8-2011

Nano-enabled synthetic biology: A cell mimic based sensing platform for exploiting biochemical networks

Piro Siuti
psiuti@utk.edu

To the Graduate Council:

I am submitting herewith a dissertation written by Piro Siuti entitled "Nano-enabled synthetic biology: A cell mimic based sensing platform for exploiting biochemical networks." I have examined the final electronic copy of this dissertation for form and content and recommend that it be accepted in partial fulfillment of the requirements for the degree of Doctor of Philosophy, with a major in Life Sciences.

Mitchel J. Doktycz, Major Professor

We have read this dissertation and recommend its acceptance:

Michael L. Simpson, Engin Serpersu, Eric T. Boder

Accepted for the Council:
Dixie L. Thompson

Vice Provost and Dean of the Graduate School

(Original signatures are on file with official student records.)

Nano-enabled synthetic biology: A cell mimic based sensing platform for exploiting biochemical networks

A Dissertation presented for the
Doctor of Philosophy Degree
The University of Tennessee, Knoxville

Piro Siuti
August 2011

ACKNOWLEDGEMENTS

I would like to first thank my advisor, Dr. Mitchel Doktycz for the opportunity to work in his lab as a graduate student. I am truly grateful for his guidance and for introducing me to many nanotechnology, microfluidics and microscopy tools.

I want to acknowledge my dissertation committee for their service. In addition to Dr. Mitchel Doktycz, Dr. Michael L. Simpson, Dr. Engin Serpersu and Dr. Eric T. Boder were immensely helpful throughout this process. I greatly appreciate the critical reviews and helpful discussions throughout my graduate career.

I would also like to extend my gratitude to Dr. Scott Retterer for taking valuable time away of his own work to introduce me to microfluidics, microscopy and AFM. I am grateful for his teaching and leadership as I took on new challenging projects. Without his efforts, this project would not be possible. I would also like to thank Dr. C. K. Choi for his experience and help with conducting and analyzing enzyme reactions, and for always having an insightful answer to my questions. Many thanks to Dr. David K. Karig and Sukanya Iyer for their contribution to the protein synthesis and quorum sensing projects.

Special thanks go to A. Nicole Billings for her help with confocal microscopy and FRAP experiments.

I would like to acknowledge the support of the Genome Science and Technology program at the University of Tennessee, Knoxville and the Biological and Nanoscale Systems Group at ORNL. This research was supported by NIH Grant EB000657. A portion of this research was conducted at the Center for Nanophase Materials Sciences, which is sponsored at Oak Ridge National Laboratory by the Division of Scientific User Facilities, U.S. Department of Energy. This work was performed at the Oak Ridge National Laboratory, managed by UT-Battelle, LLC, for the U.S. DOE under Contract No. DE-AC05- 00OR22725.

I would like to thank all of the lab members that I worked with, my fellow classmates, and my officemates for their support and friendship. Finally, I would like to extend my sincerest gratitude to my family for all of their encouragement and support through this process.

ABSTRACT

Exploring and understanding how the smallest scale features of a cell affect biochemical reactions has always been a challenge. Nanoscale fabrication advancements have allowed scientists to create small volume reaction containers that resemble the physical scale of cell membranes. Engineers seek to use biological design principles to manipulate information and import new functionality to such synthetic devices, which in turn, play a crucial role in allowing them to explore the effects of physical transport and extreme conditions of temperature and pH on reaction systems. Engineered reaction containers can be physically and chemically defined to control the flux of molecules of different sizes and charge. The design and testing of such a container is described here. It has a volume of 19 pL and has defined slits of 10-200 nm. The device successfully contains DNA and protein molecules and has been used to conduct and analyze enzyme reactions under different substrate concentrations and a continuous cell-free protein synthesis. The effect of DNA concentration and slit size on protein yield is also discussed.
Glucose oxidase and horseradish peroxidase were loaded in the small volume container and fed with a solution containing glucose and Amplex Red™ to produce Resorufin. Fluorescent microscopy was used to monitor the reaction, which was carried out under microfluidic control. Enzyme kinetics were characterized and compared with conventional scale results.

Continuous cell free protein synthesis in arrays of nanoporous, picoliter volume containers has also been achieved. A multiscale fabrication process allows for the monolithic integration of the containers and an addressable microfluidic network. Synthesis of enhanced green fluorescent protein (eGFP) in the nanoporous containers continues beyond 24 hours and yields more than twice the amount of protein, on a per volume basis, than conventional scale batch reactions. These picoliter, nanoporous containers provide new ways for quick determination of enzyme kinetics and continuous protein synthesis in microfluidic systems. They can be used in a wide variety of applications such as drug discovery, clinical diagnostics and high-throughput screening.

TABLE OF CONTENTS

Chapter 1 Introduction 1
1.1. Synthetic Biology 3
1.2. Mimicking cells 8
1.3. Vesicle systems 9
1.4. Water in oil emulsion systems 11
1.5. Nanotechnology approach in cell mimicking 12
1.6. Silicon and glass micromachining methods 15
1.7. Polymers and plastic materials 17
1.8. Microfluidic technologies 21
Chapter 2 Determine and tune membrane permeability, through control of membrane pore properties to control the flux of small molecules and proteins 24
2.1. Introduction 24
2.2. Materials and Methods 28
2.2.1. Microfluidic device fabrication 28
2.2.2. Device packaging and general imaging techniques 29
2.2.3. Loading of nanoporous reaction vessels 31
2.2.4. Bacterial growth and media 33
2.2.5. Protein purification and SDS-PAGE 33
2.2.6. Fluorescence Recovery After Photobleaching (FRAP) 36
2.2.7. Functional demonstration of size exclusion and molecular containment 36
2.2.8. Containment of fluorescein and EGFP 37
2.3. Results and discussion 37
2.3.1. Device fabrication 37
2.3.2. Fluorescence Recovery After Photobleaching (FRAP) 38
2.3.3. Functional demonstration of size exclusion and molecular containment 40
2.4. Conclusions 49
Chapter 3 Enzymatic reactions in nanoporous, picoliter volume containers 51
3.1. Introduction 51
3.2. Materials and Methods 56
3.2.1. Microfluidic device 56
3.3 Results and Discussion 61
3.3.1. Single Enzyme Reactions 61
3.3.2. Coupled Enzyme Reactions 64
3.4. Conclusion 76
Chapter 4 Cell-Free Transcription/Translation in picoliter volume containers 77
4.1. Introduction 77
4.2. Materials and Methods 79
4.2.1. Device Fabrication 79
4.2.2. Cell Free Translation 82
4.2.3. Characterization 84
4.3. Results and Discussion 84
4.4. Conclusion 91
Chapter 5 Continuous protein production in nanoporous, picoliter volume containers under continuous flow conditions 92

5.1. Introduction 92
5.2. Materials and methods 94
5.2.1. Device Fabrication 94
5.2.2. Cell Free Transcription/Translation 95
5.2.3. Quantifying Cell-Free Transcription/Translation Reactions 97
5.3. Results 98
5.3.1. Cell Free Transcription/Translation 98
5.3.2. Quantifying Protein Synthesis and Release 101
5.4. Discussion 106
5.5. Conclusions 111
Chapter 6 Conclusions and future directions 113
6.1. Summary 113
6.2. Future Directions 114
List of References 120
VITA 137

LIST OF TABLES

Table Page

Table 3-1: Michaelis-Menten Kinetic Variables for Coupled Enzyme Reactions 75
Table 5-1: Summary of protein synthesis rates and yields 109

LIST OF FIGURES

Figure Page

Figure 1-1: Materials, fabrication techniques and applications for BioMEMS devices.. 16
Figure 2-1: Scanning electron micrographs of containment vessels 27
Figure 2-2: Fabrication steps of the cell mimic device..... 30
Figure 2-3: Reaction device fabrication..... 32
Figure 2-4: SDS-PAGE of different concentrations of purified EGFP 35
Figure 2-5: Fluorescence Recovery After Photobleaching. 39
Figure 2-6: Diffusion of fluorescent polystyrene beads 41
Figure 2-7: Diffusion of plasmid DNA. 42
Figure 2-8: Silicon dioxide deposition..... 44
Figure 2-9: Diffusion of EGFP and fluorescein..... 46
Figure 2-10: Lumped Capacitance Diffusion model. 47
Figure 2-11: Experimental diffusion data vs. the diffusion model 50
Figure 3-1: A nanoporous, picoliter volume platform for enzyme reactions 55
Figure 3-2: Resorufin standard curve 58
Figure 3-3: Single enzyme reactions on 4 minute PECVD devices. 63
Figure 3-4: Sealed device and an array of enzyme reactions..... 65
Figure 3-5: Coupled enzyme reactions on 7 minute PECVD 66
Figure 3-6: Coupled enzyme reactions with different HRP concentrations 67
Figure 3-7: Fluorescently measured coupled enzyme reactions. 69
Figure 3-8: Michealis-Menten plots..... 71
Figure 3-9: Lineweaver-Burk reciprocal plots..... 72
Figure 4-1: Wafer with 8 chips and sealed device. 80
Figure 4-2: Scanning Electron Microscope (SEM) images of the device. 81
Figure 4-3: Plasmid encoding for EGFP. 83
Figure 4-4: Standard curve of EGFP in (a) cell mimic device (b) plate reader 85
Figure 4-5: Cell-free transcription/translation in cell mimic devices.. 86
Figure 4-6: Cell-free transcription/translation with different DNA concentrations.. 88
Figure 4-7: Cell-free transcription/translation in no pore cell mimic devices.. 89
Figure 4-8: Cell-free protein expression in (a) plate reader and (b) no slit device.. 90
Figure 5-1: A cell mimic platform for continuous protein production. 96
Figure 5-2: Continuous protein production in cell mimic devices. 100
Figure 5-3: Protein synthesis recovery after photobleaching. 102
Figure 5-4: Fluorescence recovery rates. 104
Figure 5-5: Blockage of protein synthesis by antibiotic treatment. 105
Figure 6-1: Sender-Receiver system in reaction devices. 117
Figure 6-2: Receiver cell activation in a plate reader. 118
Figure 6-3: Activating receiver cells caged inside of a reaction device. 119

Chapter 1
Introduction

The cell is the fundamental unit of biological systems. It has the ability of sensing, processing information and responding to changes in the environment. The cell operates under a wide range of environmental conditions and consists of complex networks of interacting molecules, which function within and outside the cell. The complexity of its networks allows for self-checking and redundancy which leads to a dynamic robustness [1]. The dimensions of the cell are well conserved and its membrane serves as a boundary for controlling the transport and detection of chemical signals between cells and their surrounding environment. The membrane of a cell is a semi-permeable lipid bilayer, which transports proteins and regulates molecular transport through its channels. It is changes in protein charge, structure and surface energy combined with membrane pore structures that precisely dictate transport and selectivity across the membrane [2-4]. The small size of the cell allows for intra and inter-cellular communication through facilitated and passive diffusion. It also allows for small fluctuations in molecular concentrations to result in significant changes in network interactions. Cells can be highly specialized and extremely diverse but still use a common set of building blocks and follow the same fundamental principles of thermodynamics and physical sciences [5]. However, understanding the organizing principles and the complexity of network interactions has been proven to be a difficult task. Therefore, emulating the properties of biological cells becomes a necessary step for better understanding the cell and the functional capabilities of its biomolecular systems.

There are many challenges and opportunities in mimicking the properties of biological cells. Recent advances in nano/micro technology and synthetic biology have created the opportunity to match the working level of a cell and gain insight into the organizing principles of molecular and network interactions. They have made possible integration of nanomaterials into engineering microscale structures that are comparable in size with a living cell and mimic its biological properties.

The objective of this thesis is to develop a cell mimic based picoliter volume device that is able to mimic functional aspects of a biological cell, and function as a universal platform to study biochemical reactions within a cellular scale system. The cellular scale, nanostructured membrane is fabricated in silicon and is used to confine DNA, enzymes, proteins, and cell free extract components. Microfluidics are used to deliver and remove materials via diffusion-mediated exchange across the membrane enabling enzymatic reactions and long-term production of functional proteins. The nanostructured membrane facilitates selective material transport and has been modified to tune material exchange. Many devices can be implemented in parallel making the platform suitable for larger scale production of a single protein or for simultaneous functional analyses of multiple proteins.

The following introduction will provide background and significance of different approaches that have been followed in mimicking cell membranes and understanding existing biological systems. Chapter 2 provides a description of the approaches taken to determine and tune membrane permeability, through control of the physical pore structures to control the flux of small molecules and proteins. Chapter 3 describes single and coupled enzyme reactions in cell mimic devices. Chapter 4 discusses exploiting the

advantages of the small volume cell mimic device to carry cell-free transcription/translation and determine the optimal DNA template concentrations required for these scale reactions. Chapter 5 extends the results presented in Chapter 4 and describes the advantages of small volume reaction containers and controlled membrane transport for a long-term continuous protein production. Chapter 6 is a summary of conclusions and future directions.

1.1. Synthetic Biology

Synthetic biology is a relatively new notion in life science. It covers a variety of disciplines such as molecular biology, systems biology, engineering and physics [6, 7]. This emerging field is working toward understanding how biological systems work, by modeling and engineering complex reaction networks, carrying out the assembly of systems in a synthetic way and defining “minimal” cells capable of sustaining life [6]. The term “synthetic biology” was first introduced in 1980 by Barbara Hobom to describe bacteria that were genetically engineered by using recombinant DNA technology [8]. The term “synthetic biology” was introduced again in 2000 by Eric Kool and other speakers at the annual meeting of the American Chemical Society in San Francisco, where the term was used to describe synthesis of unnatural organic molecules which can function in living systems [6]. The classical meaning of synthetic biology is the use of synthetic molecules for obtaining a quantitative understanding of existing biological systems. More recently, it has achieved a broader notion by attempting to recreate in unnatural chemical systems [9] the properties of living systems such as heredity, self-organization at the cellular scale, and directed evolution in order to “redesign life” [6, 10, 11]. Synthetic

biologists try to understand “natural” biology by carrying out biological assembly in a synthetic way. They also seek to use interchangeable parts from living systems that can be tested and used as building units for systems that may or may not have analogues in natural living systems [6]. This engineering approach may be applied to all levels of biological structures from molecules to cells to organisms [7]. The efforts of synthetic biology can be better categorized as a “top-down” or “bottom up” approach. The “top-down” approach uses entire genomes, as blueprints to better understand gene function in a cell. A key focus is on constructing minimal cells by the reduction of genomes in order to determine the minimal number of genes capable of sustaining life [12-15]. Rewriting a complete genome can enable a better understanding of gene function by observing differences in observed and predicted behavior of cells. A few groups are working on creating bacteria with chromosomes that have been completely synthesized from synthetic oligos [16]. This can be accomplished stepwise [17] or by inactivating and removing the entire genome of the bacteria and replacing it with a whole in vitro synthesized genome[16]. Another goal of the “top-down” approach is to test theories about the minimum number of genes required for bacterial survival and replication [18-20]. It can also develop minimal living systems which can then serve as units that can be augmented for specific purposes [21]. The “top down” approach has been based on the stipulation that closely related genomes have genes that are required for those species but are not required for basic life. Therefore, to test theories of the minimum number of genes required for bacterial replication, a systematic removal of “indispensable” genes by mutating them one gene at a time has been applied to the genomes of *Escherichia coli* and *Mycoplasma* bacteria [16, 17, 22]. Another goal of the “top-down” approach is to

create bacteria with globally mutated genomes rather than truncated ones, which can make possible the extension of the genetic code with unnatural amino acids[23] and prevent functional exchanges of genetic material with natural species, therefore decreasing the chance of environmental contamination [16]. However, there are many challenges to this approach such as the presence of false “essential” and “dispensable” genes and the fact that more than a third of the discovered essential genes have unknown functions [15].

On the other hand, the “bottom-up” approach follows the strategy of constructing engineered genetic circuits or simplified systems to better understand molecular and cellular regulatory processes and to obtain simple systems with desired capabilities [5, 7, 24-26]. The genomic-based information and the control mechanisms that are being obtained from this approach are making possible redirection of living systems by engineering specific genetic circuits such as toggle switches, repressilators and logic switches [27-30]. These engineered gene circuits can be used to test theoretical models, and advance our understanding of biological complex systems[31]. The engineering community has taken “bottom-up” synthetic biology a step further. They seek to extract interchangeable parts from living systems, which could be tested, validated and reassembled to create devices with optimized metabolic pathways for the production of desired reagents [6, 32-34]. A great variety of synthetic networks have been applied in cells by rearranging regulatory components into genetic oscillators [29], artificial population control based on quorum sensing [35], a bistable circuit [30], and a sender-receiver system [36]. Noireaux *et al* constructed cell-free gene circuits consisting of engineered repression cascades and transcriptional activation. In these cascades, the

protein products of the first stage were used as input activators or inhibitors of the next stage. Using this approach, they constructed one-, two-, and three-stage gene expression cascades, which were used to study parameter ranges and basic principles of genetic circuit assembly [31, 37]. Elowitz and Lieber designed an artificial oscillator module from three regulating genes [29]. This “repressilator” was wired into the circuits of *E. coli* and induced periodic on-off switching of genes. The periodic on-off switching was visible by coupling the module to the synthesis of green fluorescent protein (GFP) [27]. Other gene modules that have been used in a “bottom up” fashion for controlling and understanding bacterial behavior are toggle switches. These switches can be flipped into an on or off state by an environmental signal or quorum sensing autoinducer [27]. A different approach was taken by Weiss and co-workers toward artificial pattern formation [35]. They generated an artificial gene network that responded to different concentrations of diffusible quorum sensing autoinducers. The artificial gene network was implemented in *E. coli* and the bacteria were grown in a Petri dish surrounded by different localized sources of autoinducers. The diffusion of the autoinducers from the sources turned on expression in bacteria and led to spatial patterning of the biofilm[35]. Other groups have also studied spatio-temporal effects induced by varying chemical “sources” via reaction diffusion in the form of genetic oscillators or pulse generators. Reaction diffusion systems have also been used to produce nano and microscale patterns [38].

In principle, systems with integrated elements that act as signal transducers, molecular sensors, and genetic regulators, can be used as simple models of biological control circuits. The reduced number of components in these systems allows for an accurate computational prediction of their behavior, which can be used to improve their

design[31]. However, the “top-down” and “bottom-up” approaches still rely on the use of biomolecules and an existing cellular environment to start and validate cellular function [5]. Modeling and analysis of these systems are difficult because of the many unknown parameters in the cell environment. Therefore, *in vitro* reconstruction of genetic circuits with known components in a cell-like environment is a possible option to overcome these limitations [31]. Designing biological devices that mimic a biological cell and allow for formation of complex systems from their basic functional parts, sense abnormal conditions and dose response in real-time, and perform metabolic and biosynthetic functions[7], can lead to a system with true “bottom-up” cell-like characteristics.

The advancements in techniques and approaches described above have created significant opportunities to modify single living cells and multicellular species [39]. However, there are also major limitations associated with these approaches such as high cost, low efficiency of scale, safety and ethical issues. Furthermore, combining non-biological with cellular techniques is often difficult, the resulting products of the genetic manipulations could be toxic to the cells and there is also the need for specialized nutrient media to grow certain genetically modified cells. Therefore, an alternative approach is to build cell-like devices that are engineered specifically to encapsulate components for certain applications [39]. These cell-like devices can function as containers for artificial cellular systems and must be able to exchange nutrients, ions, regulatory molecules and remove waste products between the device and the environment. Internal organization of compartments could be used for localized production and micron-scale assembly line formation [31].

1.2. Mimicking cells

Mimicking cells has been the focus of researchers for many decades. Several efforts have been employed for the development of platforms that mimic and apply functional aspects of the cell and its ability to contain pico/nanoliter volumes of liquid on reaction effectiveness [39-44]. These small volume containers have a variety of different nomenclature such as cell mimics, minimal cells, cell-like entities, nanoreactors, artificial cells and in vitro compartmentalization devices. A common feature of these platforms is their ability to contain small volumes of liquid and reduce the number of molecules needed to carry out a function. Due to their small volume, they can also establish favorable local conditions for protein functions and eliminate the need for mixing [5]. Therefore, the small volume containers are ideal for understanding self-organization at a cellular scale and studying single molecule reactions. They are also useful as platforms for understanding molecular reaction systems and questions involving the origin of life [4, 5, 45-49]. A more practical use for biomimetic devices is for high-throughput screening [50, 51] or synthesis of products that are toxic to natural cells [52-54]. Furthermore, the containers can be used for drug delivery, chemical sensing, signal amplification, detection of nonsense or frame-shift mutations in marker genes [55-57], protein production [58-65] including pharmaceutical proteins [66, 67] and patient-specific vaccine candidates [66, 68], synthesis of drug transporters[69], toxin detection [70] and preparation of nanomaterials [71-73]. Finally, cell-mimic devices can be used to study evolutionary aspects of the cell and also study stochastic effects on the performance of artificial gene networks [31]. However, the parallel pursuits for creating functional

mimics of cells have the containing membrane as a distinguishing feature from each other.

1.3. Vesicle systems

There are many different materials that have been used to mimic the membrane of a cell. Self-assembled vesicles prepared from amphiphilic molecules are the most common approach for the formation of synthetic membranes. These structures can be formed from synthetic molecules such as block copolymers [72, 74], or from lipids. Block copolymers consist of at least two parts of different solubility, which gives them the ability to self-assemble into a variety of structures including vesicles mimicking a cell membrane [5, 75, 76]. Depending on the type of polymer, molecular weight and block ratio, different vesicles with a wide range of physical and chemical properties can be created and used for reagent delivery, chemical sensing and reaction containment [75-77]. Enzyme activity can be conserved inside polymersomes, which makes these vesicles applicable for sensing and stimulus response. They have also been used for incorporation of natural energy-transducing membrane proteins and demonstrated the potential use of these systems for energy conversion processes of natural systems [5].

Membranous vesicles consisting of lipid bilayers have been used in laboratories for more than 40 years. Lipid bilayer vesicle preparation is a mature field that has been used for many years by the pharmaceutical industry in cosmetic preparations and as drug delivery agents [39]. These self-assembling structures formed from lipids are called liposomes. They were first prepared in the 1965 by Bangham and his team and can be prepared by different techniques [39, 78, 79]. The first liposomes were called multi

lamellar vesicles (MLVs) because they consisted of hundreds of concentric lipid bilayers [39]. Since the multilamellar characteristic can be a limitation, small unilamellar vesicles (SUVs) were prepared by sonicating MLVs. The liposomes consist of natural components and they have distinct advantages over other vesicles. They can be created in cell comparable scales and can allow for pore-forming proteins to be incorporated. Liposomes that allow small molecules to pass through but retain macromolecules can also be prepared by choosing short-chain lipids [39]. Although many neutral small molecules can diffuse through the walls of the lipid bilayer, their permeation properties can be regulated based on the chain length and composition of their lipids. Liposomes can contain chemical reactions and have been useful in understanding diffusion, permeability and other physical properties of the cell membrane. They can also protect enzymes from degradation and help in better understanding the biological properties of a cell membrane [5]. Liposomes have been used to study many gene-based reaction systems such as protein production involving a gene sequence, mainly green fluorescent protein (*gfp*) gene, with a promoter and cell-free extract [80-85]. Complex genetic reactions have also been achieved in liposomes. A two-stage genetic network stage was demonstrated by Ishikawa *et al*, where the protein produced in the first stage is required for activating protein synthesis in the second [86]. Noireaux *et al* has demonstrated other multi-stage reaction systems [44]. Many groups have also shown that enzymes entrapped inside of a liposome can be used for catalyzing reactions [87, 88], for metabolizing toxic reagents [89], or for diagnostic applications [90].

1.4. Water in oil emulsion systems

Water in oil (w/o) emulsions have also been used to create small volume biomimetic devices. Femtoliter volume containers can be prepared by stirring a mixture of oil, aqueous solution and appropriate surfactants [42, 91-93]. Strong shaking or ultrasonication can be used to make even smaller size droplets [94]. Microfluidics technology has also been used to generate droplets of defined composition and size. This approach allows for easy manipulation where mixing and compartmentalization of reagents can be obtained by the merging of microfluidic flow streams[5, 95]. Since w/o techniques can create a large number of small volume reaction containers, they have been used for a variety of applications such as quantifying genetic variation within individual alleles [96], amplifying and characterizing complete genomic libraries [97, 98], linking genotypes with phenotypes and high-throughput screening and selection [99, 100]. In these approaches, the genes or whole genomes together with specific polymerases and the reagents for transcription/translation are contained inside the aqueous compartment. Direct assessments of specific protein functions can be made. On the other hand, the amount of reagent available and inhibitory byproduct formation, limit the reaction inside the vessel since reagent exchange within the oil phase is unlikely. Researchers are trying to enhance reagent transport in and out of the w/o emulsion reaction vessel by allowing individual vessels to physically contact or fuse with each other [91, 101, 102].

Self-assembly based simply on molecular recognition, may not be enough to produce all the desired structures of different spatial and temporal order. Therefore, developing artificial systems, which can be used for the assembly of synthetic structures,

are necessary [31]. Engineered synthetic spatio-temporal gene networks have been developed by Isalan *et al* to emulate *Drosophila* embryonic pattern formation [103]. They modeled embryonic cells using a spatially extended expression network, which was formed by using “gene”-coated paramagnetic beads that were held in place by magnets in a reaction chamber. Gradients of activators that were generated from different local sources in the network were able to activate repressor protein production from bead-immobilized genes. Diffusion of the newly produced repressor protein, led to a spatial modulation of gene expression patterns resembling gap formation in the *Drosophila* embryo [103]. This chip-based expression system is of interest for studying the spatio-temporal effects and synthetic developmental systems *in vitro* [31].

Major advantages of these cell mimic devices are their ability to self-assemble and to be produced with simple techniques. However, the small volume reaction containers described above, do not have long-term stability. They are relatively fragile and sensitive to temperature, stress, and pH. They are also easily damaged by low mechanical stress, which makes them unable to survive most micro- and nanoscale fabrications. The fixed dimensions of their pores can also limit their applicability. Therefore, a more robust reaction platform with a defined volume, pore sizes and design could be advantageous.

1.5. Nanotechnology approach in cell mimicking

Advancements in nanotechnology and microfabrication techniques have allowed researchers to work at the atomic and molecular levels [104]. They can match the working scale of a living cell and provide platforms and cell mimic devices that can be

used for a bottom-up construction of nanosystems with cell-like characteristics. Nanotechnology has provided the tools and technology platforms to better understand biological systems by having the ability to arrange molecules into objects of several length scales and also to disassemble objects into molecules. This is achieved by rearranging matter using ‘weak’ molecular interactions such as hydrogen bonds, van der Waal forces, various surface forces and electrostatic dipoles[104]. Nanotechnology was initially classified into wet and dry nanotechnology. Wet nanotechnology includes living biosystems whereas dry nanotechnology is searching for approaches to engineer man-made structures at the nanoscale level and to integrate these structures into more complex systems [104]. Although nanotechnological approaches may differ from the evolving systems found in nature, many concepts such as surface interactions of various shapes, self-assembly and self-repair can be used as inspiration for nanotechnology [104]. Model biological systems models and biotechnology combined with the tools and investigation platforms that are provided by nanotechnology have led to a new branch of nanotechnology called nanobiotechnology. It applies nanoscale techniques and principles to better understand biological systems. It also uses biological materials and principles to create devices that can be integrated from the nanoscale level [104]. The approach used by nanobiotechnology has uncovered many fundamental biological processes and key advancements have been made in understanding biological processes such as self-assembly and self-organization [105, 106], self-repairing, nanoscale surgery, eco-toxicology [107], pollution by nanoparticles [108], protein dynamics, synthesis and targeted delivery of drugs [109], enzyme reactions and cell signaling [104, 110, 111]. Other contributions include development of color changing nanoscale systems for

displaying protein unfolding events[112], using rectified Brownian motion to explain kinesin motion along microtubules and chemomechanical energy conversions of intracellular processes [113]. Nanobiotechnology is also playing an important role in emerging areas such as the study of tissue regeneration mechanisms, realistic molecular modeling of soft matter, and understanding energy supply and conversion in the cell [104].

Nanobiotechnology has been combined with Micro-Electro-Mechanical Systems (MEMS), which are miniature devices that integrate electrical and mechanical components on a silicon substrate [114]. These devices vary in size between nanometer to millimeter level. Applications of MEMS in biology and chemistry have led to the creation of new platforms called BioMEMS (biological or biomedical Micro-Electro-Mechanical Systems). BioMEMS have been taken a step further to create Lab-on-a-Chip, which is a device or a system of devices that are used to perform a combination of biological and clinical assay analysis on a single mimic device [114]. Mimicking the principles and concepts of biology have led to the controlled self-assembly of arrays of nanoparticles, macromolecular crystals and devices for use in nanoelectronics. Structure replication [12], mimicking photosynthesis [115], neuromorphic engineering [116] and the development of bioreceptors and biomarkers, are more examples of using biological paradigms to create semibiological hybrids and artificial nanoscale devices [104]. Different fabrication techniques such as drilling, etching, molding or embossing have been used to create new devices of various sizes, which are based on concepts and principles from natural systems. They have been synthesized from a wide variety of materials such as oxide films being etched by ion beam [117, 118], track etching

nanopores in polymer films [119], using soft lithography [120] and from carbon nanotubes [121, 122]. These devices can enhance our ability to interface and understand basic questions regarding biological functions such as mimicking photosynthesis [123], creating large molecular structures [106], neuromorphic engineering [116], and developing bioreceptors and biomarkers [104]. These small volume devices can relieve the need for structures or devices for mixing, decrease the number of molecules required for carrying out a reaction and decrease analysis time and rapid heat exchange when compared to traditional analytical systems [124]. They can also be modified to control the flux of different size molecules and can facilitate kinetic studies [125-128]. For example, these small volume devices have been developed and used for single molecule enzymology [129, 130], cell-free protein synthesis [63, 131-134], high-throughput screening [71, 131], and novel functional assays [70, 135]. BioMEMS devices are fabricated using mainly two categories of materials. The two categories are (1) silicon and glass and (2) polymers and plastic materials (Figure1.1).

1.6. Silicon and glass micromachining methods

Silicon and glass micromachining methods of fabrication are the most popular approach for cell mimic device formation, especially since they use a wide variety of technologies for bulk micromachining, lithography and surface machining. Silicon methods of fabrication start with single crystalline silicon wafers, which undergo different deposition techniques for a number of layers such as silicon dioxide, polysilicon, metal, and silicon nitride. Wet or dry etching techniques can also be

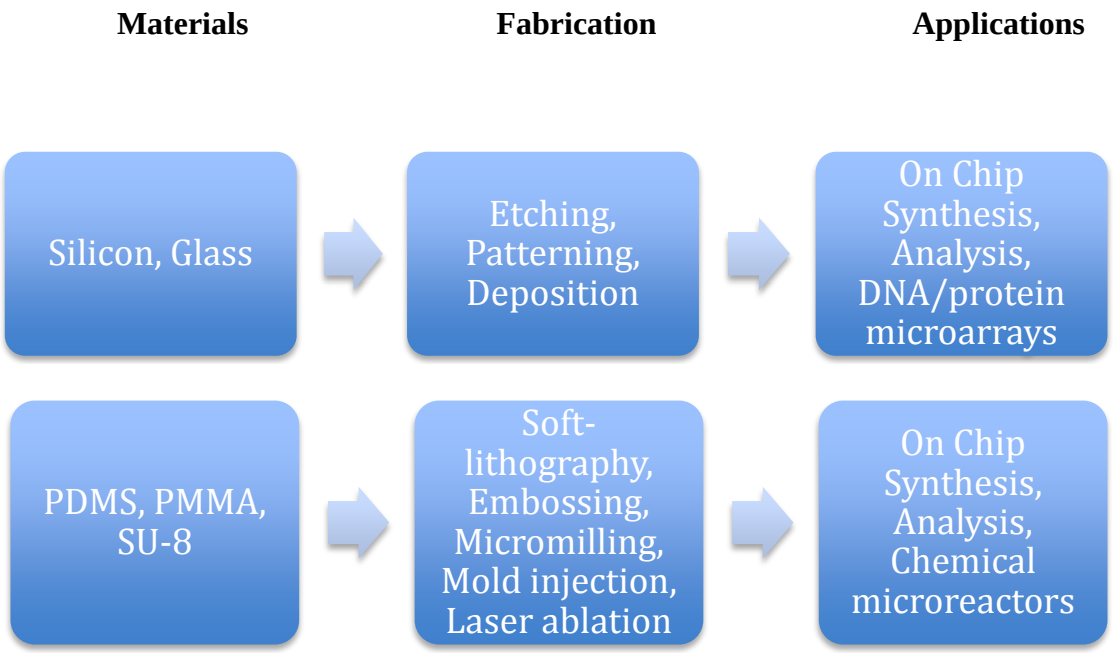

Figure 1-1: Materials, fabrication techniques and applications for BioMEMS devices.

used to make the device and/or the microchannel. The pores in the membrane of the device are usually made by making holes through the synthetic material. Common techniques used to achieve this are track etching, anodic oxidation, and ion beam etching [114, 136].

Glass methods of fabrication are also as popular as silicon, mostly due to favorable properties of glass such as high chemical resistance, high mechanical strength, wide optical transmission range and high electrical insulation. Glass can be photo patterned using dopant photosensitive materials or it can be etched using buffered hydrofluoric acid with metal masking layers and photoresist [114, 137]. Glass channels with straight walls can be also obtained by using deep RIE [138]. Although micromachining techniques are widely used, silicon and glass based devices have some drawbacks such as their surface characteristics may not be well suited for all biological applications. Other drawbacks include the need for expensive equipment and facilities, they are also labor intensive, require highly specialized skills and can be costly to manufacture. Therefore, a less expensive, less specialized and faster method for device fabrication is necessary to promote a widespread use of microfluidic devices in biology [139].

1.7. Polymers and plastic materials

In the past few years, more research groups have started to use plastic materials and polymers for fabricating BioMEMS. The main reasons for using these materials are their low cost and multi-functionalities [140, 141]. There are a wide variety of plastic materials and polymers with different physical, chemical and biological properties, which

makes them adaptable for different applications. It is also easier to interface biological tissues to the polymer materials. Their bio-degradability, lack of immuno-inflammatory initiation and lower toxicity allow for in vitro applications of devices made from these materials. The methods used to fabricate these microdevices include soft lithography, hot embossing, mold injection, micromilling and laser ablation [142]. Soft lithography is the most popular alternative approach to silicon and glass micromachining. It was first developed in 1974 at Bell Labs when researchers developed a new technique to use a lithographic master for molding soft materials [139]. Soft lithography has been used to pattern surfaces and fabricate microchannels via stamping, molding and embossing. Typically, soft lithography refers to the molding of polymers and different plastic materials, using photoresist masters. Polymers are the most common material used for soft lithography and BioMEMS fabrication. They have unique properties such as biological and chemical compatibility, easy fabrication, good thermal properties, optical transparency and high electrical insulation[114]. Polymer enzymes are usually synthesized using soft lithography techniques. Commonly used polymers for soft lithography are PDMS, PMMA and SU-8. PDMS is a hydrophobic polymer, which is prepared by mixing a curing agent with a pre-polymer [143]. PDMS can be cured by heat or UV light and based on its properties it is considered an ideal material for soft lithography [144]. It is optically transparent, durable and self-seals ability to a wide range of surfaces. It also has a modifiable interfacial energy, which makes its surface dynamic and overall a good material for building micro-fluidic devices and channels [114]. Porous membrane devices can be formed by micromolding the PDMS. In this procedure, degassed PDMS is poured over a patterned substrate and left to cure for 1-2 hours. The

impression of the pattern of the substrate is then left on the PDMS after it is cured around the etched substrate. Therefore, the design features of a PDMS device are only limited by the master from which it is molded. Devices that are formed this way have been shown to have pores as small as 30 nm [145]. PDMS is biocompatible and devices prepared from this material have been used in a variety of applications such as culturing bacteria and mammalian cells, protein production and enzyme kinetics. Micromachining and photolithography have been used to fabricate complex masters to mold PDMS microstructures, including ones with multidimensional layers [146].

Soft lithography has also been used to describe hot embossing techniques, which are used to transfer a pattern from a metal master or a micromachined quartz to a flexible plastic sheet. The plastic sheet becomes imprinted to the master by applying heat and high pressure. Many plastic printed surfaces can be formed from one micromachined master and then bonded to plastic covers to form microchannels [147]. The most commonly used plastic for hot embossing is polymethylmethacrylate (PMMA), which is the least hydrophobic of most common plastics. It is also known as Plexiglass, Acrylic, Lucite etc, and was originally used as resist material for Lithography, Electroplating and Molding techniques (LIGA techniques) [137]. It is thermoplastic and noncrystalline in nature with a 92% optical transparency [148]. It can be reused many times by reheating and reshaping it into different forms. It also possesses many other features such as high chemical resistance, low frictional coefficient and good electrical insulation. The surface of PMMA can be modified by oxygen plasma exposure or X-ray irradiation in order to modify its surface properties for biomedical applications [114, 137]. Hot embossing of PMMA enables construction of low cost devices and is appropriate for finalized device

design. However, it can be time consuming and expensive if new features need to be added to the platform since a new micromachined master is required. SU-8 is another polymer that is commonly used as a material for BioMEMS applications. It is in a liquid form consisting of a solvent, an epoxy resin and a photoacid generator. Generally it is used for making simple and inexpensive thick photoresists for high aspect ratio structures. It has good temperature and chemical resistance and can be patterned to create nearly vertical sidewalls [114]. Other approaches for constructing microfluidic devices consist of micromolding or using photodefinable polymers. Micromolding is inexpensive and takes advantage of thermoplastic polymer materials, which are heated past their glass transition temperature and are molded into a lower temperature master. Photodefinable polymers are used to create devices that are called microfluidic tectonics. These devices are relatively cheap and are constructed using lithography, photopolymerizable materials and laminar flow.

Synthetic membranes have many advantages over membranes made from biological components. They are more robust and can withstand a wide range of environmental conditions such as pHs, temperatures and pressures, which makes them easier to integrate with micro-scale systems. It is also feasible to develop synthetic devices with specific material composition, dimensions and design, which make them very flexible for a wide range of applications. The challenge for synthetic cell membranes remains the efficiencies and multifunctionality that is present in a biological membrane.

1.8. Microfluidic technologies

No matter what material is used to make cell mimic devices, these devices still cannot perform high-throughput experiments at a cellular scale or under a variety of specific environmental conditions. Microfluidic technologies can overcome these limitations by taking advantage of the same microfabrication techniques used to pattern cell mimic devices on silicon, glass or PDMS wafers[149]. The low cost of production and small-scale give microfluidics the ability to perform procedures such as biological and chemical sensing, high-throughput screening and genetic analysis[149]. The laborious and time-consuming efforts to save chemical compounds and conduct high-throughput screening applications have led to miniaturization of existing technologies and the introduction of nanoliter dispensing systems and high-density plate formats[150]. Microfluidic chips are small platforms that consist of channel systems connected to liquid reservoirs via tubing systems. The fabrication of microfluidic chips usually requires cleanroom facilities and consists of a variety of materials and fabrication techniques. However, the majority of microfluidic devices are simple planar microchips fabricated on silicon, glass or polymers via photolithography [150-152]. Due to short distances and high surface to volume ratio, transport times of mass and heat are shortened in microfluidic channels and multi-step reactions can be easily performed. Most microfluidic devices are miniaturized versions of macroscale systems and they do not take full advantage of the properties unique to the microscale. However, the number of microfluidic devices that operate under continuous flow and take advantage of the effect of laminar flow and diffusion in microscale is growing. Operating under continuous flow allows for on-line analysis, combination of multiple reaction steps, and shortened

reaction times, resulting in faster optimization of reaction parameters [150]. The small size of microfluidics also allows for the incorporation of multiple aspects of modern biology or chemistry labs onto a single microfluidic device. These integrated microfluidic devices are called Lab-on-a-Chip (LOC) or micro-Total Analysis Systems (μ-TAS) and they have been used for different techniques such as Polymerase Chain Reaction (PCR), Fluorescence Activated Cell sorting (FACS) and cell culturing [150]. Many Lab-on-a-Chip devices can include multiple analysis steps such as cell sorting and concentration, growth and detection followed by cell lysing and PCR. Recent advances in fluorescent imaging techniques combined with microfluidics have created opportunities to study signaling networks and perform live cell experiments [149]. Fluorescent imaging can be performed within microfluidic devices by taking advantage of the small-scale of microfluidics, which allows for subcellular manipulations of molecules and highly specific control of the cellular microenvironment [153]. Furthermore, visualization of molecular movement within whole cells conducted in high-throughput microfluidics, allows for large-scale determination of dynamic properties such as spatial and temporal characterization, which have recently been used to develop mathematical models of biological systems [153, 154]. Burns *et al* fabricated a microfluidic platform with nanoliter DNA analysis devices with integrated heaters, temperature sensors and fluorescent detectors. The platform was used to perform sample loading, mixing, PCR, electrophoresis and detection simultaneously in a single chip [155]. Mathies group also developed 16, 48 and 96 microchannel electrophoresis microchips, which were used for genotyping and DNA sequencing [156].

Here, we have developed a cell mimic based picoliter volume device in a microfluidic platform that is able to mimic functional aspects of a biological cell. It operates under continuous flow and takes advantage of the effect of laminar flow and diffusion in microscale. Materials are delivered and removed via diffusion-mediated exchange across the membrane enabling enzymatic reactions and long-term protein production. The nanostructured membrane has been modified to control and facilitate material exchange and transport. Many devices have been implemented in parallel making the platform suitable for larger scale production of a single protein or for simultaneous functional analyses of multiple enzymes and proteins.

Chapter 2
Determine and tune membrane permeability, through control of membrane pore properties to control the flux of small molecules and proteins

2.1. Introduction

Understanding the physical phenomena that influence microscale interactions is a key factor when working with microfluidics and cell mimic devices. Therefore, new microscale devices must be made to take advantage of forces that are dominant at the microscale. Surface area to volume ratio, laminar flow and diffusion are three main physical characteristics that influence the performance of microfluidic devices[139]. Laminar flow is a fluid flow regime in which the velocity of a particle in a stream is not a random function of time [139]. Due to the short length of a microfluidic channel, the flow is generally laminar, which allows for precise calculation of mass transport as a function of time, using parameters such as fluid properties and channel geometry. Consequences of laminar flow in microfluidic channels include the ability to flow two or more streams in contact with each other without mixing, which allows for creating well-formed packets of fluid[139]. Since laminar flow allows for different reagents to perfuse barrier-free next to each other, localized treatment of cells can be easily achieved in microfluidic platforms. Chemical gradients with sub-cellular resolution can also be constructed by combining laminar flow with a controlled mixing by diffusion[149].

Diffusion is another important factor to be considered when working with microfluidic devices. It is defined as the process by which, based on the Brownian motion, a concentrated group of particles in a given volume will spread evenly over time

so that throughout the volume there is a constant average concentration. Diffusion is measured in one dimension by the equation $d^2=2Dt$, where d is the distance that the particle moves in a time t, and D is the diffusion coefficient of the particle. Therefore, the time it takes the particle to travel over a distance is proportional to the square of that distance [139, 149]. The diffusive motion of a particle over large distances is negligible, but it can account for a significant portion of mass transport when considered on the micro-scale. An additional consideration is the relative amount of surface area exposure, which increases dramatically in a microfluidic device. This can cause increased heat conduction and faster diffusion. Therefore, the effect of diffusion becomes very important and must be accounted for in small volume devices.

In a living cell, volume containment and material diffusion are controlled by the physical structure of the cell membrane. Therefore, mimicking the cell membrane must take into account the approaches that the membrane of a living cell uses to gate and select the types of molecules that are allowed to diffuse through it. The strategies used to convey gating abilities of a cell mimic device could be classified according to the desired type of selectivity, such as electrochemical, chemical or physical. Gating by electrochemical selectivity can be achieved by changing the surface charge of the channel walls by applying electric potentials. It can also be achieved by changing the surface charge of the molecule or species by controlling the ionic strength of the solution or by controlling the external pH. Strategies that use chemical selectivity can involve functionalizing the surfaces of the nanopores with a reactive molecule. Specific species will bind to the reactive molecule at the entrance of the nanopores to block or allow flow

through them. Physical selectivity can be achieved by decreasing or increasing the size of the membrane pores, thereby achieving a physical restriction of flow through the pores. The cell mimic device described here (Figure 2.1) uses physical selectivity for transport and mixing of materials across its membrane. During the transmembrane diffusion, the diffusivity (D_o) of a specific molecular species depends on the viscosity of the medium in which it is suspended, the temperature of the medium and the hydrodynamic radius of the species. Effective diffusivity (D_{eff}), also referred to as apparent diffusivity, can dramatically change based on binding interactions of the molecules with pore surfaces and steric hindrance of molecular motion. More dramatic changes to effective diffusivity (D_{eff}) can occur by increases in pore length and reductions in pore radius, which translate into significant changes in pore surface area to open volume ratio. Effective diffusivity of a given molecule at the nanoscale level is also influenced by phenomena such as single file diffusion and ionic selectivity [157, 158]. The rate of molecular transport per unit of membrane area depends also on the size and number of pores (open volume fraction). It is the architecture of the membrane that enables functionality, therefore defining and implementing a strategy for tuning membrane permeability by controlling the physical pore width is the primary focus of this chapter. More specifically, we demonstrate functional size exclusion and molecular containment. Fluorescence recovery after photobleaching and a Lumped Capacitance Model are used for predicting transport measurements and transient changes in concentration within a nanoporous reaction vessel under moderate external flow.

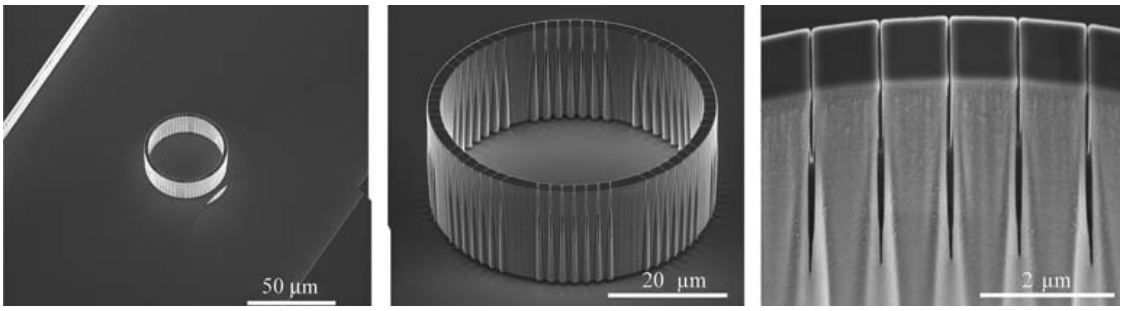

Figure 2-1: Scanning electron micrographs of containment vessels for assessing diffusive loss taken prior to filling and sealing show the integration of porous vessels within a microfluidic channel (left), the overall device size and pore locations (center) and nominal pore size (right). Images were taken at a 30° stage tilt.

2.2. Materials and Methods

2.2.1. Microfluidic device fabrication

The small volume reaction devices were fabricated as described in Retterer et al [159]. A 400 silicon wafer with a h100i crystal orientation was used to fabricate the devices. The etch mask for the reaction devices was defined by spin-coating the wafer with NANO PMMA 495 A4 electron beam resist (Microchem Corp., Newton, MA) at 2500 rpm for 45 seconds and baking it on a hotplate for 10 min at 180° C. The geometry of the reaction container and optical alignment marks for subsequent processing were exposed using a JEOL JBX9300-FS electron beam lithography system operating at 100 kV and 2 nA. The patterns were developed for 1 min in 1:3 methyl isobutyl ketone (MIBK):isopropyl alcohol (IPA), rinsed with IPA, and dried with nitrogen. Afterwards, they were exposed to a brief oxygen plasma (10 sccm, 150 mT, 100 W, 6 s) before depositing 15 nm of chromium via electron beam evaporation. Then the wafer was soaked in acetone, and rinsed with IPA and water. The rinsing leaves behind a chromium etch mask in the areas exposed by the electron beam. Conventional contact alignment optical lithography was then used to define the microchannel masks. The wafer was treated with MicroPrime MP-P20 (Shin-Etsu MicroSi, Inc., Phoenix, AZ), which was was spin-coated at 6000 rpm. JSR Micro NFR 016 D2 55cp (JSR Micro Inc., Sunnyvale, CA) was then used as the etch mask for the microchannels. It was also spin-coated at 6000 rpm. NFR is a negative photoresist and it is more resistant to cracking during the cryogenic etching process. Next, the wafer was baked on a hotplate at 90°C for 90 seconds, exposed, and baked for an additional 90 seconds at 90°C. CD26 (Microchem

Corp., Newton, MA) (<5% tetramethylammonium hydroxide) was used to develop the samples for 20 seconds, until the microchannels were visibly developed. The wafer was then rinsed with water, dried with N_2 and baked for 3 min at 180°C. To remove any organic solvent and resist residue left on the exposed silicon, the wafer was exposed to a brief oxygen plasma (10 sccm O_2, 150 mT, 400 W, 1 min). Oxford Plasmalab 100 using a cryogenic silicon etching process was used to etch the wafer by exposing samples to a plasma of SF_6 and O_2 at 110°C. Reaction vessels and channels were etched to a depth of 15 mm at a rate of approximately 3 mm/min. After cryogenic etching was completed, exposing the wafer to another oxygen plasma and briefly soaking it in chromium etchant removed mask materials. Oxford Plasmalab 100 plasma enhanced chemical vapor deposition system was used after the removal of the etch mask materials to deposit silicon dioxide on the structures. The duration of the deposition was 2, 4, 5, 6 and 7 minutes to control final pore dimensions and tune size selectivity of the nanoporous reaction vessels. The resulting silicon wafer contains eight identical chips. Each chip is 4 cm long and consists of 2 channels, each with an array of 18 reaction containers. The cylindrical container is 2 μm thick with 8 sets of 7 slits. Slits range in size from ~5-200 nm wide and 10 μm deep [63, 159]. For the experiments described here, the container has a volume of ~19 pL (Figure 2.2).

2.2.2. Device packaging and general imaging techniques

Polydimethylsiloxane (PDMS), prepared from a Sylgard 184 silicone elastomer kit (Dow Corning, Midland, MI), was used to seal the channels and the containers after devices were filled with the reaction components or different solutions. PDMS was mixed at a

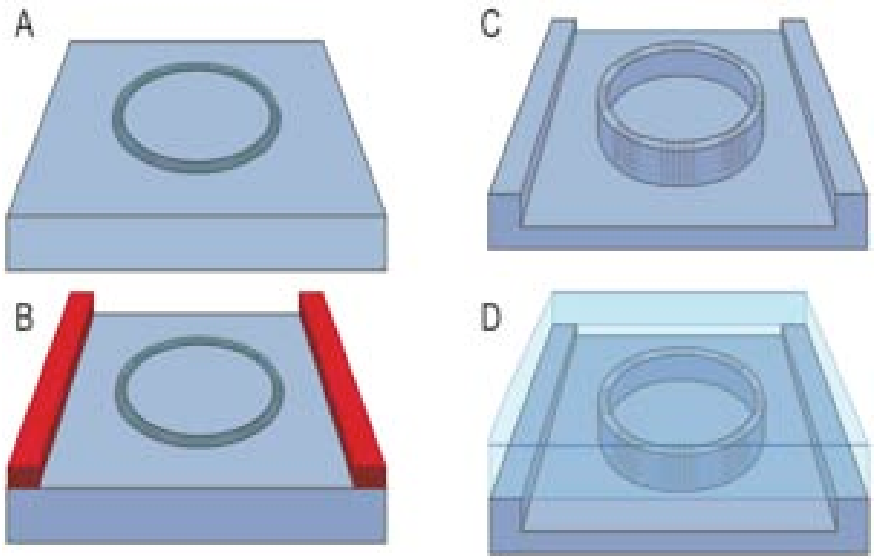

Figure 2-2: Fabrication steps of the cell mimic device. The fabrication of the silicon containment vessels is a top-down process that uses both electron beam and optical lithography. (a) Electron beam lithography is used to define the vessel geometry including the overall size, pore structure and appropriate alignment marks. (b) Contact lithography is used to define the larger microfluidic structures. (c) A single cryogenic silicon etching process is used to transfer the two dimensional pattern into silicon. Masking materials are then stripped and the device is coated with a thin PECVD oxide to add additional control to pore size. (d) A PDMS layer is added on top of the chip to enclose the system.

10:1 w/w ratio, degassed and cured for approximately 1 h at 70°C. Then, it was cut into 4 mm thick pieces matching the microfluidic chip size. Holes were made at the ends of the channel for the inputs and output of the network using an 18-gauge blunt tip needle and fitted with tygon tubing and appropriate gauge needle and syringe. The packaged chip measured approximately 4 cm long by 15 mm wide. The number and type of individual reaction vessels can be modified from one chip to the next. Each chip configuration consisted of two channels with 18 vessels in each of two channels, spaced at equal intervals along the channel. Each array of 18 devices can be imaged simultaneously in the viewing area of a Zeiss Axioscop epifluorescent microscope with a 10x objective.

2.2.3. Loading of nanoporous reaction vessels

Prior to sealing with PDMS, the chips were treated with a 1 mg/mL solution of bovine serum albumin for 60 min, to prevent nonspecific adsorption of reaction constituents to the device walls. An adapted cell microinjection system, which consists of a hydraulic manipulator with manual injection pump attached to a Burleigh micromanipulator was used to fill individual vessels. Pulled micropipettes with tip diameters of two microns (Small Parts Inc., Logansport, IN) were loaded with the desired reagent by backfilling them using a flexible polyimide needle (World Precision Instruments, Sarasota, FL). Chips were manually filled under a stereomicroscope by touching the filled pipette into the center of the reaction vessels. The amount of material injected in the device was dictated by the volume of the device structure and viscosity of the filling solution. For DNA containment experiments solutions contain 4% glycerol to reduce the risk of overfilling devices (Figure 2.3).

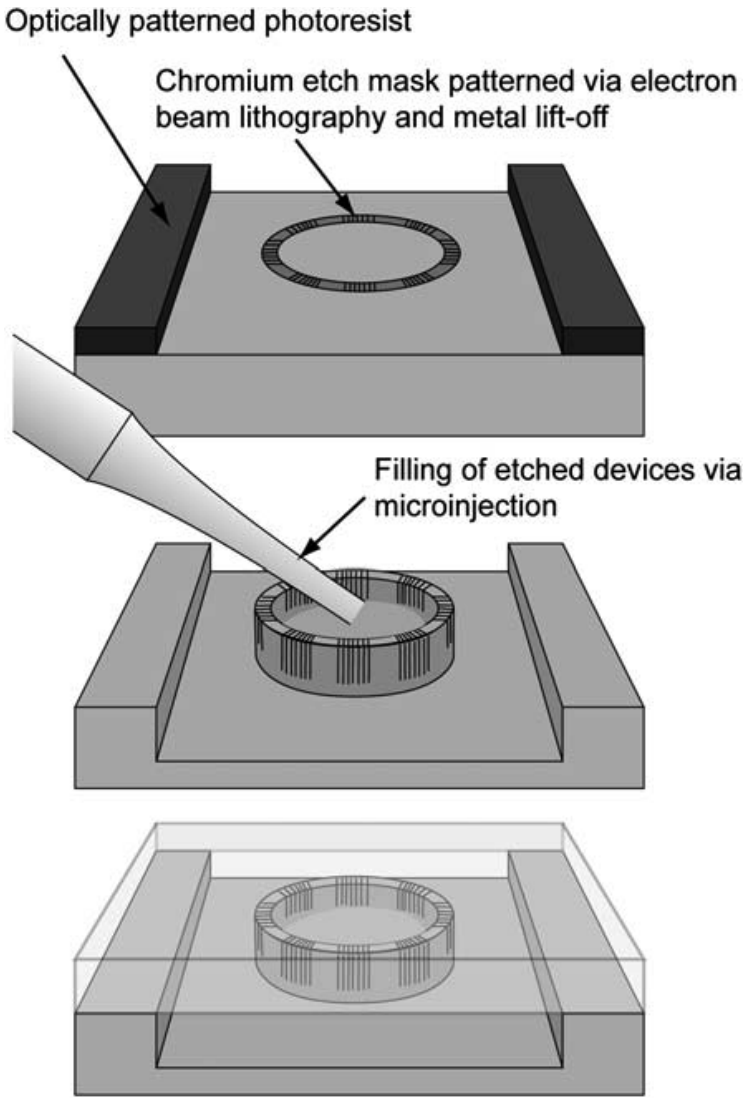

Figure 2-3: Nanoporous reaction devices are fabricated within microfluidic channels by combining electron beam lithography and metal lift-off techniques with contact photolithography to define the reaction vessel and channel geometries (top). The pattern is transferred into the exposed silicon using cryogenic silicon etching and individual vessels are filled with reactants via microinjection (middle). The entire chip is then sealed with PDMS (bottom) [159].

2.2.4. Bacterial growth and media

E. coli strains BL21 (DE3) (Invitrogen) were grown in Luria-Bertani (LB) medium, which was supplemented with 50 μg/ml ampicillin since the plasmid used has an ampicillin resistance gene. *E. coli* cultures were grown at 37°C unless otherwise noted. Plasmid DNA (5.4 kb) used in the DNA containment and labeling experiments was constructed by recombining a gene for enhanced GFP (EGFP) into pDEST17 (Invitrogen) to allow expression of 6 His-GFP from a T7 promoter. The plasmid pDEST17 was transformed and propagated in chemically competent BL21 (DE3) (Invitrogen) cells. Briefly, transformation was conducted as follows. The pDEST17 plasmid was thawed a room temperature and the BL21 (DE3) (Invitrogen) cells were thawed on ice. Then, 3 μl of plasmid was added to 100 μl of cells, which were then left on ice for 30 minutes. Afterwards, the cells were heat-shocked for 45 seconds at 42°C and put on ice for 2 minutes. The cells were then added to 400 μl of LB with ampicillin and placed at 37°C for 45 minutes under continuous shaking. About 200 μl was added in Petri dishes treated with ampicillin and were left to grow overnight. Colonies grown on these plates were later used to grow more cells for plasmid and protein purifications. Plasmid DNA was purified from the transformed Escherichia coli BL21 (DE3) cells (Invitrogen) using a Qiagen Plasmid Midiprep Purification kit (Valancia, CA) according to the manufacturer's instructions.

2.2.5. Protein purification and SDS-PAGE

Production of EGFP was carried out using the plasmid described above to transform E. coli BL21 (DE3) cells. IPTG was added to a final concentration of 1 mM to

induce expression of 6 His-GFP. The transformed cells were grown at 30°C overnight and 0.5 ml of the overnight culture was used to inoculate 100 ml of LB media. The culture was incubated at 37°C until it reached an OD_{600} of 1.0. Cells were centrifuged for 20 minutes at 5000 rpm and resuspended in 15 ml of BugBuster™ (Novagen) supplemented with 15 µl of 100 mg/ml lysozyme. Protein degradation was prevented by supplementing the samples with Halt™ protein inhibitor cocktail (Pierce Biotechnology, Rockford, IL) according to the manufacturer's instructions. The cell lysate was incubated at 4°C for 30 minutes and was sonicated (3 pulses, 30 second duration) with a Branson Digital Sonifier. The lysate was then centrifuged at 14,000 rpm for 30 minutes and the supernatant was applied directly to His-Select Nickel Affinity Gel column (Sigma, Saint Louis, MO). The column was then washed with 10 column volumes of wash buffer and eluted with 2 column volumes of wash buffer containing 500 mM imidazole.

Dialysis was conducted to change the buffer from elution buffer to TRIS buffer. The purified EGFP was added to an Amicon Ultra-15 filter column (Millipore) to exchange the elution buffer with 20 mM of TRIS buffer since the imidazole that is present in the elution buffer degrades the protein after a few days of storage in -80°C. After the extraction procedure, both the insoluble and soluble fractions were boiled in sodium dodecyl sulfate (SDS) sample buffer and 5 µl was loaded on a 12% TRIS-HCl polyacrylamide gel (Bio-Rad) to test purity. The gel was electrophoresed for 1 hour at 100V. The gel was stained with comassie blue stain overnight and destained with a methanol solution for 12 hours (Figure 2.4).

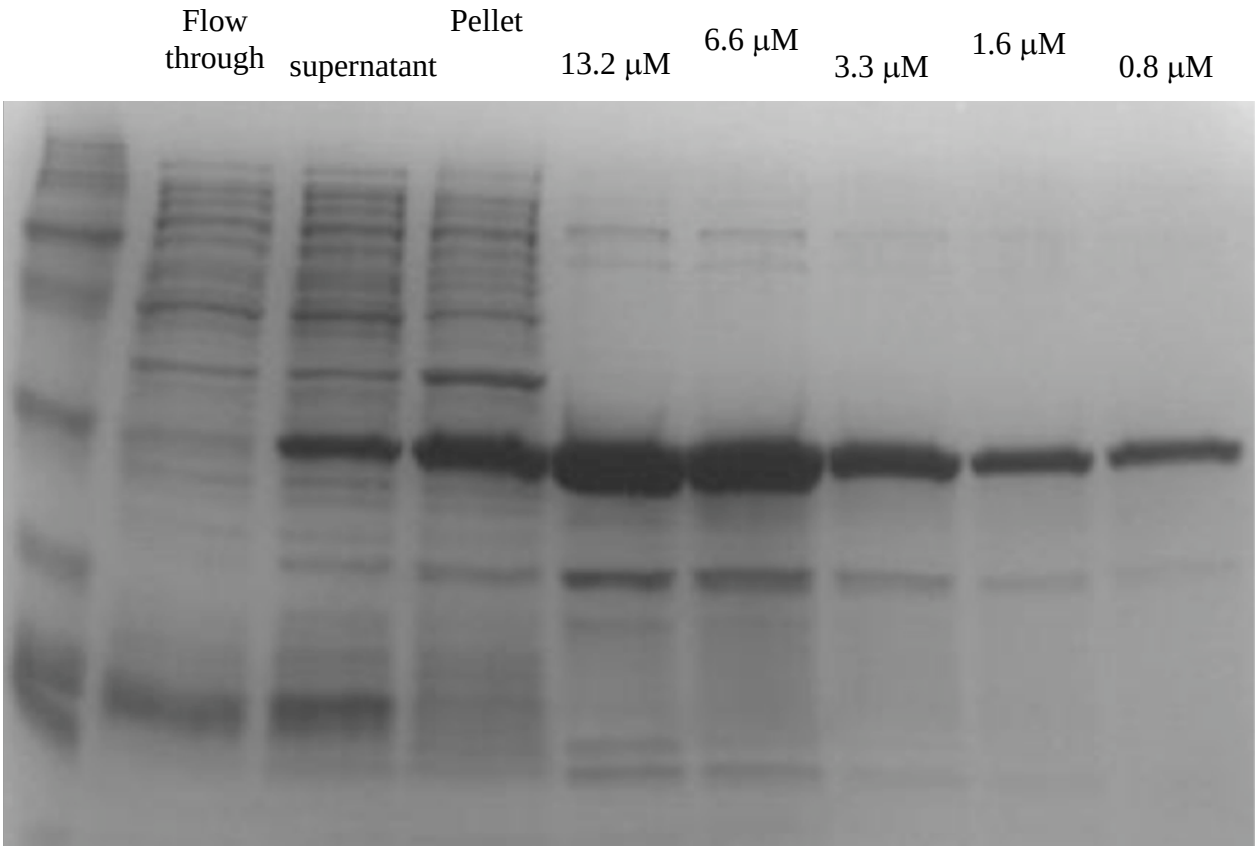

Figure 2-4: SDS-PAGE of different concentrations of purified EGFP

2.2.6. Fluorescence Recovery After Photobleaching (FRAP)

To evaluate the rate of transport of EGFP through the pores of the cell mimic device fluorescence recovery after photobleaching (FRAP) was conducted on devices that had undergone 4, 5, 6 and 7 minute duration of PECVD silicon dioxide deposition. The experiments were conducted by first filling the device and the microfluidic channel with 6.6 μM EGFP. The experiments were performed on a Leica TCS SP2 scanning confocal microscope equipped with a Leica HCX PL APO 63X oil immersion objective lens. Leica LCS software (version 1537) FRAP application was used to collect pre-bleach, bleach and post-bleach images. Bleaching was performed with a 40 μm diameter circular region-of-interest (ROI), which corresponds to the size of the cell mimic device. The bleach pulse was applied by setting the 488-nm line of a 25 mW argon-krypton laser to acousto-optic tunable filter (AOTF) of 100%. Fluorescence recovery was measured at an AOTF of 2-3% laser power. All the parameters of the FRAP experiments are briefly described as follows. 1) Select “GFP” reading. 2) Switch microscope control from visual to scan. 3) Set Pinhole to 250. 4) Set Beam expander to 3. 5) Set Format 256 x 256. 6) Set Mode xyt. 7) Set speed 1000 Hz. 8) Set laser bleach intensity to 100%. 9) Set pre-bleach images to 3. 10) Set bleach to 150 laser pulses and post-bleach to 200 laser pulses. 11) Set laser intensity for image to 3% of bleach.

2.2.7. Functional demonstration of size exclusion and molecular containment

To demonstrate the functional size range for exclusion using the 200 nm pore devices, microchannels were loaded with solutions of 100 nm and 350 nm Fluorsbrite latex beads at a flow rate of 10 μL/h. Care was taken to insure that air bubbles were not

trapped in the reaction vessels. Fluorsbrite 100 nm and 350 nm latex beads used in size exclusion experiments were obtained from Polysciences Inc. (Warrington, PA). Images were taken every 5 minutes for 1 hour.

DNA containment and labeling experiments were carried out by filling reaction vessels with DNA concentrations ranging from 30 to 240 ng/μL in buffer. A labeling solution consisting of ethidium bromide (EtBr) at a concentration of 100 μg/mL was injected into the microchannel. Images were captured before adding EtBr, immediately after adding EtBr, and after 30 min under flow at a flow rate of 10 μL/h. Ethidium bromide and other reagents were purchased from Sigma Aldrich.

2.2.8. Containment of fluorescein and EGFP

Flow experiments were conducted by first filling the reaction vessels with a 100 mg/mL solution of fluorescein and different EGFP concentrations. Under a steady flow of 10 μL/h ensembles of reaction vessels were imaged. A Retiga firewire camera and QCapture software were used to capture fluorescent and bright field images. Care was taken to ensure that exposure times, binning and other relevant camera settings were maintained to allow reasonable comparisons to be made between experiments. A shutter was used to minimize photobleaching when images were not being captured.

2.3. Results and discussion

2.3.1. Device fabrication

A combination of optical and electron beam lithography were used to achieve the desired device geometries and fabrication. Eight chips were completed per wafer using

batch fabrication. Multiple wafers could be produced due to the relative short electron beam lithography write time (~45 min per wafer). Completed cell mimic devices had an inner diameter of 40 microns, a 2 μm thick wall, and 56 pores (8 sets of 7 pores). Structures and channels were 15 μm tall, with heights measured using physical profilometry. The internal volume of the structures was approximately 19 picoliters. A diameter of 40 μm was chosen because of the relative ease with which the devices could be imaged and filled using microinjection (Figure 2.2 and 2.3).

2.3.2. Fluorescence Recovery After Photobleaching (FRAP)

Fluorescence Recovery After Photobleaching (FRAP) has been an important technique in determining diffusion of fluorescently labeled proteins across the cell membrane. With this technique, a high intensity pulse is used to photobleach an area of the cell and the movement of unbleached molecules from surrounding areas into the bleached area and vice versa is recorded by time-lapse microscopy. The idea behind this method is to measure the ability of a fluorescent molecule to move around over time. The diffusion coefficient (D) of the fluorescent protein is related to both its rate and extent of recovery (Figure 2.5a). FRAP has been widely used to help define the fluid mosaic model of cell membranes and to measure the lateral diffusion of various membrane or cytoplasmic constituents. It has also been used to determine if a protein is able to move within a membrane. Simulating a mathematical reaction-diffusion model and deriving the diffusion coefficient and binding or dissociation constants by parameter estimation, is the best approach towards a quantitative interpretation of FRAP data [160, 161].

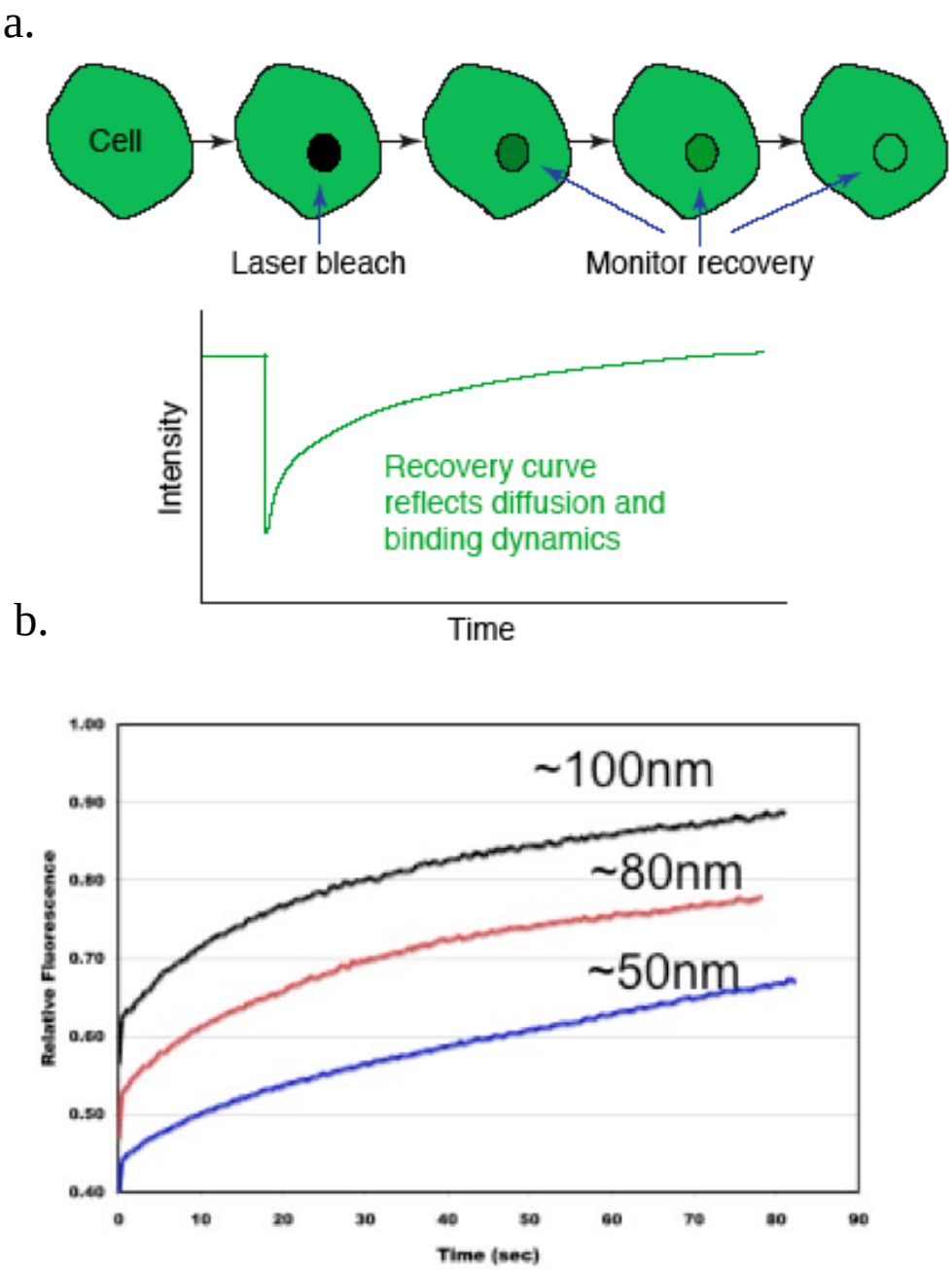

Figure 2-5: Fluorescence Recovery After Photobleaching. (a) Presentation of data collected during a FRAP experiment. Fluorescence is collected before and after photobleaching occurs. Over time, the unbleached molecules diffuse into the photobleached area and the amount of fluorescence increases [161]. (b) Fluorescent recovery of reaction vessels with different nominal pore sizes.

Here, FRAP has been adapted to measure the rate of EGFP fluorescence recovery over time within the reaction device. This provides a measurement of diffusion of eGFP through the pores of cell mimic devices that have undergone 4, 5, 6 and 7 minute duration of PECVD silicon dioxide depositions. Fluorescence recovery occurred in all the devices (Figure 2.5b). In order to fit the recovery data with a mathematical diffusion model, a Matlab (The Math Works, Natick, MA) code is being written by a staff scientist at ORNL and it is still an ongoing process.

2.3.3. Functional demonstration of size exclusion and molecular containment

In separate experiments, 100 and 350 nm beads were injected into microfluidic channels containing cell mimic devices with 200 nm pores. 100 nm beads easily entered the vessels while 350 nm beads were excluded. Figure 2.6 demonstrates that vessels have a functional pore size, and size distribution between 100 nm and 350 nm.

In DNA labeling experiments 240 ng/μL, 120 ng/μL, 60 ng/μL and 30 ng/μL of 5.4 kb plasmid DNA were loaded in reaction vessels using a microinjection system. DNA containment experiments were carried out in reaction vessels with a 200 nm pore and minimal silicon oxide coating. The cell mimic device was successful in containing the DNA while allowing small molecules to cross the reactor membrane and intercalate the DNA. A fluorescent response proportional to DNA concentration (Figure 2.7) was apparent in images taken 30 min after ethidium bromide was introduced through the microfluidic channel. A limited degradation of the fluorescent signal was observed over time indicating that the DNA was contained within the reaction vessels over extended periods.

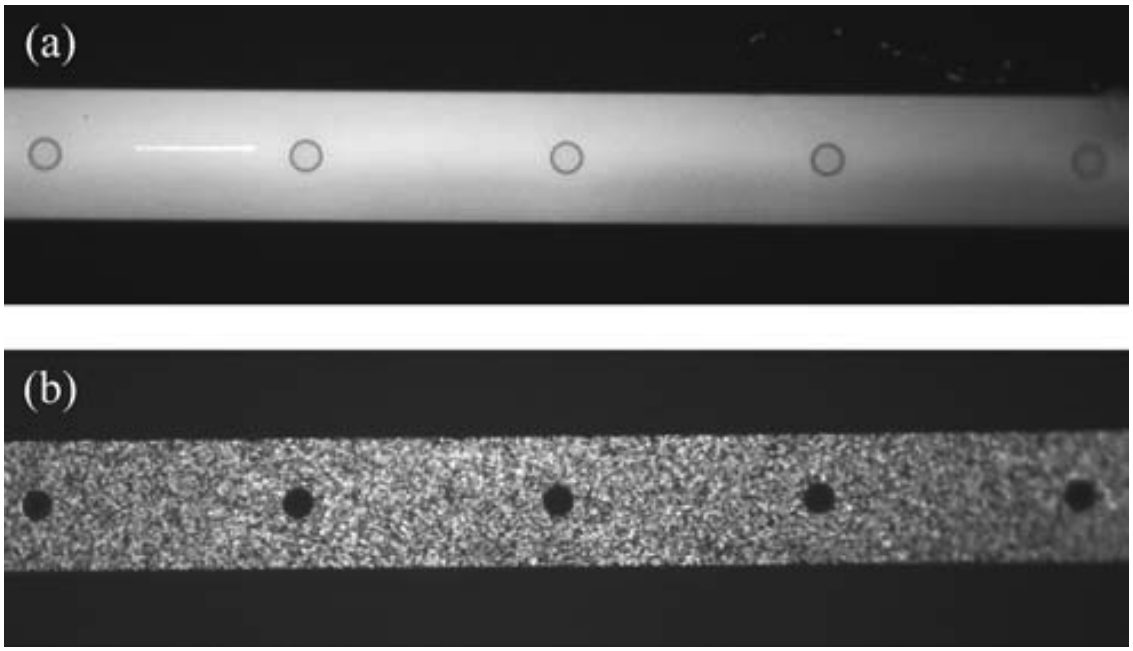

Figure 2-6: Fluorescent polystyrene beads were introduced into microchannels at modest flow rates. (a) 100 nm diameter beads diffused through the reaction vessel membrane as expected, while larger (b) 350 nm beads were excluded.

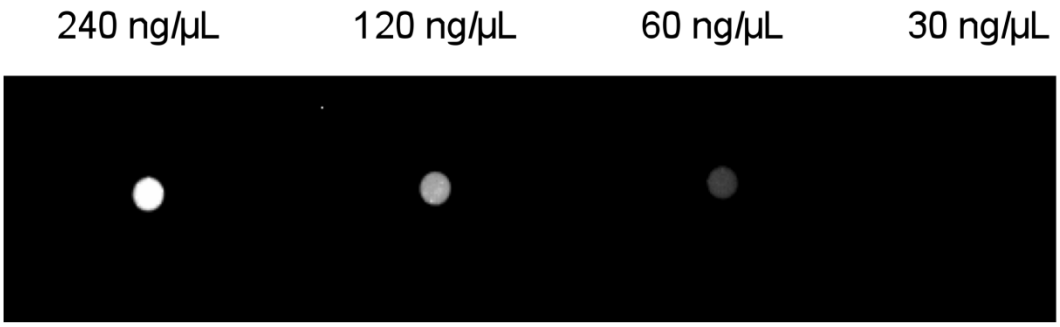

Figure 2-7: Plasmid DNA was loaded into reaction vessels with a minimal silicon dioxide coating at different concentrations (240 ng/µL – 30ng/µL) corresponding to the total mass shown. Plasmid DNA was labeled in situ with ethidium bromide. Fluorescence was evident immediately and did not diminish, indicating that plasmid DNA is retained, and small molecules are able to traverse the membrane and react with the plasmid.

A 5.4 kb plasmid has a computationally and experimentally predicted radius of gyration between 80 and 240 nm [162, 163]. This suggests an overall diameter that fluctuates near the value that is the width of the pore (200 nm). The absence of fluorescent material outside of the vessels and the persistence of fluorescence from the labeled DNA after 60 min indicate that the plasmid is not able to freely diffuse through the reaction vessel membrane. Ultimately, to control the transport of specific proteins or small molecules across and between reaction vessels, the pore size and surface charge or functionality would need to be tuned further. Therefore, we examined the use of plasma enhanced chemical vapor deposition to reduce pore size (width) and limit the flux of molecules such as fluorescein and EGFP across the vessel membranes. Individual chips containing devices were subjected to different durations PECVD silicon dioxide depositions. Plasma enhanced chemical vapor deposition can further change the width of the pores by depositing thin films of silicon dioxide from the gas state into the solid state on the device. The longer the device undergoes this procedure, the greater the oxide is deposited and the smaller the width of the pores becomes. Since there is a considerable reduction in pore size as more silicon dioxide is deposited on the reaction vessels (Figure 2.8), it would be difficult to directly measure the effective gap size through the entire thickness of the membrane using imaging techniques. Therefore, the effect of silicon dioxide deposition on pore size can be indirectly assessed by measuring the retention of GFP (~30 kDa) and fluorescein (~300 Da). A comparison of retention of different size proteins such as GFP and fluorescein within devices that have different amounts of silicon dioxide depositions was carried out. Individual device chips were subjected to 4,

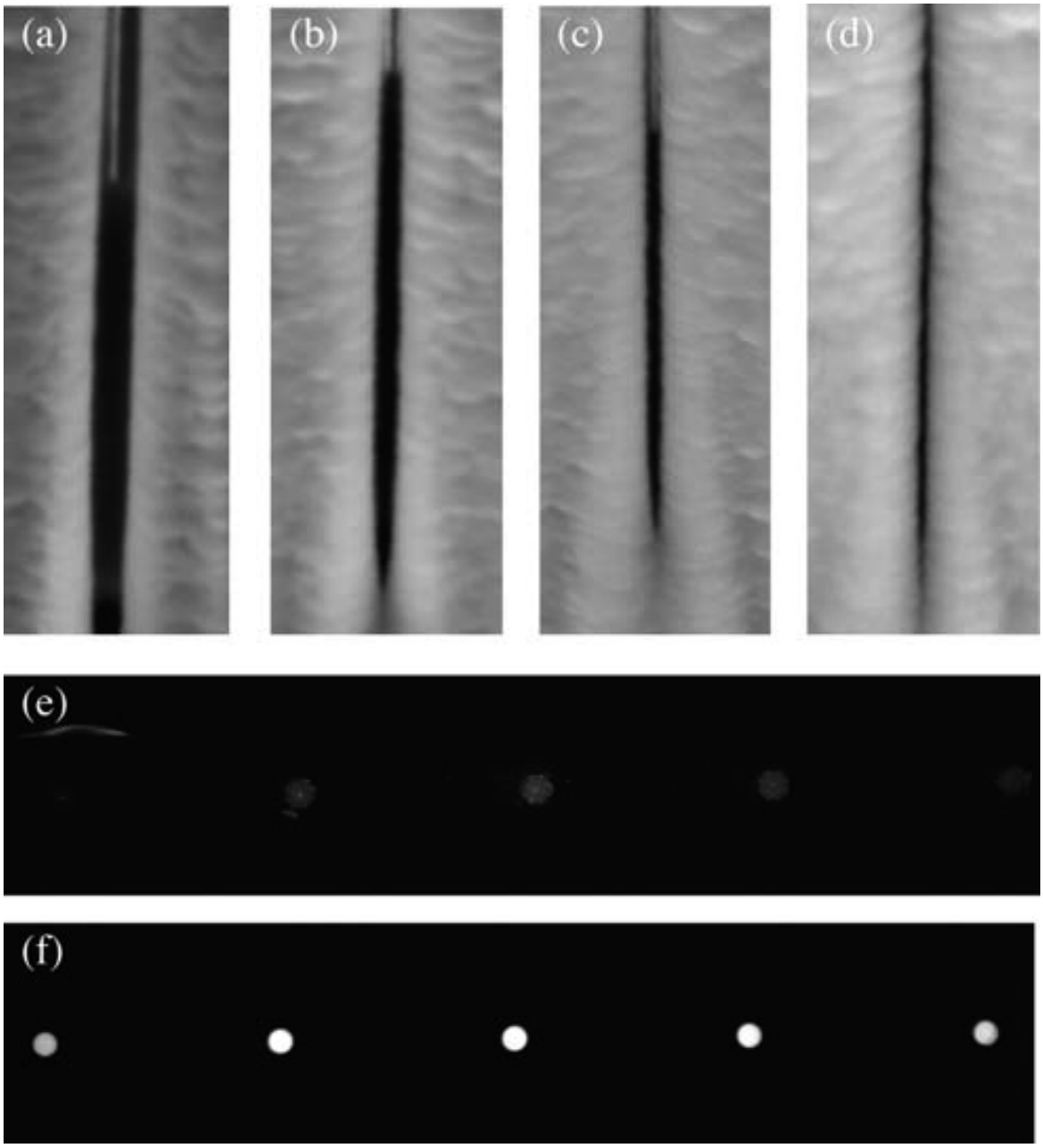

Figure 2-8: The deposition of silicon dioxide on membrane structures can be used to reduce pore width. Pores are shown after (a) 2, (b) 4, (c) 6, and (d) 8 min of PECVD silicon dioxide deposition. The retention of green fluorescent protein was observed after 5 min in reaction vessels coated with silicon dioxide for (e) 4 min (100 ms digital camera exposure) and (f) 6 min (50 ms digital camera exposure). Each of the devices shown was filled with the same concentration of EGFP.

5, 6, and 7 minute duration of PECVD silicon dioxide depositions. The fluorescein and EGFP diffusion experiments (Figure 2.9) showed a quick diffusion of both molecules out of devices that have 4 and 5 minute duration of PECVD silicon dioxide depositions. Devices with 6 and 7 minute PECVD retained GFP and fluorescein much longer.

Based on Fick's law, a Lumped Capacitance Model for predicting transient changes in concentration within a nanoporous reaction vessel under moderate external flow was prepared and used to fit the fluorescein and eGFP diffusion data (Figure 2.10). This module was used to determine the effective gap size of devices that were subjected to 4, 5, 6, and 7 minute duration of PECVD silicon dioxide deposition. The following assumptions were made for this model: a) External concentration of the species diffusing from the device is effectively zero since the channel is under a continuous flow. b) The solution inside the cell mimic device is well mixed and c) The change in concentration across the nanoporous membrane of width Δx is assumed to be linear.

Using Fick's law, the rate of mass (m) loss from the reaction vessel can be expressed as follows:

$$\frac{dm}{dt} = -DnM_w A_{pore} \frac{dC}{dx}$$

D is the diffusivity of the species of interest (fluorescein or EGFP), n is the number of pores, M_w is molecular weight, A_{pore} is the cross sectional area of a single pore and is the product of the pore height and width ($h_p w_p$), C is concentration and x is the thickness of the membrane. Discretizing this expression based on the assumptions enumerated above

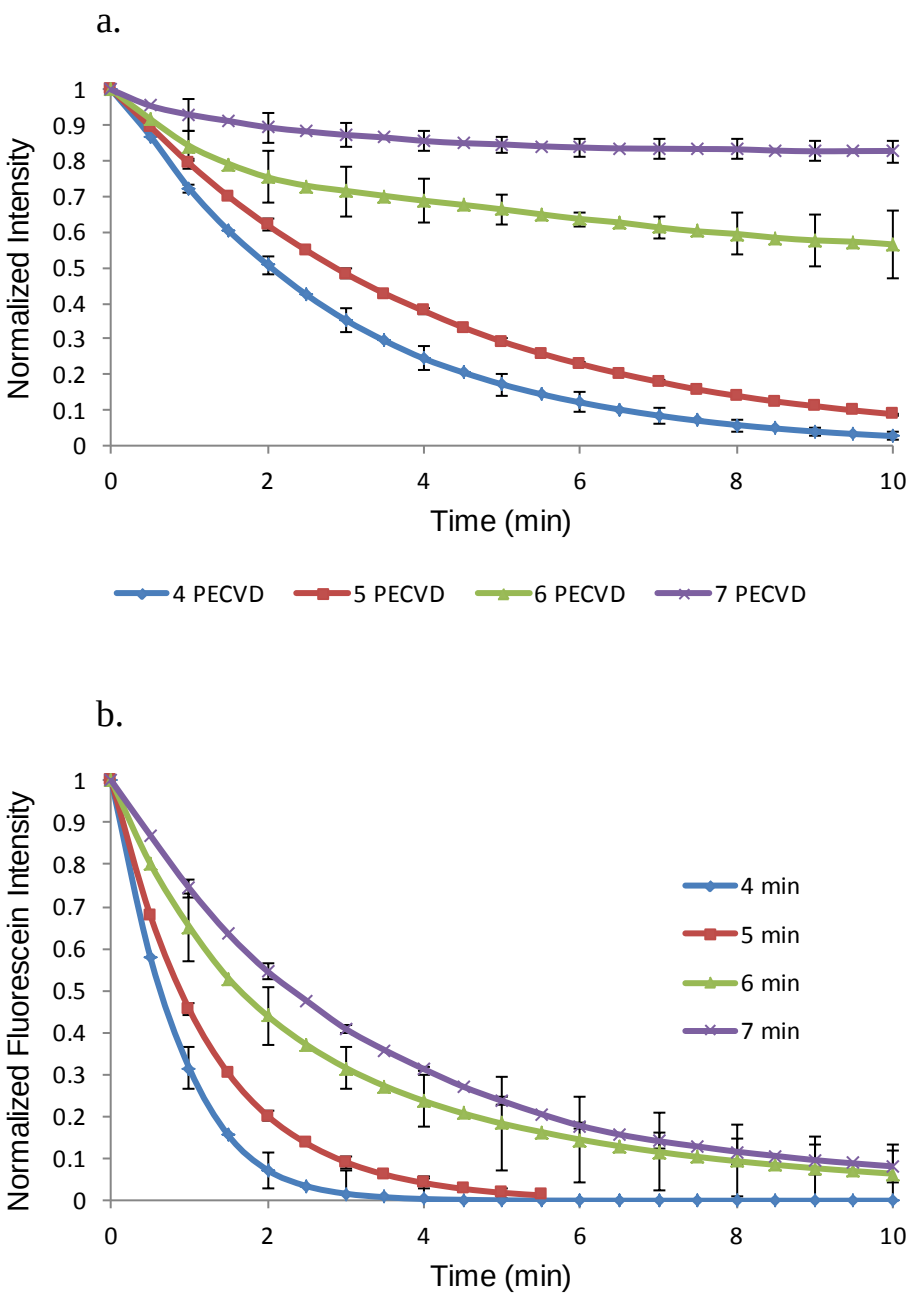

Figure 2-9: Diffusion of EGFP and fluorescein on cell mimic devices that have undergone 4, 5, 6 and 7 minute PECVD. (a) Diffusion of GFP. (b) Diffusion of fluorescein. The graphs represent the average intensity recorded from 3 individual reaction containers during 3 separate diffusion experiments. Error bars representing +/- one standard deviation are shown at 1 minute intervals for clarity.

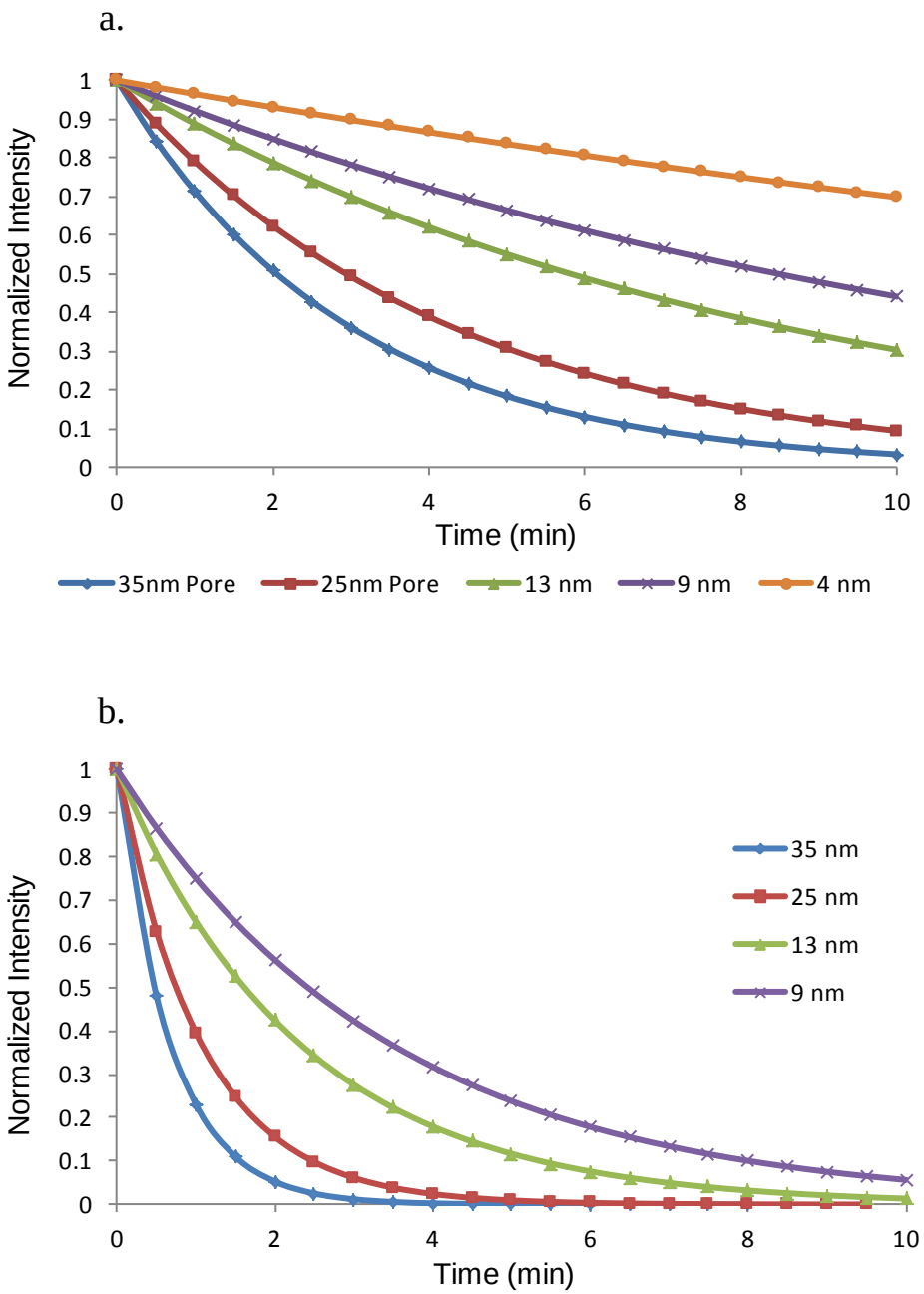

Figure 2-10: Lumped Capacitance Diffusion model (a) EGFP and (b) fluorescein for predicting transient changes in concentration within the cell mimic device with different pore widths of 35, 25, 13 and 9 nm under moderate external flow.

for a short time increment *Dt*, the change in concentration can be expressed as:

$$\Delta C = \frac{-Dnh_p w_p}{V\Delta x}(C_{in} - C_{out})\Delta t$$

where *V* is the total volume of the reaction vessel. Using the above equation and noting that the concentration outside of the vessel is assumed zero, the following expression can be written for the concentration within the vessel at *t+Dt*.

$$C_{in}^{t+\Delta t} = C_{in}^{t} - \frac{Dnh_p w_p}{V\Delta x} C_{in}^{t}\Delta t$$

or

$$C_{in}^{t+\Delta t} = C_{in}^{t}\left(1 - \frac{Dnh_p w_p \Delta t}{V\Delta x}\right)$$

Therefore the concentration within the vessel for an arbitrary time t+kDt can be given as:

$$C_{in}^{t+k\Delta t} = C_{in}^{t}\left(1 - \frac{Dnh_p w_p \Delta t}{V\Delta x}\right)^{k}$$

This final equation was used to calculate the predicted normalized concentration within porous reaction vessels for a desired period of time. The cell mimic dimensions were 15µm high, 40µm diameter, 2µm membrane thickness, and literature based diffusion coefficients for fluorescein and EGFP were $1.6 * 10^{-10}$ m^2/s and $1.0 * 10^{-11}$ m^2/s respectively [164, 165]. The 56 slit-shaped pores were estimated to be 10µm deep. Graphs of concentration over time were calculated using a time step of 10 seconds and different pore size widths for expected diffusivities for fluorescein and EGFP [159]. Comparing the experimental diffusion data of EGFP and fluorescein on devices that were

subjected to 4, 5, 6, and 7 minute duration of PECVD silicon dioxide depositions, with the diffusion model based on different pore size widths, we determine that 4 minute PECVD corresponds to ~35 nm pore width, 5 minute PECVD corresponds to ~25 nm pore width, 6 minute PECVD corresponds to ~13-15 nm pore width and 7 minute PECVD corresponds to ~5-10 nm pore width (Figure 2.11). EGFP has a cylindrical shape with axis lengths of 2.4 and 4.2 nm; therefore a 7 minute PECVD device with a calculated pore width of ~5-10 nm should predominantly retain the protein when compared to shorter durations of PECVD. However, the comparable size of the 7 minute PECVD pore and eGFP may also lead to clogging of the pores as time progresses.

2.4. Conclusions

The results presented in this chapter show that nanoporous, cellular-scale reactors can be created and modified using multi-scale fabrication techniques such as electron beam and contact lithography, cryogenic etching and plasma enhanced chemical vapor deposition. Size modification of the device pores can allow for the retention of larger species that represent information or functionality within a reaction system while allowing smaller materials to freely pass through the porous membrane. Such reaction vessels may prove useful in fundamental studies of protein-based complex reaction systems and will enable the development of responsive sensors and therapeutic platforms that rely upon the on-demand conversion or production of biological materials. The concepts of controlled flux and scaled transport presented in this aim can drive the design of synthetic reaction vessels, which will then lead to more complex systems and networks such as single and coupled enzyme reactions and cell-free transcription/translation.

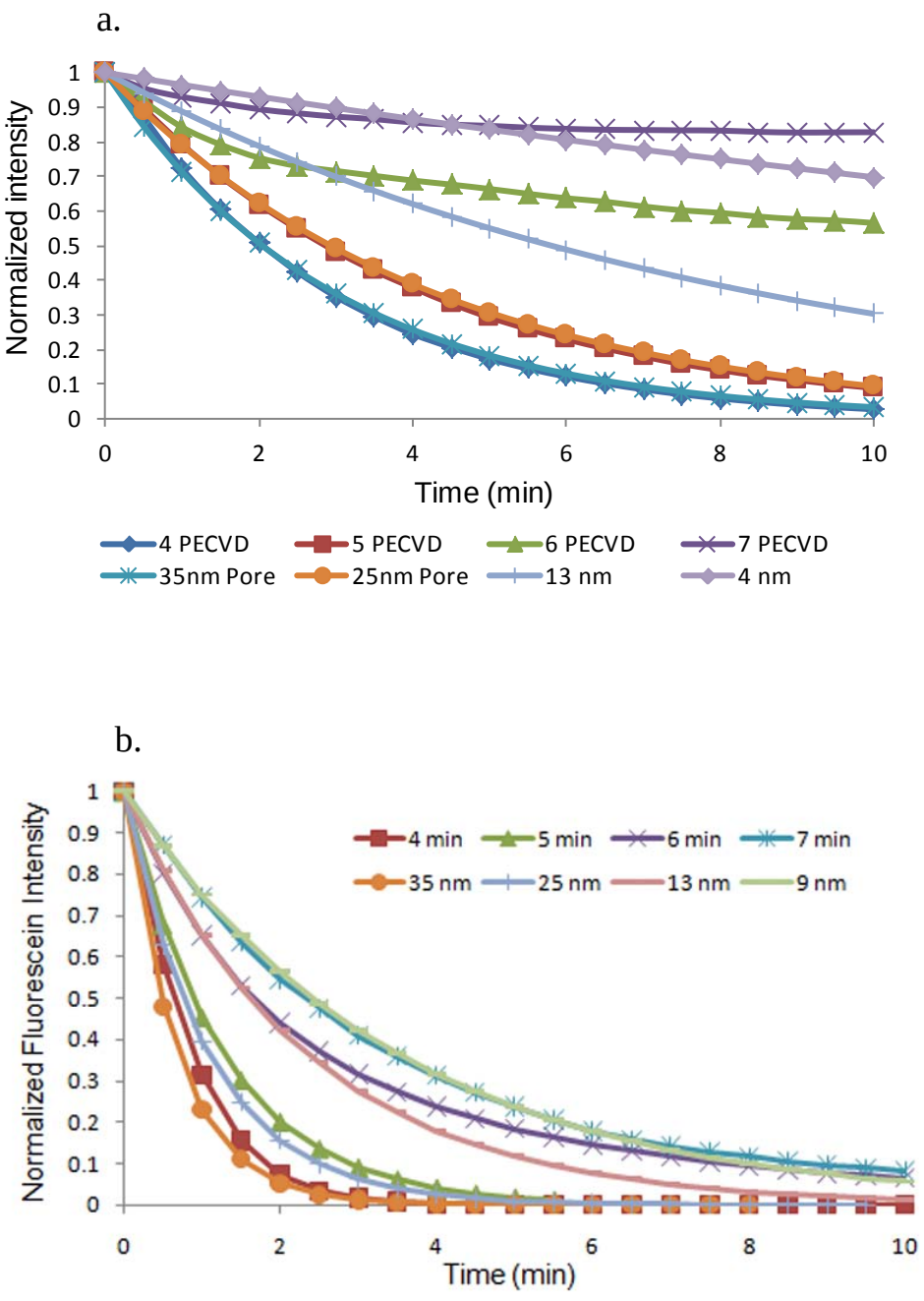

Figure 2-11: Experimental diffusion data vs. the diffusion model. a) Normalized EGFP diffusion data for devices that have undergone 4, 5, 6 and 7 minute PECVD vs. the diffusion model for pore widths of 35, 25, 13 and 4 nm. b) Normalized fluorescein diffusion data for devices that have undergone 4, 5, 6 and 7 minute PECVD vs. the diffusion model for pore widths of 35, 25, 13 and 9 nm.

Chapter 3
Enzymatic reactions in nanoporous, picoliter volume containers

This chapter is based on a manuscript about to be submited to *Analytical Chemistry*, Siuti, P.; Retterer, S.T.; Chang Kyoung Choi and Doktycz, M.J., "Enzymatic reactions in nanoporous, picoliter volume containers,"

Data, images, and text relevant to this study are included in this chapter. Images are presented in color where they were published in black and white. Under the direction of the co-authors, I conducted the experiments, analyzed the resulting data, and drafted the manuscript. The co-authors responded with editorial comments and additional text where needed.

3.1. Introduction

Enzymes are responsible for catalyzing and increasing the reaction rates of almost all chemical reactions that occur inside and outside a cell, which makes them important for understanding biological interactions at the molecular level [166]. They have and continue to play a key role in biological sensing and information processing. Our understanding of enzymes has improved rapidly in the past decades, and extensive studies have been done to explain rate enhancements by enzyme catalysis[167]. In combination with structure determination and genetic engineering, many new approaches and biochemical methods have also been developed. They have provided more details about enzyme reaction mechanisms such as charge stabilization and turnover rates [168, 169]. However, there is still more to discover about enzymes mode of action, structural interactions, analytical capacity and sensitivity. A main challenge for reaching this goal is that biocatalyst optimization and analysis is limited by the impracticalities of conventional enzyme screening techniques due to sample consumption, inability to

remove inhibitory byproducts and the number of experiments that need to be performed[170]. Therefore, different approaches that allow for faster screening of enzyme reactions, small sample consumption and mimic the natural small volume and crowded conditions of biological cell compartments are necessary.

Advances of micro and nanotechnology have enabled engineering of systems at the scale of biological cells [171], which has led to a rapid growth in the field of micro-total analysis systems (μ-TAS) and enzyme microreactor engineering[172]. Recently, several small volume reaction containers have been created in different materials, shapes and pore sizes such as liposomes [173-176], water in oil (w/o) emulsions[5], nanoliter wells defined in polydimethylsiloxane (PDMS) [177, 178], and hydrogel-based microreactors [179]. These small volume devices can relieve the need of structures for mixing, decrease the number of molecules required for carrying out a reaction, decrease analysis time and rapid heat exchange when compared to traditional analytical systems [124]. They can also be modified to control the flux of different size molecules and facilitate kinetic studies, help in analysis of the affinity and action of enzymes toward new drug candidates, and offer the potential to screen hundreds of combinations of enzyme and substrates in a parallel way [125-128].

Most of the efforts for designing microdevices for biosensing and studying enzyme kinetics have focused on miniaturizing batch mode reactors or microreactors that operate in a continuous mode by immobilizing enzymes on a solid support [128]. Miniature batch mode reactors have been used in a variety of approaches. Mao et al developed a technique for creating multiple batch microreactors in micrometer-size glass capillaries or in microfabricated channels. They used the batch microreactors to study

enzyme kinetics under different values of temperature and/or pH [180]. Jung et al developed polydimethyl siloxane (PDMS) femtoliter-scale chambers for studying single-molecule enzyme kinetics and sensitivity [181]. However, miniaturized batch reactors have drawbacks such as their inability to remove inhibitory byproducts and the “dead time”, which is the time it takes the reactant to mix before kinetic data are collected [128]. Microreactors that operate in a continuous mode have addressed most of the shortcomings of the batch reactors by removing inhibitory byproduct build up, reactor dead time and reducing material consumption. The initial practice of such small volume containers and microfluidic systems for analyzing enzyme kinetics was based on the transportation of reagents and samples through a system of micrometer dimension channels with electrokinetic flow for controlling dilution and mixing. This approach has demonstrated a 4-fold reduction in enzyme and substrate consumption over conventional methods [182]. Burke et al conducted a stopped-flow enzyme assay using a microfabricated mixer, which consumed 6 nL enzyme and was completed in 60 s [183]. Later, other approaches have been developed such as centrifugal microfluidic system which could carry out enzymatic assays through colorimetric detection [184], and the usage of immobilized enzymes within or on microchannels for a continuous and stopped-flow analysis of enzyme kinetics [124, 128, 185-188]. These approaches have allowed for automation of enzymatic assays and for reduction of time and reagent consumption. However, there are still drawbacks for microreactors operating under continuous flow. Such drawbacks include better control of the flux of different size molecules and recovery of the enzyme requires extra steps for separation of unreacted substrate and product from the enzyme solution [128]. Immobilizing enzymes onto solid surfaces can

also be a drawback since it can damage the structure of the enzyme, thus leading to potential alteration of the intrinsic kinetic rates or loss of activity [124]. Many of these shortcomings can be addressed by designing devices with pores small enough to contain the enzymes inside and remove the inhibitory byproducts, while operating in a continuous mode. Such a device is capable of communicating and exchanging chemical information with its surroundings.

Reported here is a nanoporous, picoliter reaction container within a microfluidic channel (Figure 3.1), which operates under a continuous flow system and has been used as a new strategy for the microscale analysis of enzyme kinetics. Individual properties of the device such as volume (19 pL) and pore size (~10 nm) can be controlled and allow for a defined flux of reagents, better diffusional mixing, and for enzymes to be trapped inside the device in their native form. The device has been used to conduct single and coupled enzyme reactions of horseradish peroxidase (HRP) and glucose oxidase (GOX) with amplex red substrate to monitor different glucose concentrations under a continuous flow system. Real-time monitoring of glucose and hydrogen peroxide catalysis within single and array reaction devices was performed and showed better sensitivity than macroscale methods. The picoliter container presented here has great potential to be used as a plaform for designing and fabricating biosensors. It can also be used for many analytical applications such as studying biochemical reactions and the effects of scale on reaction efficiency, screening of substrates, and a continuous-flow analysis of enzymes and their kinetic characteristics.

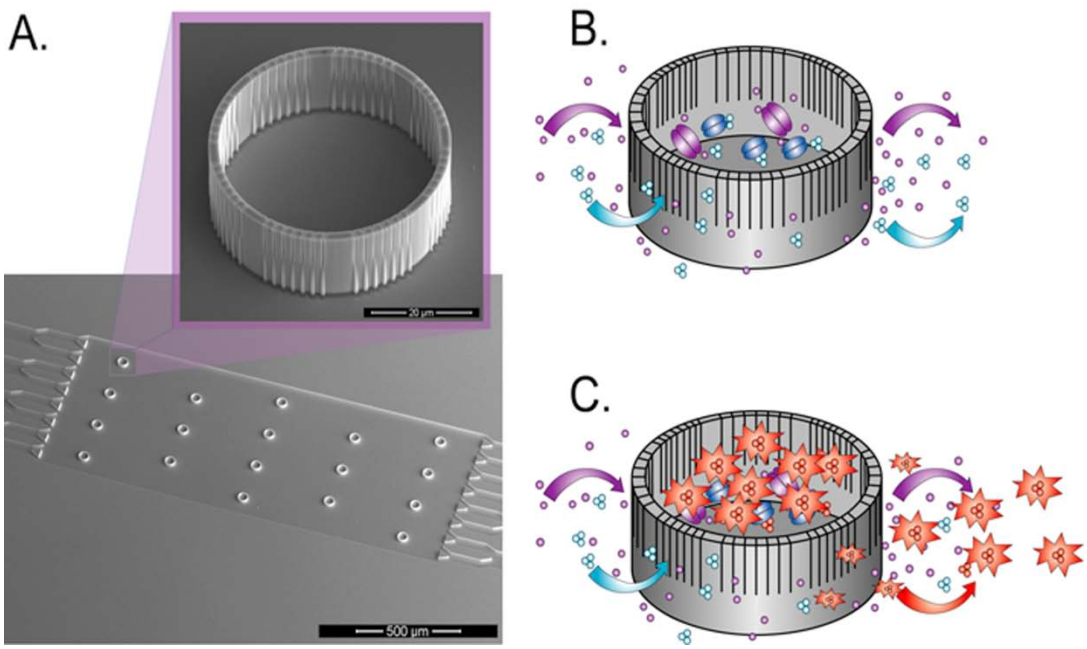

Figure 3-1: A nanoporous, picoliter volume platform for enzyme reactions. (a) SEM micrograph of a microfluidic device with an array of 18 reaction containers. The inset SEM micrograph shows a single reaction container. The slits have a limiting aperture of 10 nm. (b) Schematic of a nanostructured reaction container where glucose oxidase, along with horseradish peroxidase, is loaded into the device using a micromanipulator. (c) Schematic of a nanostructured reaction container is shown in operation. The microfluidic channel and device are sealed with PDMS. The channel is used to continuously deliver glucose and amplex red and remove resorufin and inhibitory biproducts from the reaction chamber to facilitate coupled enzyme reactions.

3.2. Materials and Methods

3.2.1. Microfluidic device

The small volume reaction devices were fabricated as previously described in chapter 2 and in Retterer et al [159]. The resulting silicon wafer contains eight identical chips. Each chip is 4 cm long and consists of 2 channels, each with an array of 18 reaction containers (Figure 3.1). The cylindrical container is 2 μm thick with 8 sets of 7 slits. Slits range in size from 5-200 nm wide and 10 μm deep [63, 159]. For all experiments described here, the container has a volume of ~19 pL.

3.2.2. Single Enzyme Reaction

Amplex Red Hydrogen Peroxide/Peroxidase Assay Kit (Invitrogen A22188) was used for enzyme reaction experiments according to manufacturer's directions. Prior to the experiments, the inner walls of the reaction device were treated with 1 mg/mL Bovine Serum Albumin (BSA) in PBS for 60 min to prevent nonspecific absorption of reagents to the surface of the device.

The solution containing 5 μM hydrogen peroxide (H_2O_2) and several horseradish peroxidase (HRP) concentrations of 0.0125u/ml, 0.025u/ml, 0.5u/ml and 1u/ml was mixed in a 1:1 ratio with 20 % glycerol and loaded into a glass micropipette with tip diameter of 2 μm (World Precision Instruments, TIP2TW1), using a flexible polyimide needle (World Precision Instruments). The cell mimic device was filled by touching the tip of the glass micropipette into the center of the device and the amount of solution injected depended on the viscosity of the solution. Several mimics were filled with only 0.0125u/ml, 0.025u/ml, 0.5u/ml and 1u/ml HRP and were used as negative controls. After

the small volume containers were loaded, the chip was covered with a 5 mm thick layer of polydimethyl siloxane (PDMS), which was used to seal the device.

Sylgard 184 silicone elastomer kit (Fischer Scientific) was used to prepare PDMS. Sylgard 184 silicon base and the curing agent were mixed in a Petri dish at a 10:1 w/w ratio, respectively. The mixture was degassed for ~30 min and cured in the oven at 70°C for 60- 90 minutes. After baking, PDMS was cut into pieces covering the chip and two holes were punched on each end of the channel using an 18 gauge blunt tip needle. Polyethylene tubes were fit into the holes to allow for the input and output of solutions in and out of the channel. The channel was then filled with working solution and kept at a constant flow of 1µL/hr, 5µL/hr and 10µL/hr. The working solution consists of 100 µM Amplex Red, 0.05 M sodium phosphate pH 7.4 and 10% glycerol. The experiments were conducted at room temperature and repeated a minimum of three times.

A resorufin standard was prepared by diluting different concentrations of 1, 2, 3, 4, 5, 6 and 7 µM resorufin (Figure 3.2). Each of the eGFP solutions contained 10 % glycerol concentration. These solutions were loaded in devices and fluorescence was measured using identical settings as for single and coupled enzyme reactions. Resorufin concentration produced in the single and coupled enzyme reactions conducted in the cell mimic devices was measured against this resorufin standard.

3.2.3. Coupled Enzyme Reaction

Amplex Red Glucose/Glucose Oxidase Assay Kit (Invitrogen A22189) was used for coupled enzyme reaction experiments according to manufacturer's directions.

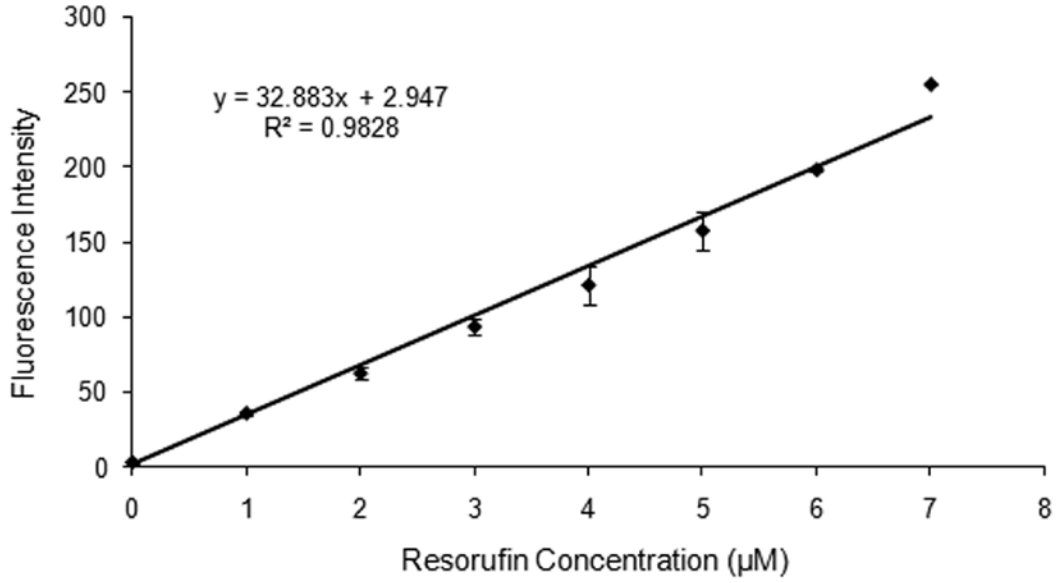

Figure 3-2: Resorufin standard curve. A standard curve showing the fluorescent intensity according to the resorufin concentration in the device. Error bars are ±1 SD.

A similar procedure was also followed for coupled enzyme reactions. Bovine Serum Albumin was used to treat the chip for ~10 min prior to the experiment for preventing nonspecific absorption of reagents to the device. In this case the solution containing 0.5 u/mL glucose oxidase (GOX) and 0.5 u/mL horseradish peroxidase (HRP) was mixed in a 1:1 ratio with 20 % glycerol which led to a final concentration of 0.25 u/ml GOX and HRP and 10% glycerol. The solution was then loaded into the device using a 2 µL glass microtip (World Precision Instruments, TIP2TW1). Several devices were filled with only 0.25 u/mL HRP or GOX and used as negative controls. The chip was then covered with PDMS and the channel was filled with working solution at a constant flow rate of 10µL/hr. The working solution consists of 100 µM Amplex Red, 1x buffer, 10% glycerol and 0.01, 0.1, 1, 5, 10 and 100 µM glucose.

The coupled enzyme reactions were conducted on devices that had undergone different plasma enhanced chemical vapor deposition (PECVD) times of 2, 4, 6, 7 and 9 min, which affects the size of the slits of the device. Several GOX and HRP enzyme concentrations of 0.0125u/ml, 0.025u/ml, 0.5u/ml and 1u/ml were tried in order to optimize the enzyme ratio.

The experiments were also conducted with different substrate concentrations of 10 µM, 100 µM, 1mM, 5 mM, 10mM and 100mM. Devices that had undergone 7 min PECVD were chosen to continue the rest of the experiments. They were loaded with a final 0.25 u/mL GOX, 0.25 u/mL HRP and 10% glycerol. The channel was then filled with working solution, which consisted of the various glucose concentrations, 100 µM Amplex Red, 0.05 M sodium phosphate pH 7.4 and 10% glycerol. Each experiment was repeated in triplicates for statistical purposes.

In order to compare coupled enzyme reactions in the device with conventional scale, coupled enzyme reactions were also conducted in a Costar 96 flat bottom well plate. The enzyme and substrate concentrations were kept the same as in the device reactions and the final reaction volume in the plate well was 100 μL. To ensure proper mixing of the reagents, the plate was shaken before each reading by the plate reader. Fluorescence was measured every 10 seconds using a Perkin Elmer HTS 7000 Plus BioAssay Reader. Each experiment was repeated in triplicates for statistical purposes.

3.2.4. Imaging and data analysis

Immediately after the channel was filled with working solution, fluorescence was monitored by measuring the intensity from time lapse images taken every 10 seconds with binning 1x1 and exposure time of 256ms. A Zeiss Axioskop 2 FS Plus epifluorescent microscope equipped with a Retiga firewire camera and a 40x dry objective (Zeiss) was used to obtain the images. A 200 W mercury arc lamp was used as light source for excitation. The Retiga firewire camera was synchronized with a Lambda SC smart shutter (Sutter, CA) and the proper filter sets were used to minimize photobleaching of resorufin during the experiments. The images were acquired as 16-bit grayscale TIFFs using acquisition software IPLab 4.0.8 (Scanalytics,Inc.). Camera settings, exposure times and binning were kept the same for all the experiments in order to allow comparisons between experiments. Image intensity values for each of the devices were calculated and plotted using MATLAB (V7.2, MathWorks).

3.3 Results and Discussion

Understanding the countless interactions carried out by enzymes and their influence in a variety of fields such as biosensors, drug discovery, medical diagnostics and organic synthesis has been an immense challenge. Addressing this challenge requires methods with high-throughput capacity, which can be used for fast screening and identification of biocatalysts, inhibitors and drug targets. Microfluidic enzyme reactors have been emerging as a valuable tool by reducing the scale of reactions and as fast analytical procedures. Microfluidic technology is especially well suited for small-scale analysis since it can be integrated with optical sensing methods and has the potential to be introduced into industrial-scale synthesis. The nanoporous, container described here enables single and coupled enzyme reactions in picoliter volumes while enabling substrate exchange and inhibitory byproduct removal.

3.3.1. Single Enzyme Reactions

To test the ability of the picoliter volume reactor to carry out enzyme reactions, effective experimental conditions for filling the devices and carrying out the reactions were first determined. Several difficulties such as overflowing, quick sample drying and air bubble formation were encountered while loading the device. These difficulties, which were due to the small volume of the container (~19 pL) and the low viscosity of the reaction mix, were overcome by examining the effects of loading different ratios of reaction mix with glycerol. Glycerol is more viscous and takes longer to evaporate than the reaction mix. A new reaction mix consisting of 10% glycerol was found to be optimal. It had an increased viscosity, which made it easier to load the device, avoid air

bubble formation, and reduce the effects of evaporation before sealing the device with PDMS. Arrays of up to 18 devices could be prepared in this manner and only a brief amount of time (~20 minutes) was needed to prepare the reaction mix, load the device and begin measurements.

Enzyme reactions are involved in all processes related to the physiological functioning of a cell. Enzymatic assays are important in many applications such as glucose sensing and monitoring, drug discovery and screening. High-throughput analysis of kinetic reaction of libraries of small molecules with specific enzymes is important for drug discovery and development, whereas screening of the activity of multiple enzyme mutants with a specific substrate is necessary for biocatalyst optimization [128]. Single enzyme reactions were conducted for the purpose of evaluating the efficacy of the device and for determining effective reaction conditions and qualitative assessment of the slits. Single enzyme reactions were successfully carried out on devices that had undergone different PECVD times. Amplex Red had penetrated through the slits of the device and was converted from colorless into red color by HRP in the presence of H_2O_2. Flow rates of 1, 5, 10 and 20 µL/hr were examined and 10 µL/hr was found to be optimal. Slower flow rates were not fast enough to remove all the resorufin that was observed diffusing out of the devices and the channel would fill with red color.

Enzyme concentration present in the device did not affect the success of the experiment since the containers turned red under all enzyme concentrations. However, it took a longer time for the devices to turn red when smaller enzyme concentrations were present. Resorufin diffused out of the container quickly and filled the channel in red color for enzyme reactions conducted on 2, 4 and 6 min PECVD devices (Figure 3.3), whereas

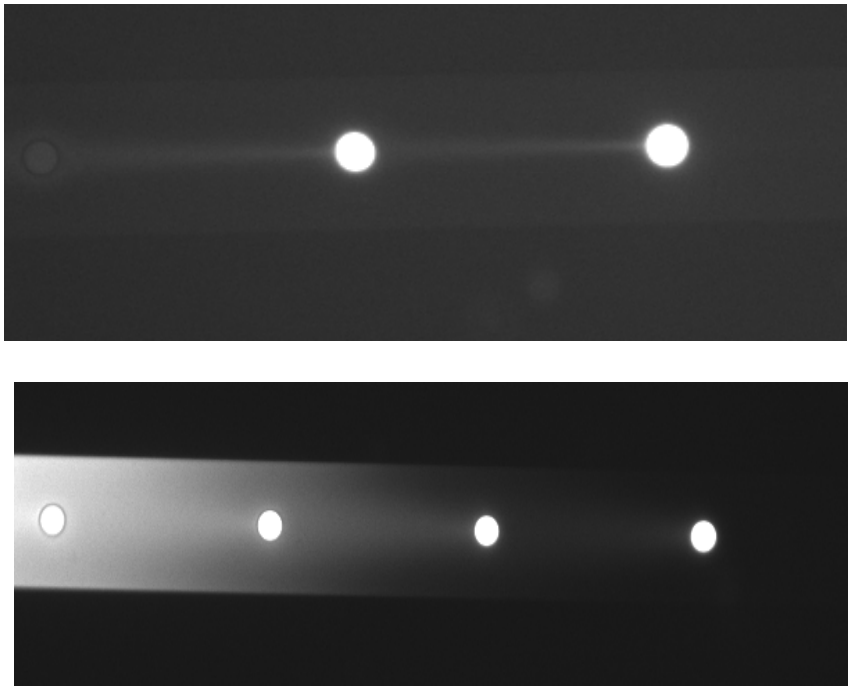

Figure 3-3: Single enzyme reactions on 4 minute PECVD devices.

7 and 9 min PECVD devices had no visible product diffusion, which combined with 10 μL/hr flow rate made it hard to detect and the channel remained colorless.

As shown in the previous chapter, since PECVD of silicon dioxide is used to further change the width of the slits by depositing thin films of silicon dioxide from the gas state into solid state on the device, the longer the device undergoes this procedure the smaller the size of the slits becomes. Therefore, the 2, 4 and 6 min PECVD devices have bigger slits than the 7 and 9 min PECVD devices and allow molecules such as glucose, amplex red, H_2O_2 and resorufin to diffuse quickly through the membrane. Devices that have undergone 7 and 9 min PECVD have slits with smaller widths (~5-10 nm), therefore they can allow slow diffusion of small molecules such as glucose, amplex red, H_2O_2 and resorufin, but prevent large molecules such as horseradish peroxidase from transporting out of the device. Since the 7 min PECVD device was able to contain the reaction, we decided to continue the rest of the experiments using this type of device.

3.3.2. Coupled Enzyme Reactions

Coupled enzyme reactions were successfully conducted in the small volume containers. Glucose and amplex red penetrated through the slits of the device and glucose was converted by GOX in the presence of oxygen into gluconolactone and hydrogen peroxide. The newly formed H_2O_2 reacted with Amplex Red in the presence of HRP to form the molecule Resorufin, which was visible due to its fluorescent red color (Figure 3.4 and 3.5). All reactions conducted with different enzyme concentrations were successful in the 7 and 9 minute PECVD coated devices (Figure 3.6).

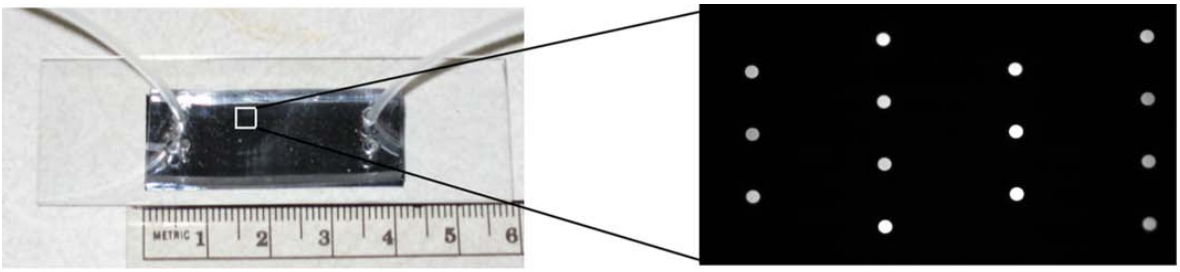

Figure 3-4: Sealed device and an array of enzyme reactions conducted simultaneously. Parallel reactions with a series of enzyme concentrations from 0.0125u/ml to 1u/ml in the devices and 10 mM glucose in the channel.

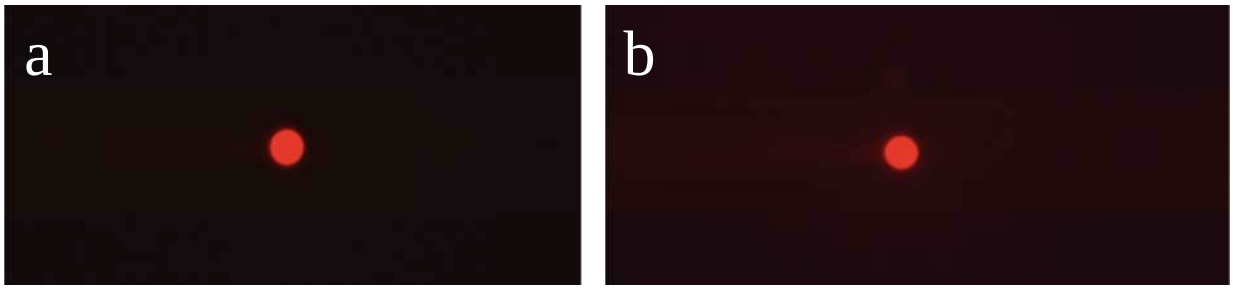

Figure 3-5: Coupled enzyme reactions on 7 minute PECVD at (a) 10 minutes (b) 70 minutes.

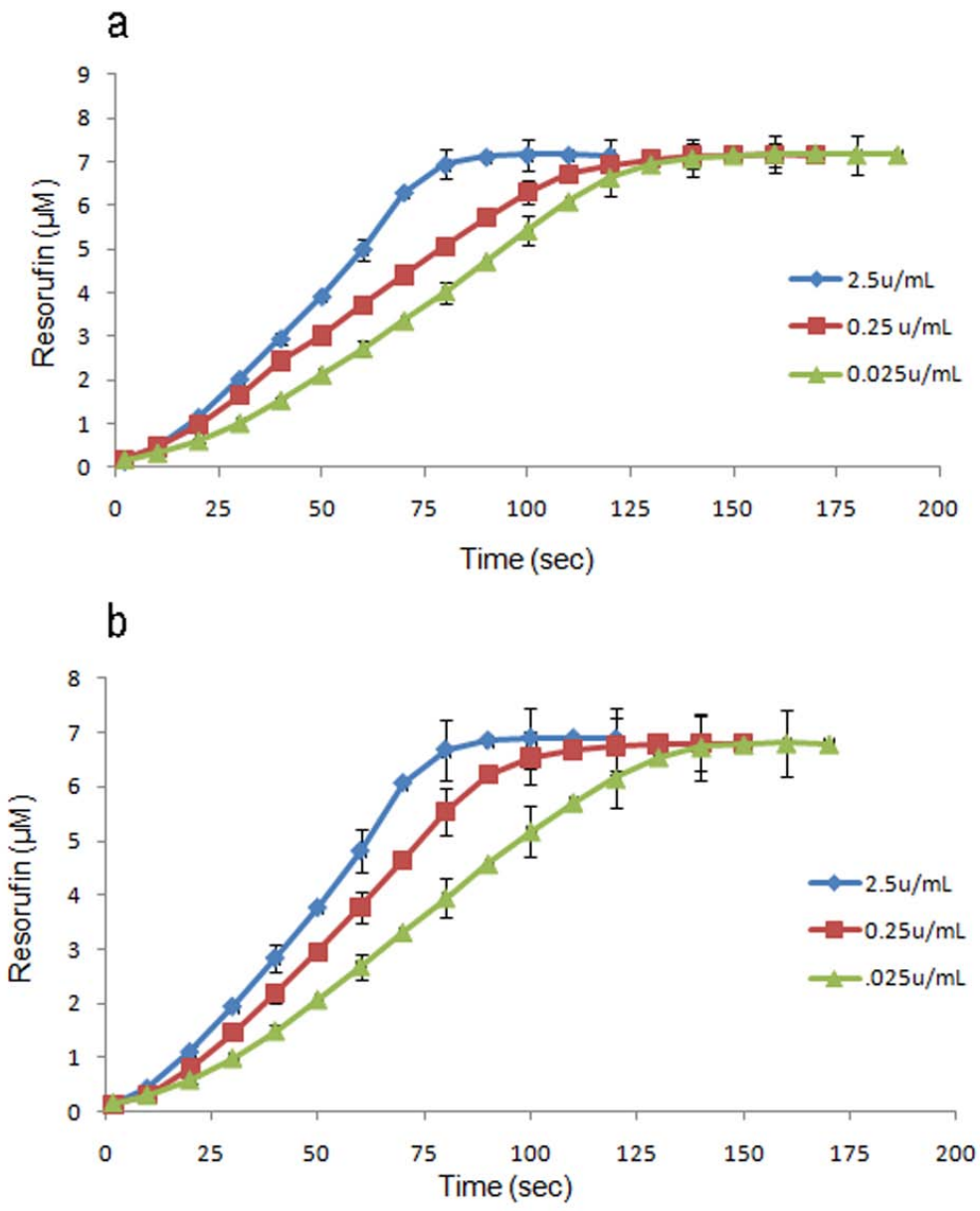

Figure 3-6: Coupled enzyme reactions with 0.25 U/ml GOX and different HRP concentrations in cell mimic devices. A) Coupled enzyme reactions on devices that have undergone 7 min PECVD. B) Coupled enzyme reactions on devices that have undergone 9 min PECVD. Each graph represents the resorufin concentration, corresponding to the observed fluorescence intensity, from three coupled enzyme reaction experiments (3 individual devices on 3 separate chips). Error bars represent +/- one standard deviation and are shown at 20 second intervals for clarity.

All reactions conducted with different enzyme concentrations were successful in devices that had undergone 7 and 9 minute PECVD (Figure 3.6). Devices that have undergone 7 min PECVD have slits with bigger widths (~5-10 nm) than the 9 minute PECVD devices, therefore they can allow a faster diffusion of small molecules such as amplex red, H_2O_2 and resorufin, but are still small enough to prevent large molecules such as glucose oxidase and horseradish peroxidase from transporting out of the device. Since the 7 min PECVD device was able to contain the reaction, we decided to continue the rest of the experiments using this type of device. GOX and HRP concentrations of 0.25 u/mL were arbitrarily chosen to continue the rest of the experiments since these concentrations had results with the smallest error bars.

Coupled enzyme reactions were also conducted with different glucose concentrations and showed to be substrate dependent (Figure 3.4 and 3.5). Higher glucose concentration increased the enzyme reaction rate in the device. The reaction reached its peak of 7-8 μM resorufin within ~150 seconds when glucose concentration was 100 mM and it took ~10 minutes when glucose concentration was 10 μM (Figure 3.7). The coupled enzyme reactions conducted in the plate reader, reached the peak of 6 μM resorufin within ~300-400 seconds for the high concentrations of glucose and it took ~30-40 minutes when glucose concentration was 100 and 10 μM (Figure 3.7). Since there is a 1:1 stoichiometry ratio between H_2O_2 and the appearance of resorufin, the turnover of H_2O_2 could be determined from calibration curves obtained from the corresponding fluorescence intensities of known concentrations of resorufin.

Enzyme kinetics were determined by measuring resorufin's fluorescence signal through time in the device, and Michealis-Menten equation was used to evaluate enzyme

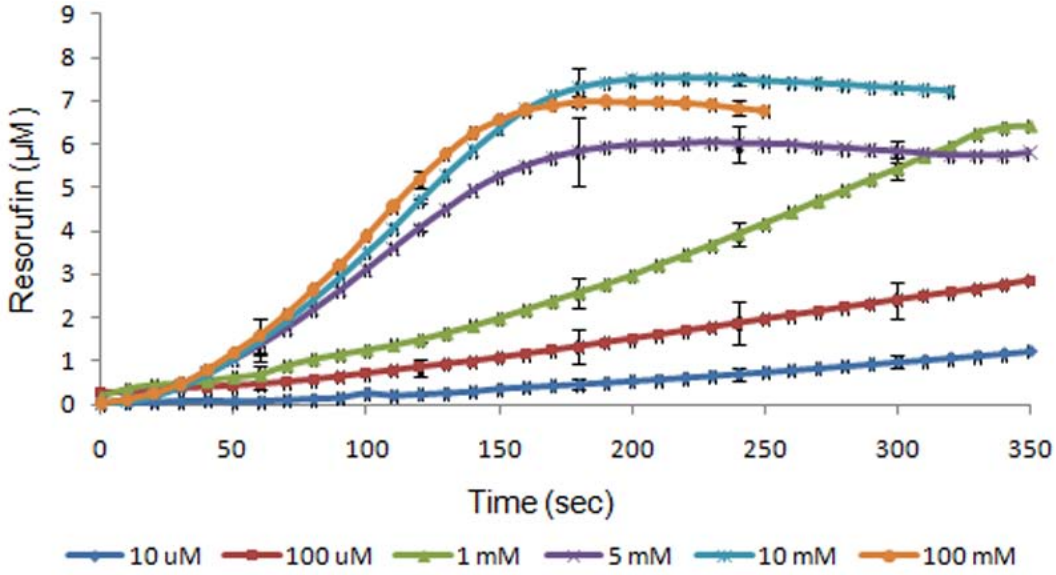

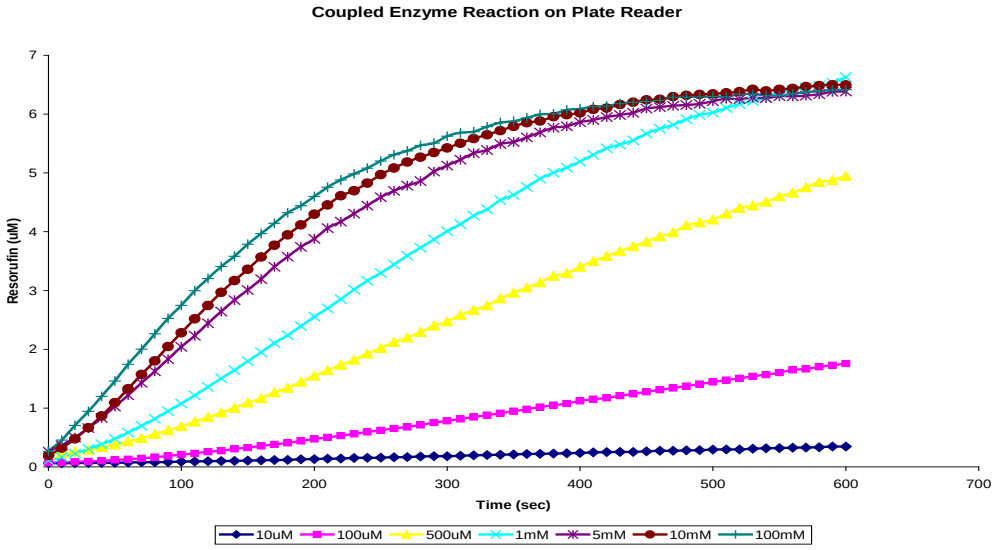

Figure 3-7: Fluorescently measured coupled enzyme reactions in picoliter volume reactors and plate reader with glucose concentrations from 10 μM to 100 mM. Time course fluorescence intensity of the product resorufin according to the increase of the substrate concentration of glucose.

kinetics of the coupled enzyme reaction. Since this is a coupled enzyme reaction and glucose oxidation is the slowest reaction step, the overall reaction rate corresponds to the catalytic rate of glucose oxidase.

$$V_0 = V_{max}[S]/(K_m + [S])$$

In this equation, V_0 is the initial rate of the enzyme reaction, [S] is the substrate concentration, V_{max} is the maximum rate which corresponds to the velocity of the reaction when the enzymes are saturated with substrate, and K_m is the amount of substrate needed for half the maximal velocity. Maximal velocity (V_{max}) was determined for each glucose concentration from the slopes of normalized fluorescence intensities as a function of time. Background fluorescence was measured for each reaction and then was subtracted from the fluorescence intensity measured in the device.

Using the rates calculated from the data in Figure 3.7, a Lineweaver-Burk plot of 1/V and 1/[S] was used to derive K_m and V_{max} (Figure 3.8).

$$1/V_0 = (K_m/V_{max})/[S] + 1/V_{max}$$

The slope of the line for the Lineweaver-Burk plot is K_m/V_{max}, the Y intercept is $1/V_{max}$ whereas the X intercept is $-1/K_m$ Coupled enzyme reactions in the device had a K_m = 1.65 ± 0.17 mM and a V_{max} = 67 ± 1.5 μM min^{-1}, whereas coupled enzyme reactions in the plate reader had a K_m= 0.75 ± 0.04 mM and a V_{max} = 25 ± 0.3 μM min^{-1}. A 2.2-2.5 times difference was observed between the K_m and V_{max} values.

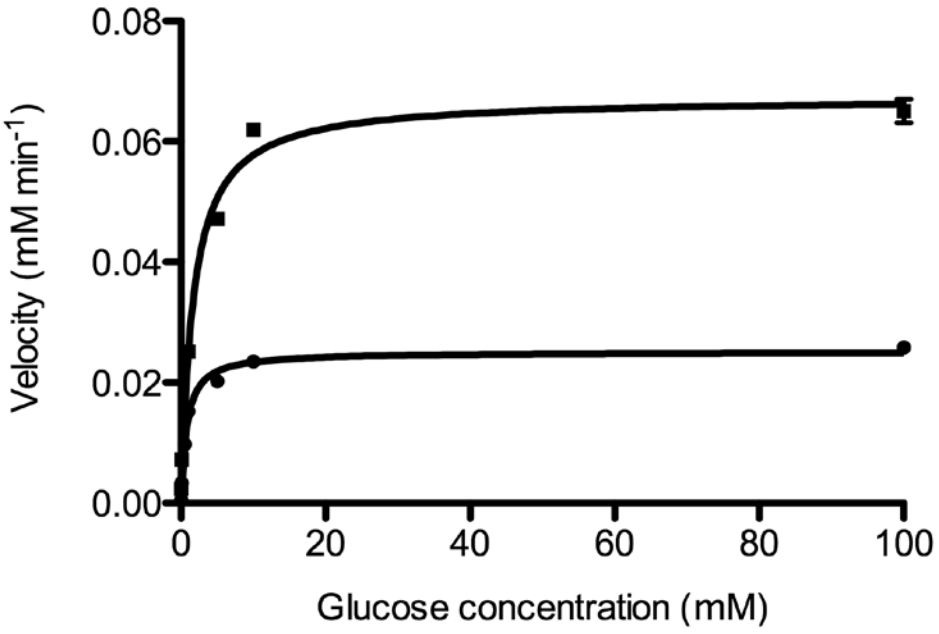

Figure 3-8: Michealis-Menten plots of coupled enzyme reactions in picoliter volume reaction device (ν) and plate reader (λ).The K_m and V_{max} for the reaction device were found to be 1.65 ± 0.17 mM and 67 ± 1.4 μM min^{-1} respectively. (b) The K_m and V_{max} for the coupled enzyme reactions in the plate reader were found to be 0.75 ± 0.04 mM and 25 ± 0.3 μM min^{-1} respectively.

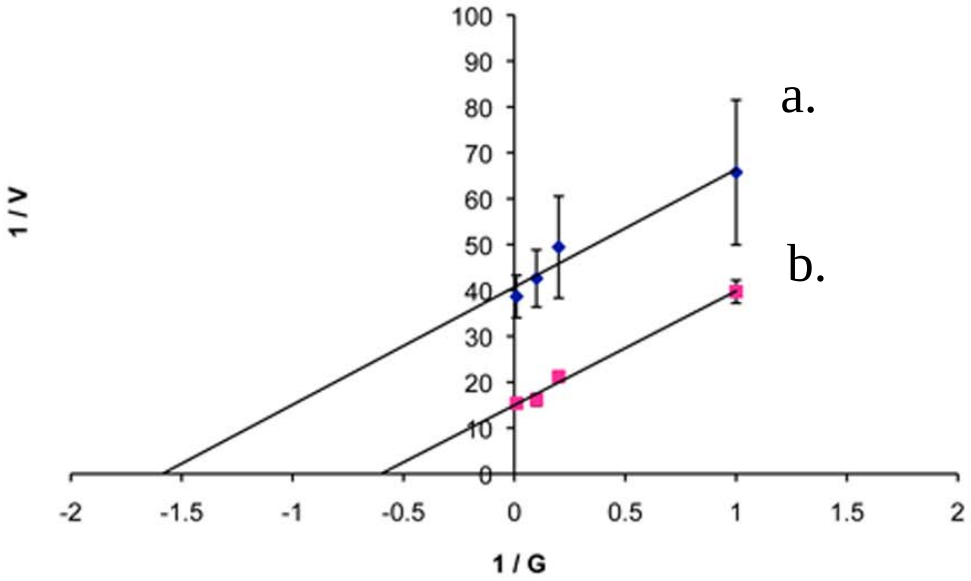

Figure 3-9: Lineweaver-Burk reciprocal plots for coupled enzyme reactions in plate reader and device. (a, blue diamond) The K_m and V_{max} for the plate reader were found to be 0.59 ± 0.01 mM and 23 ± 0.8 μM min^{-1} respectively. (b, pink square) The K_m and V_{max} for the coupled enzyme reactions in the device were found to be 0.587 ± 0.02 mM and 49 ± 1.4 μM min^{-1} respectively.

One possible reason that the device and plate reader reactions have different K_m and V_{max} values could be that product inhibition takes place in the batch reactions. The plate reader is a closed system and the reaction of high concentrations of glucose with glucose oxidase produces an excess of H_2O_2, which can oxidize resorufin to nonfluorescent resazurin. Therefore it makes it seem as if less enzymes were present in the reaction and less product was formed at a longer time. On the other hand, the small reaction device with its nanometer size slits prevents build up of H_2O_2 and therefore allows for a better determination of enzyme kinetics. However, the effect of product loss from the reaction device should also be taken into consideration. Since resorufin is a small molecule, it can diffuse out of the device and may not be accounted during enzyme kinetics. The diffusion experiments described above show that ~40% of fluorescein diffuses out of a 7 min PECVD device within 2 minutes, which is the time that it takes for most of the enzyme reactions to reach V_{max}. Fluorescein has a comparable size with resorufin therefore it can be assumed that ~40% of the product leaves the reaction device before V_{max} is reached, which should increase V_{max}. However, since substrate, amplex red and H_2O_2 are also transported through the pores of the device at the same time that resorufin is diffusing out, the amount of product that diffuses out and is not included in kinetics calculations should be much smaller than 40%. Nevertheless, a model that accounts for diffusion of all small molecules involved in the reaction is necessary in order to have a more realistic V_{max}.

Nevertheless, a model that accounts for diffusion of all small molecules involved in the reaction is necessary in order to have a more realistic V_{max}. Substrate mass diffusion in and out of the device and better mixing can also allow for a higher V_{max} in

the device. Mass diffusion is a key point when considering enzyme reactions in small volume containers. The best situation is when diffusion of substrate and product is not the rate limiting process, which leads to better estimation of enzyme kinetics. The Michaelis-Menten model, for low substrate concentrations, is directly depended on the diffusion rate of the substrate into the device (Table 3.1). In this diffusion-controlled system, there is a linear correlation between the reaction rate results and the substrate concentration [190]. This diffusion-limited linearization of the catalytic rate applies for low substrate concentrations whereas the high substrate concentrations still represent the Michaelis-Menten model. As shown in the fluorescein diffusion data, product is leaving the device at a fast rate even for devices that have undergone 7 minute PECVD. Therefore, optimization of the width of slits is a necessary step for an unbiased evaluation of enzyme kinetics. Since both enzymes are too big to diffuse out of the device, optimization for the diffusion of glucose, amplex red and resorufin are the main factors. Therefore, a deterministic model of diffusion and enzyme conversion is a necessary step.

The enzyme microreactor described here offers a number of practical advantages that go beyond real time monitoring and optimization of reaction systems. It has a relatively thin membrane, the pores of which can be tuned to allow a wide range of exchange rates. It can also be designed in an array platform, which allows for fast, high-throughput screening of several enzymes and substrates simultaneously, drug discovery and clinical diagnostics.

Table 3-1: Michaelis-Menten Kinetic Variables for Coupled Enzyme Reactions

	Reaction Device	**96-well plate**
$\mathbf{K_m}$	1.65 ± 0.17 mM	0.75 ± 0.04 mM
$\mathbf{V_{max}}$	67 ± 1.5 μM min^{-1}	25 ± 0.3 μM min^{-1}

3.4. Conclusion

Here we described a nanoporous, picoliter reaction device, which under continuous-flow is used to measure enzyme kinetics in a microfluidic system. This platform has several significant advantages such as (1) the device is integrated with microfluidics to manipulate the surrounding environment and provide a fast and convenient monitoring of the activity of different enzymes; (2) the multi device platform allows for a high-throughput screening of several enzymes and substrates; (3) the enzymes are trapped inside the device in their native form and (4) the devices can be prepared with a controlled nanometer-size porosity which allows for fast mass transfer kinetics and removal of inhibitory byproducts. These picoliter reaction devices will have a key role in probing biological systems and better understanding self-organization at the micro scale. They could also interact with biological systems, sense abnormal conditions and respond with appropriately dose reagents.

Chapter 4
Cell-Free Transcription/Translation in engineered picoliter volume containers

This chapter is based on a manuscript reprinted from *2009 First Annual Ornl Biomedical Science & Engineering Conference: Exploring the Intersections of Interdisciplinary Biomedical Research,* Siuti, P.; Retterer, S.T.; Chang Kyoung Choi; Fowlkes, J.D.; Doktycz, M.J.; , "Cell free translation in engineered picoliter volume containers," pp.1-4, Copyright (2010), with permision from IEEE Xplore Digital Library

Data, images and text relevant to this study are included in this chapter. Images are presented in color where they were published in black and white. Under the direction of the co-authors, I conducted the experiments, analyzed the resulting data, and drafted the manuscript. The co-authors responded with editorial comments and additional text where needed.

4.1. Introduction

Synthetic biology is a relatively new discipline that can help to elucidate many of the mysteries of cell biology and enable us to develop new applications related to the fabrication of nanostructures and biomaterials, medicine, biosensing and energy production [5, 72, 102]. By combining genes, synthetic biologists are successfully inserting the equivalent of chemical factories into microorganisms that enable new forms of cellular control and enhance our understanding of basic cellular operations. Advancements in nanotechnology have created opportunities for synthetic biologists to match the scale of biological system components and create biologically inspired devices [5]. One example is cell mimics, where the cell's small volume and controlled flux is mimicked in order to carry out reaction systems. These small volume devices can establish favorable conditions for protein production and function. They can also be used

to understand biological systems, study single molecule reactions and examine self organization at the cellular scale [5, 45, 46, 191, 192]

Commonly, liposome vesicles are used as model systems to mimic the function of the cellular membrane. Since these vesicles are made of natural lipids, they are biocompatible with membrane proteins, which can be used to facilitate material exchange [5, 72, 74, 78]. Water in oil emulsions have also been used to create small reaction volumes [91, 102]. However, the long-term stability of liposome vesicles and water in oil emulsion structures can be problematic [5]. Additionally, such systems are difficult to integrate with synthetic control mechanisms and devices, which leads to the need for more robust and reliable vesicles.

Microfabrication and nanotechnology based techniques can be used to create such robust reaction containers from inorganic materials. The small volume devices can be used for a variety of applications including: high throughput screening [135], enzyme kinetics [130], analysis of single cells [193] and cell-free protein synthesis [5, 132, 135, 194]. They can be patterned in different materials, shapes and pore sizes and can be physically or chemically modified to control the flux of molecules of different sizes and charges so that they mimic some of the characteristics of a natural cell. Such a silicon based device is described here. It can be used for studying biochemical reactions and the effects of scale and compartmentalization on reaction efficiency. The cylindrical container is 2μm thick with 8 sets of 7 slits spaced around the perimeter. Slits are etched in the same processing step as the device and can range in size from 30-200 nm wide and 10 nm deep. Devices can be created without slits as well. These small volume containers can be used to characterize reaction systems and material organization in a fluid

environment. They can also be used to “self assemble” reaction systems. Further, the device allows for controlled transport between the local environment and the contained volume through the synthetic membrane. Cell-free transcription and translation reactions conducted in this container would be useful for producing functional proteins as needed for biomedical applications. Reported here is the use of a picoliter volume containers (Figure 4.1) to conduct cell-free protein synthesis. Further, the optimal DNA concentration and the time required for maximal protein yield in the device is determined.

4.2. Materials and Methods

4.2.1. Device Fabrication

Reaction containers were fabricated using semiconductor processing techniques to define membrane characteristics. Feature fabrication was achieved using electron beam and optical lithography, followed by cryogenic etching and plasma enhanced chemical vapor of silicon dioxide. Each fabrication run, results in a silicon wafer with 8 completed chips. Each chip consists of 2 channels with 15 containers per channel (Figure 4.2a, b). For the experiments described here, the resulting containers have a volume of ~19 pL and are made with either no slits or 200nm slit sizes.

The Sylgard 184 silicone elastomer kit was used to prepare Polydimethylsiloxane (PDMS), which is used to seal the top of the devices. Sylgard 184 silicon base and the curing agent were mixed together in a Petri dish at a 10 to 1 ratio, respectively. The homogeneous mixture was degassed in a desiccator for ~30 min until the air bubbles

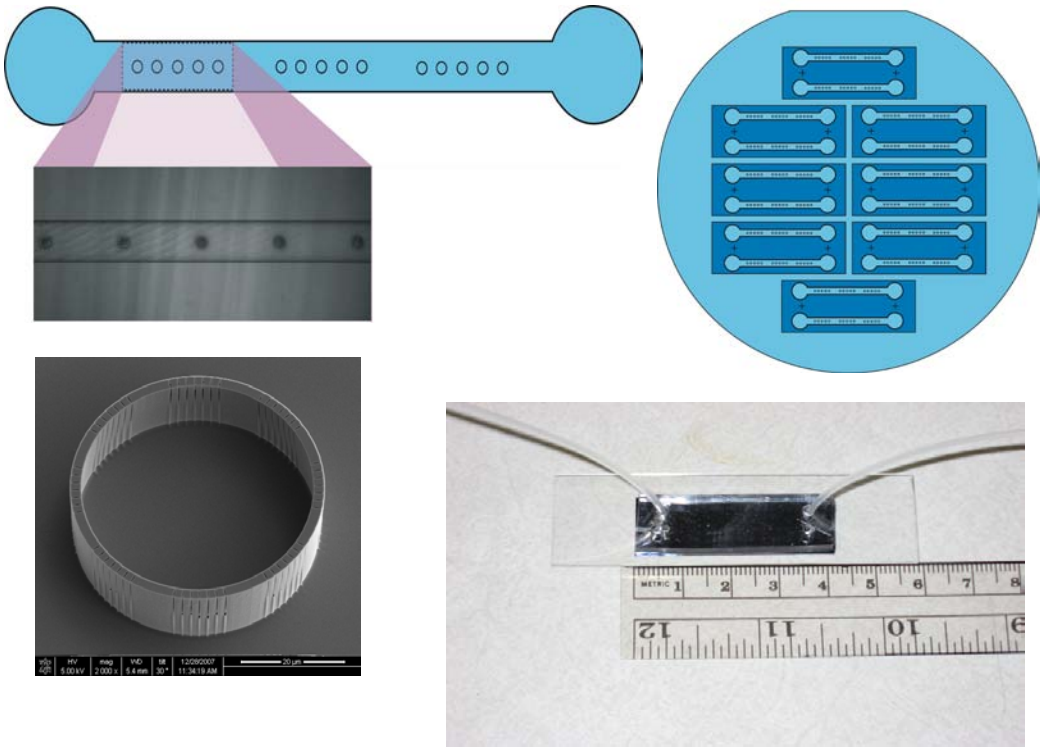

Figure 4-1: Wafer with 8 chips and sealed device.

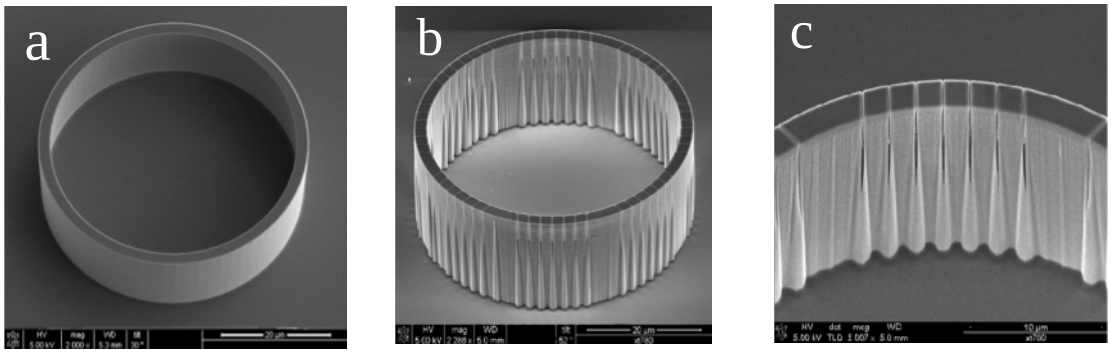

Figure 4-2: Scanning Electron Microscope (SEM) images of the device (a) Container with no slits (b) Container with 200 nm slit size (c) 200 nm slits.

were removed and was later placed in the oven at 70˚C for 60- 90 minutes. After baking, PDMS was cut into pieces in the shape of the chip and two holes were created on each end of the channel to allow for the input and output of the reaction mixture (Figure 4.2c).

4.2.2. Cell Free Translation

Escherichia coli (*E. coli*) T7S30 Extract System for Circular DNA reaction kit (Promega TB219) was used for transcription/translation experiments according to the manufacturer's directions. For the template, enhanced green fluorescent protein (EGFP) gene was cloned into pDEST17 (Invitrogen), which allows expression of EGFP from a T7 promoter (Figure 4.3). The solution containing the DNA template and the cell free transcription/translation mix was mixed in a 1:1 ratio with 8 % glycerol and placed in the cell mimic using a glass tip with 2 μm orifice (World Precision Instruments, TIP2TW1). After the structures were loaded, the chip was covered with a 5 mm thick layer of PDMS. The channel was then filled with *E. coli* S30 cell free extract and small metabolites. The experiment was incubated at 37˚C. EGFP fluorescence was visualized using a Zeiss Axioskop 2 FS Plus epifluorescent microscope. A similar procedure was also followed for cell-free transcription/translation in containers containing no slits. In this case, the DNA template was mixed with *E. coli* T7S30 cell free extract and small metabolites in a 1:4 ratio, and a final 4 % glycerol concentration. The entire reaction mixture was then loaded into the device using a 2 μL glass microtip (World Precision Instruments, TIP2TW1). Several mimics were filled with *E. coli* T7S30 cell free extract and were used as negative controls. The chip was then covered with PDMS and fluorescence was measured. The experiment was incubated at 37˚C. In order to compare cell-free

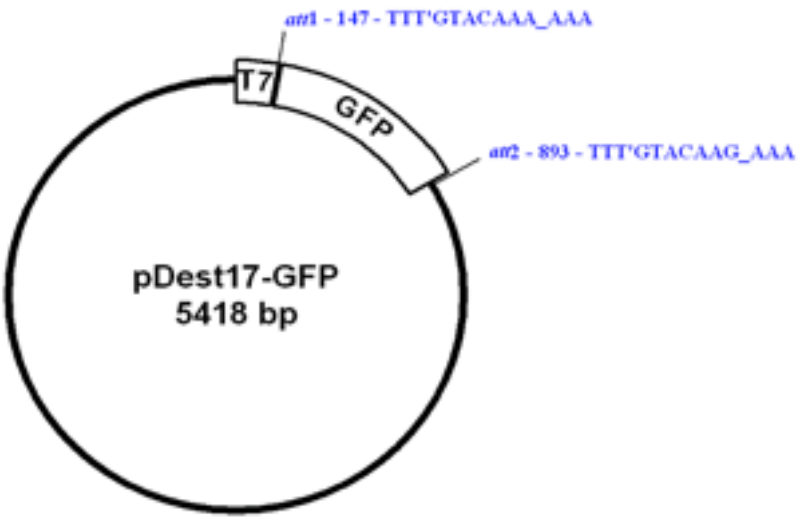

Figure 4-3: Plasmid encoding for EGFP. The plasmid is based on the pDEST17 vector backbone with a T7 inducible promoter. The size of the plasmid is 5418 bp.

translation in the device with conventional scale reactions, cell-free translation was also conducted in a Costar 96 flat bottom well plate (Figure 4.4a). The concentrations and temperature were kept the same as in the device reactions. The final reaction volume in the plate well was 50 µL and fluorescence was measured every 10 minutes using a Perkin Elmer HTS 7000 Plus BioAssay Reader.

4.2.3. Characterization

An EGFP standard was prepared by diluting purified GFP protein to concentrations of 26.2, 13.1, 6.55, 3.275, 1.64, 0.82, 0.41, 0.205 and 0.103 µM EGFP. Each of the EGFP solutions contained 4 % glycerol concentration. These solutions were loaded in no pore devices and fluorescence was measured using identical settings for devices with no pores or with 200nm pores. EGFP concentration produced in the cell-free transcription/translation reactions in the no slit and 200 nm slit size mimics was measured against this EGFP standard. For all the experiments, images were taken every 10 minutes using a dry 40x objective at an exposure time of 500 milliseconds. A 3CC syringe with a 19 gauge needle was used to flow the reaction mix into the channel.

4.3. Results and Discussion

To test the ability of the microfabricated picoliter volume containers to carry out biochemical reaction systems, cell-free protein synthesis experiments using no slits and 200 nm slit size devices (Figure 4.5) were carried out. Due to the low viscosity of the reaction mix and the small volume of the container (19 pL), we encountered several

a.

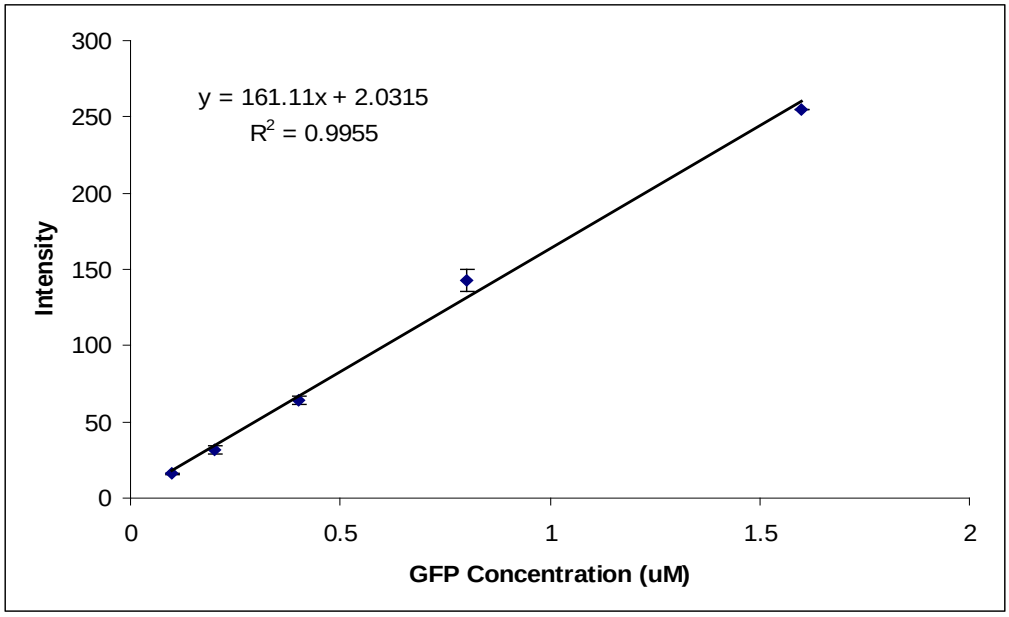

b.

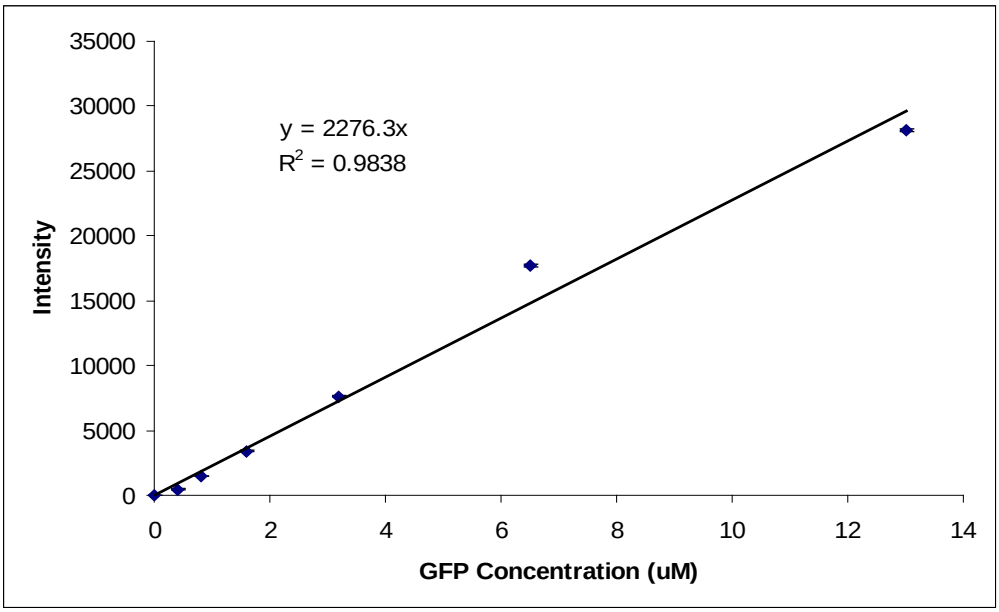

Figure 4-4: Standard curve of different EGFP concentrations in (a) cell mimic device (b) plate reader

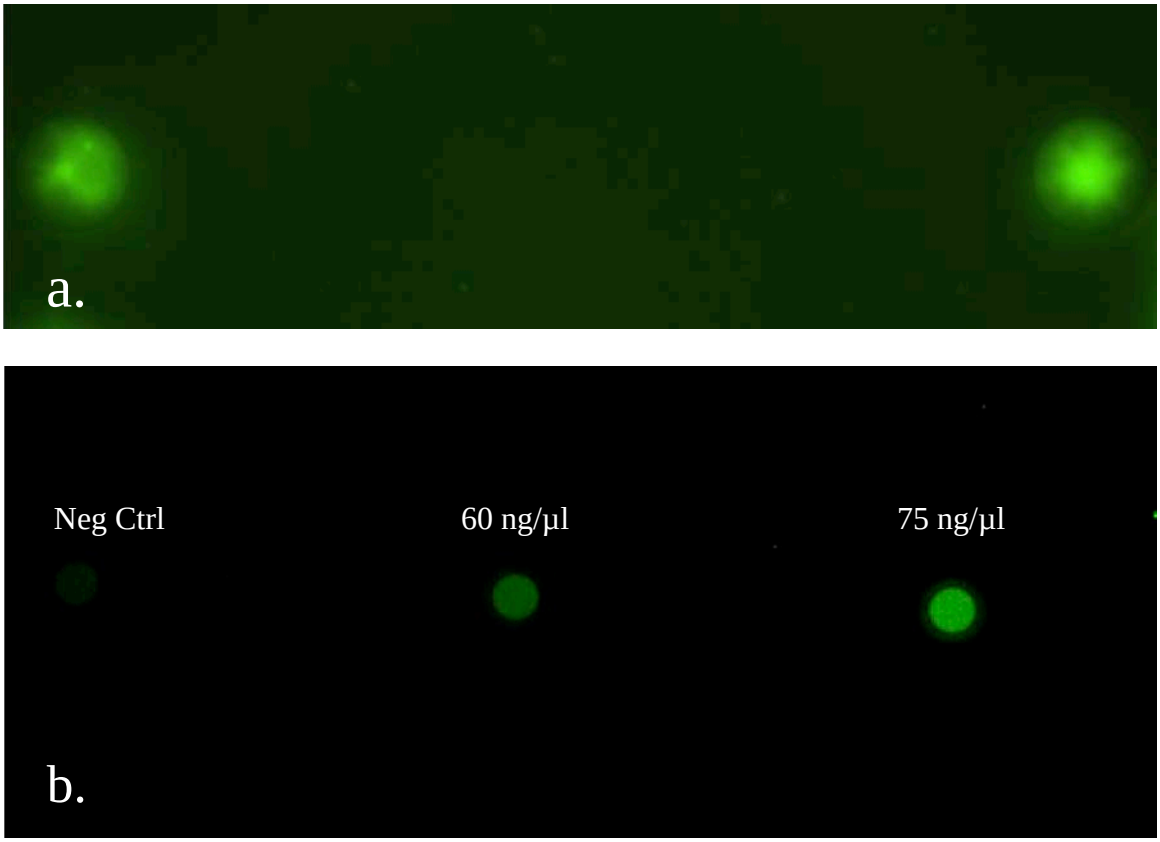

Figure 4-5: Cell-free transcription/translation in cell mimic devices. (a) Container with 200nm slit size (b) Container with no slits.

difficulties when loading the device. These difficulties consisted of overflowing the device at the time of loading, air bubble formation inside the device and quick drying of the sample immediately after loading. In order to overcome these difficulties, the reaction was mixed with different solutions that altered viscosity and evaporation time.

Evaluated solutions included polyethylene glycol (PEG), 1% alginate, glycerol, dimethyl sulfoxide (DMSO), agar, dimethylformamide (DMF) and several sucrose concentrations. All these solutions increased viscosity of the reaction mix making it easier to load the devices. Evaporation of the reaction mix after loading the device was also overcome. Protein production was also evaluated and it was significally decreased. In many cases it was completely inhibited. Alginate was the only solution of those tested that increased protein yield, however it was difficult to handle when loading the device as cross-linking of the mixture would often occur. The most useful solution, which did not significantly decrease cell free transcription/translation was glycerol. There was a small decrease in protein yield when using glycerol, but the increased viscosity made it easier to load the device and air bubble formation was avoided. Therefore, several glycerol concentrations were tested and the lowest one, which still allowed effective loading of the devices and avoided evaporation was determined to be 4% glycerol concentration.

Cell-free transcription/translation experiments were successful for small volume containers that contained no slits and 200 nm slits (Figure 4.6). The reaction yield was consistent in the no slit devices and the optimal DNA concentration was determined. It was found that 90 ng/μL DNA concentration had the highest EGFP yield (Figure 4.8) followed by 75 ng/μL.

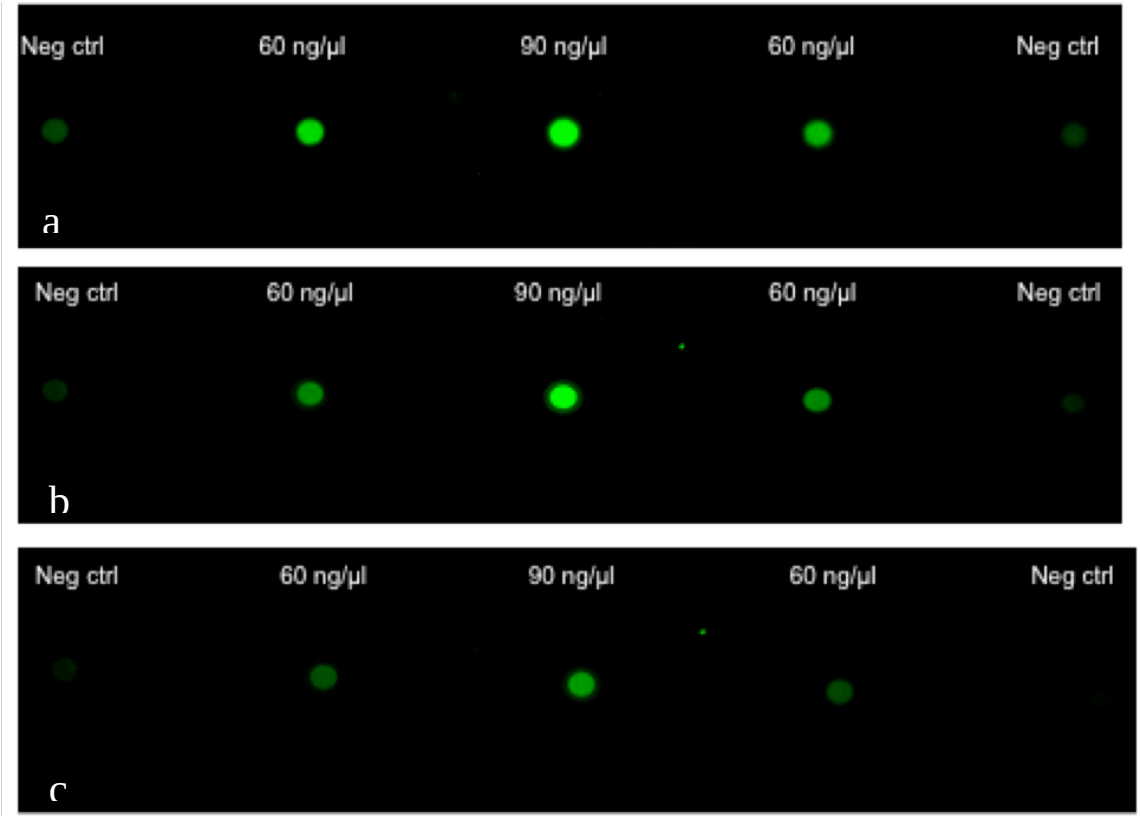

Figure 4-6: Cell-free transcription/translation in no pore devices with different DNA concentrations. Reaction after (a) 60 minutes (b) 90 minutes (c) 120 minutes.

a

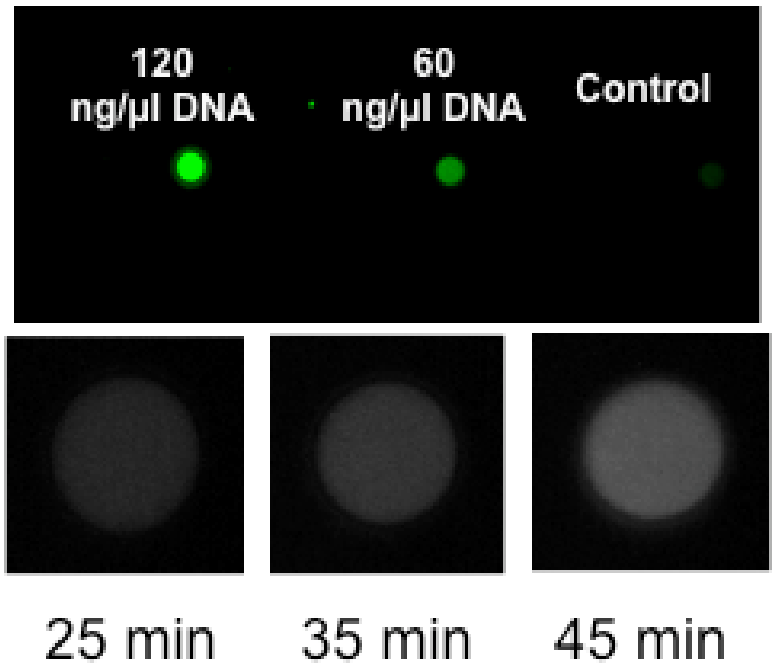

b

Figure 4-7: Cell-free transcription/translation in no pore cell mimic devices. (a) Protein production with different template concentrations of 120, 60 and 0 ng/µL DNA (b) Time progression of cell-free transcription/translation of 120 ng/µL DNA template on a no pore cell mimic device.

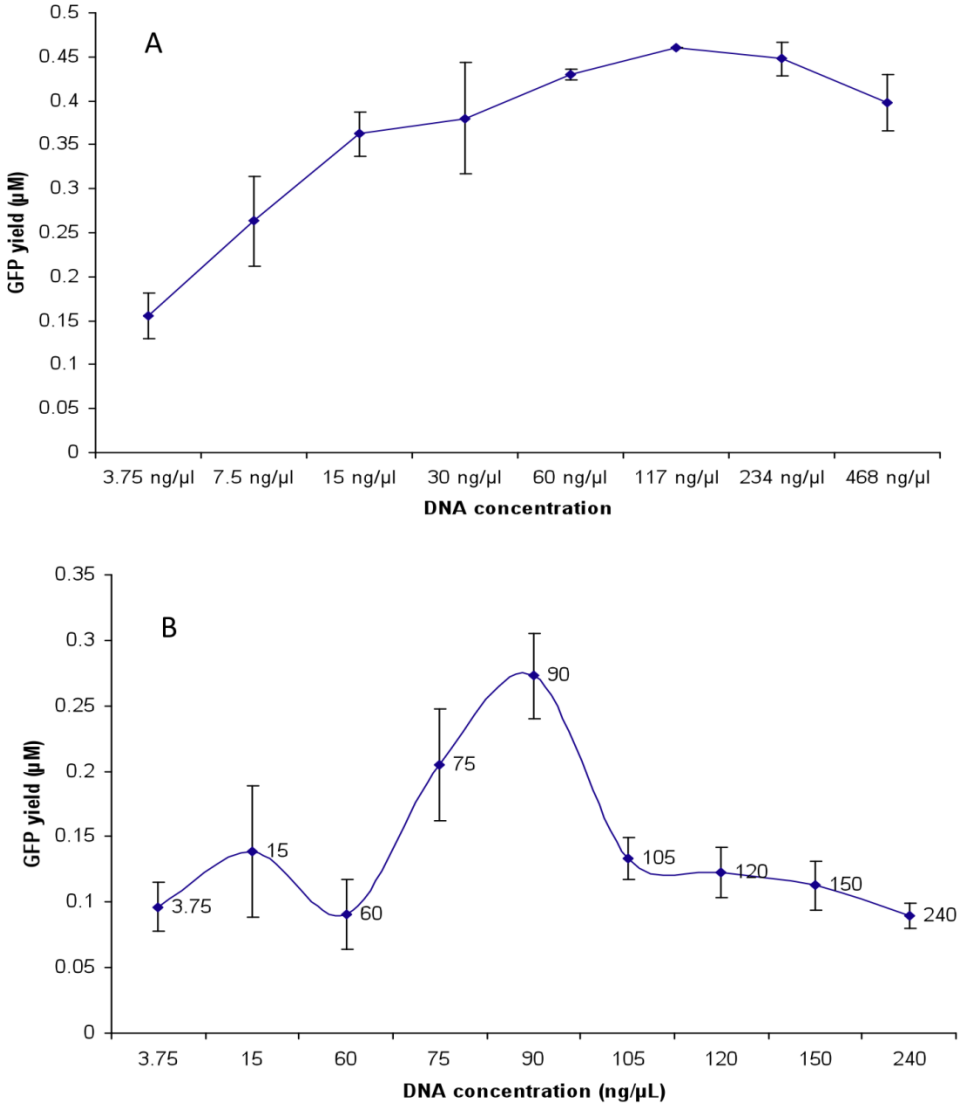

Figure 4-8: Cell-free protein expression in (a) plate reader and (b) no slit device. The graph represents the protein concentration, corresponding to the observed fluorescence intensity, from three protein synthesis experiments (3 individual devices on 3 separate chips). Error bars represent +/- one standard deviation.

The other concentrations tested had a similar EGFP yield of ~ 0.1 μM. When compared to experiments carried out at the conventional scale (50μL), a plateau was reached at template concentrations greater than 60 ng/μL (Fig. 4.8). Cell-free transcription/translation in 200nm slit size cell mimic devices was more difficult to achieve and typically GFP was produced throughout the entire microfluidic channel. This could be caused by (a) GFP leaking out of the device through the slits after it was produced or (b) the mRNA leaking out and translation occurring in the channel instead of only in the device. GFP observation in the channel was eliminated when the buffer was flowed through the channel using gravity. Under these conditions, GFP was detected only in the reaction chamber. Therefore, a better understanding of the effect of pore size and viscosity on cell mimic loading and protein production is necessary.

4.4. Conclusion

In this chapter we demonstrated cell free transcription/translation in the picoliter reaction devices with no pores or with 200 nm pore size. The reaction yield was consistent in the no pore devices and the optimal DNA concentration was determined. Optimal template concentration required for eGFP production was also determined.

Chapter 5
Continuous protein production in nanoporous, picoliter volume containers under continuous flow conditions

This chapter is based on a manuscript submited to *Lab on a Chip,* Siuti, P.; Retterer, S.T.; and Doktycz, M.J., "Continuous protein production in nanoporous, picoliter volume containers,"

Data, images and text relevant to this study are included in this chapter. Images are presented in color where they were published in black and white. Under the direction of the co-authors, I conducted the experiments, analyzed the resulting data, and drafted the manuscript. The co-authors responded with editorial comments and additional text where needed.

5.1. Introduction

Protein production is fundamental to the function of biological systems and is the technological cornerstone for the manufacture of biological therapeutics. A growing amount of genetic information has highlighted the need to rapidly screen protein activity [195] while protein-based “biologics” are emerging as an important class of pharmaceuticals [196-198]. Conventionally, protein production is carried out using live host cells. However, protein degradation, insolubility, cytotoxicity and yield [199, 200] can complicate this approach. Cell-free methods are a promising alternative and use isolated components of a cell’s transcription and translation machinery to express proteins from DNA-based instructions [56, 201].

Cell-free methods have proven practical for preparing proteins that are difficult to express in vivo, including complex macromolecular assemblies and membrane proteins[67, 202-204]. Since other aspects of cellular metabolism are not necessarily required, problems associated with conflicting reactions, codon biases, protein solubility

and toxicity can be avoided. Further, conditions can be customized to facilitate protein folding [56, 205] or gene expression [206]. Although, the cell-free nature of the reaction can enable greater control of reaction conditions, and potentially focus energy requirements towards protein production, problems associated with reaction optimization, reaction extent and product yield persist.

One origin of these shortcomings is the concurrent depletion of reaction nutrients and the build-up of reaction byproducts that inhibit protein synthesis[207]. This can abbreviate the reaction period and results in low protein yields. Spirin's introduction of reagent exchange to cell-free protein synthesis marked a major advance [82]. By continuously supplying reactants and removing byproducts through a membrane, maintenance of protein synthesis for up to several days was possible. Modifications to this approach continue to increase protein yield over that of batch reactions [55, 56, 59, 207-209]. Typically, components that can facilitate or interfere with optimal protein production are added or removed from the system [60]. The development of the PURE system, where individual components of the transcription/translation machinery are expressed, purified and combined for cell free transcription/translation, marked another significant development [81]. Using just essential components can facilitate optimal protein production, provided peak conditions are identified and all essential reactions are accounted for. Nevertheless, the development of the PURE system represents a significant step forward in the engineering of complex biochemical reactions for specific application.

Continuous exchange reactions are typically carried out at fairly large scales when compared to the biological cell. Further, they often lack sophisticated control over the

membrane properties and resultant material exchange. Significantly reducing the scale of cell free translation reactions can facilitate functional screening of proteins[63, 70, 131, 134] and exploit the scaling advantages of a biological cell [5]. Small volumes enable efficient diffusion-based mixing. Furthermore, the increase in surface area to volume allows for greater control over material flux with the environment [210]. Mimicking such aspects of the cell may improve cell free translation. Here we demonstrate the advantages of a "cell mimic" device for such purposes. A cellular scale, nanostructured membrane fabricated in silicon, is used to confine DNA instructions and cell free extract components. Microfluidics are used to deliver and remove materials via diffusion-mediated exchange across the membrane (Figure 5.1) enabling long-term production of functional proteins. The nanostructured membrane facilitates selective material transport and can be modified to tune material exchange. Many devices can be implemented in parallel making the platform suitable for larger scale production of a single protein or for simultaneous functional analyses of multiple proteins.

5.2. Materials and methods

5.2.1. Device Fabrication

The small volume reaction vessels were fabricated as previously described in Retterer et al [159]. Briefly, patterning of the reaction vessels and microfluidic network was achieved using a combination of electron beam and optical lithography respectively. Patterning was followed by cryogenic silicon etching to simultaneously create the nanoporous structures and fluidic network. Subsequent plasma enhanced chemical vapor deposition (PECVD) was performed to further reduce pore apertures. Each fluidic

network contains two inlets arranged in a Y-configuration and one outlet. The resulting silicon wafer contains eight identical chips. Each chip contains two channels, each with an array of 18 reaction containers (Figure 5.1). The individual reaction containers and the microfluidic channel are ~15 μm tall. The containers are 40 μm in diameter, resulting in a volume of ~19 pL, and possess 56 nanoscale slits. The limiting aperture of the slits is on the order of 10 nm as determined by ion beam milling and cross section analysis [211]. Polydimethylsiloxane (PDMS), prepared from a Sylgard 184 silicone elastomer kit (Dow Corning, Midland, MI), was used to seal the channels and the containers after devices were filled with the reaction components. Holes were made at the ends of the channel for the inputs and output of the network and fitted with tygon tubing and appropriate gauge needle and syringe.

5.2.2. Cell Free Transcription/Translation

Cell-free transcription/translation experiments were assembled in the containers using *Escherichia coli (E. coli)* S30T7 High-Yield Protein Expression System reaction kit (Promega TM306) with minor modifications to the manufacturer's directions. A pDEST17 (Invitrogen) plasmid with a cloned enhanced green fluorescent protein (EGFP) gene controlled by a T7 promoter was used as DNA template. The reaction container was filled with a mixture containing the DNA template, T7S30 Extract and S30 Premix Plus in a 1:2:1 ratio, respectively. The same mixture, with nuclease-free water used in place of the DNA template, was used as a negative control. To fill the containers, a glass capillary with a 2 μm orifice (World Precision Instruments, TIP2TW1) was used. Subsequently, the chip was covered with PDMS. To supply the reaction with secondary energy

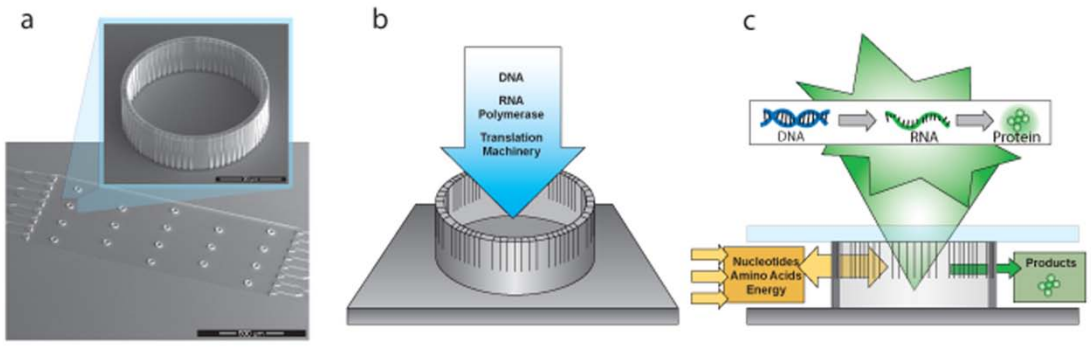

Figure 5-1: A nanoporous, picoliter volume cell mimic platform for continuous protein production. (a) SEM micrograph of a microfluidic device with an array of 18 reaction containers. The inset SEM micrograph shows a single reaction container. (b) Schematic of a nanostructured reaction container where transcription/translation reaction mix, along with DNA template is loaded and sealed with PDMS. (c) The microfluidic channel continuously delivers and removes materials from the reaction chamber to facilitate cell free protein synthesis.

source, amino acids, rNTPs, tRNAs, and salts required for translation, *E. coli* S30 Premix Plus from the kit was flowed through the fluidic network. The chip was incubated at 37˚C using a stage warmer.

Images of the cell free transcription/translation reaction were collected every 5 minutes for the duration of the experiment using a Zeiss Axioskop 2 FS Plus epifluorescent microscope equipped with a 200 W mercury arc lamp and a 40x objective. The images were collected using an exposure time of 400 ms using a Retiga firewire camera synchronized with a Lambda SC smart shutter (Sutter, CA) to minimize unwanted photobleaching of the EGFP during the experiments. Image acquisition software IPLab 4.0.8 (Scanalytics, Inc) was used to acquire the images. Programs to calculate and plot image intensity values were written using ImageJ and MATLAB (V7.2, MathWorks). To allow quantitative comparisons between experiments, binning, exposure times and camera settings were kept the same.

For comparison, conventional scale cell-free transcription/translation experiments were carried out in Costar 96 well flat bottom microwell plates using a Perkin Elmer HTS 7000 Plus BioAssay Reader. These reactions were assembled to a final volume of 50 µL using both the manufacturer recommended concentration and the same concentration ratios as used in the cell mimic containers.

5.2.3. Quantifying Cell-Free Transcription/Translation Reactions

An EGFP standard was prepared by standard methods[63] by diluting purified EGFP protein to concentrations ranging from 26.2 to 0.103 µM EGFP and loading them in the channel. Fluorescence was measured using identical settings as for the

experiments. GFP concentration produced in the cell-free transcription/translation reactions was measured against this EGFP standard.

For quantifying new protein synthesis in the devices, cell-free transcription/translation reactions were assembled and carried out as described in section B. Reaction progress was monitored by collecting images every 5 minutes for up to 25 hours. At selected times, the reaction containers were photobleached by opening the shutter for a total of 2.5 minutes. Photobleaching and the subsequent fluorescence recovery rate were measured at time points of 3, 6, 9, 12, 15, 18, 21 and 25 hours. The fluorescence recovery rate was measured against the EGFP standard.

For halting new protein synthesis in the devices, the cell-free transcription/translation reactions were carried out as described above but treated with chloramphenicol at selected time points. For these experiments, Chloramphenicol at a concentration of 5 μg/mL in *E. coli* S30 Premix was introduced into the second inlet channel as the flow from the first inlet channel was stopped. After a 1 hour treatment with the Chloramphenicol solution, the feed solution was switched back to the *E. coli* S30 Premix Plus. Images were collected every 5 minutes for the duration of the experiment.

5.3. Results

5.3.1. Cell Free Transcription/Translation

To test the ability of the cell mimic devices to carry out cell-free protein synthesis, effective experimental conditions for filling the devices and carrying out the reactions were first determined. Several difficulties such as overflowing, quick sample drying and air bubble formation were encountered while loading the device. These

difficulties, which were due to the small volume of the container (~19 pL) and the low viscosity of the reaction mix, were overcome by examining the effects of loading different ratios of T7S30 Extract and S30 Premix Plus. The T7S30 Extract is more viscous and takes longer to evaporate than S30 Premix Plus. A reaction mix consisting of a 2:1 ratio of T7S30 Extract to S30 Premix Plus was found to be optimal. The new reaction mix had an increased viscosity, which made it easier to load the device, avoid air bubble formation, and reduce the effects of evaporation before sealing of the device with PDMS. Arrays of up to 18 devices could be prepared in this manner and only a brief amount of time (~20 minute) was needed to prepare the reaction mix, load the device and begin measurements.

Long periods of protein synthesis were achieved by flowing S30 Premix Plus through the microfluidic channel surrounding cell mimic devices. Devices were filled with a reaction mix consisting of a 2:1 ratio of T7S30 Extract to S30 Premix Plus (commercial products from Promega) along with DNA encoding EGFP. A 2:1 ratio of extract to premix was found to provide an optimal viscosity for efficiently filling devices. The S30 Premix Plus contains an ATP-regeneration system, amino acids, tRNAs, rNTPs and appropriate salts needed for protein production. Diffusion of these materials into the cell mimic devices replenishes essential metabolites needed for cell free protein synthesis. Flow rates of 1, 5, 10 and 20 μL/hr were examined and 5 μL/hr was found to be optimal. Slower flow rates were difficult to maintain for long periods using the syringe pump-based pumping system while higher flow rates needlessly consumed materials.

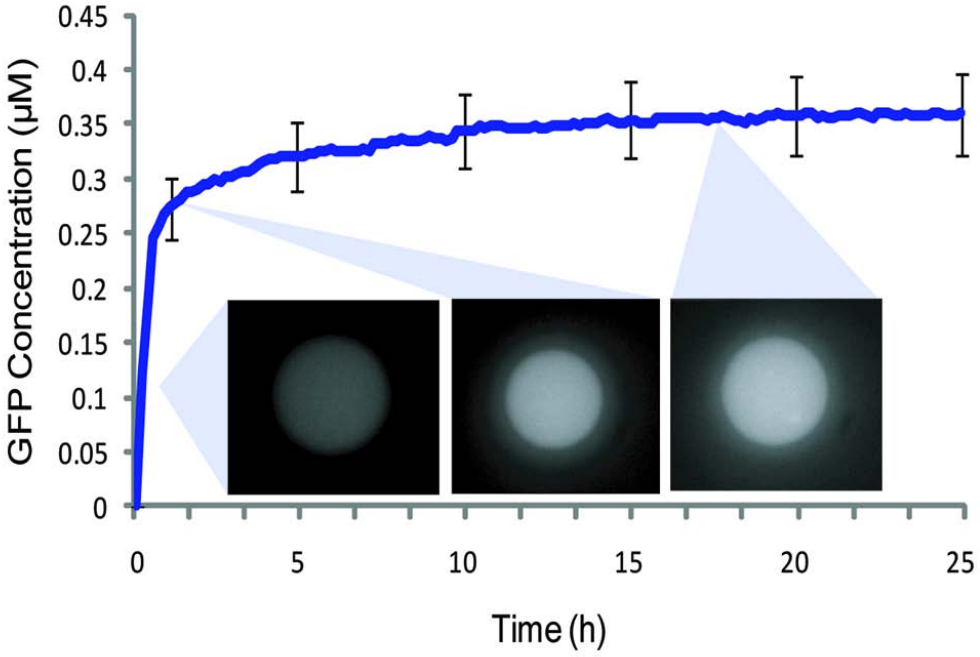

Figure 5-2: Continuous protein production in cell mimic devices. Protein synthesis was achieved by flowing S30 Premix Plus at a flow rate of 5 μL/hr through the microfluidic channel surrounding cell mimic devices that were loaded with DNA and other reaction components. Representative fluorescent micrographs of the cell mimic devices taken a different time points are shown. The graph represents the average intensity recorded from 3 individual reaction containers during 3 separate cell-free translation experiments. Error bars representing +/- one standard deviation are shown at 5 hour intervals for clarity.

The EGFP protein concentration in a cell mimic device, as determined from fluorescent imaging and comparison to standards, was found to increase for the first 1-2 hours and then reached a plateau that was maintained for the next 24 hours. Additional engineering of an appropriate fluid delivery system will be needed to consistently carry reactions well beyond 24 hours. The maximum concentration observed in the cell mimic device was 0.35 μM. For comparison, standard 50 μL batch reactions were carried out in microwell plates using the similar reaction conditions. Standard 1:1 ratios of T7S30 Extract to S30 Premix Plus as well as the 2:1 ratio used in the cell mimic devices were examined. The maximum observed GFP concentrations were similar and found to peak at 3.5-4 μM after 3 hours.

5.3.2. Quantifying Protein Synthesis and Release

In order to determine if new protein is continuously synthesized throughout the experiment, the cell free translation reactions were photobleached at selected time points. A recovery in EGFP fluorescence would indicate new protein synthesis (Figure 5.3). In each case, an individual cell mimic device was exposed to 2.5 minutes of excitation light. Fluorescence recovery was observed and reached a maximal value within 1-2 hours. This value was maintained throughout the remainder of the experiment. When bleaching occurred at later time points, a new steady state was observed at a lower signal level. The fluorescence recovery rates are summarized in Figure 5.4. A steady decrease in the recovery rate, which is related to the rate of new synthesis, is observed as reaction time progresses. Some decrease in this rate may be due to damage to proteins besides EGFP

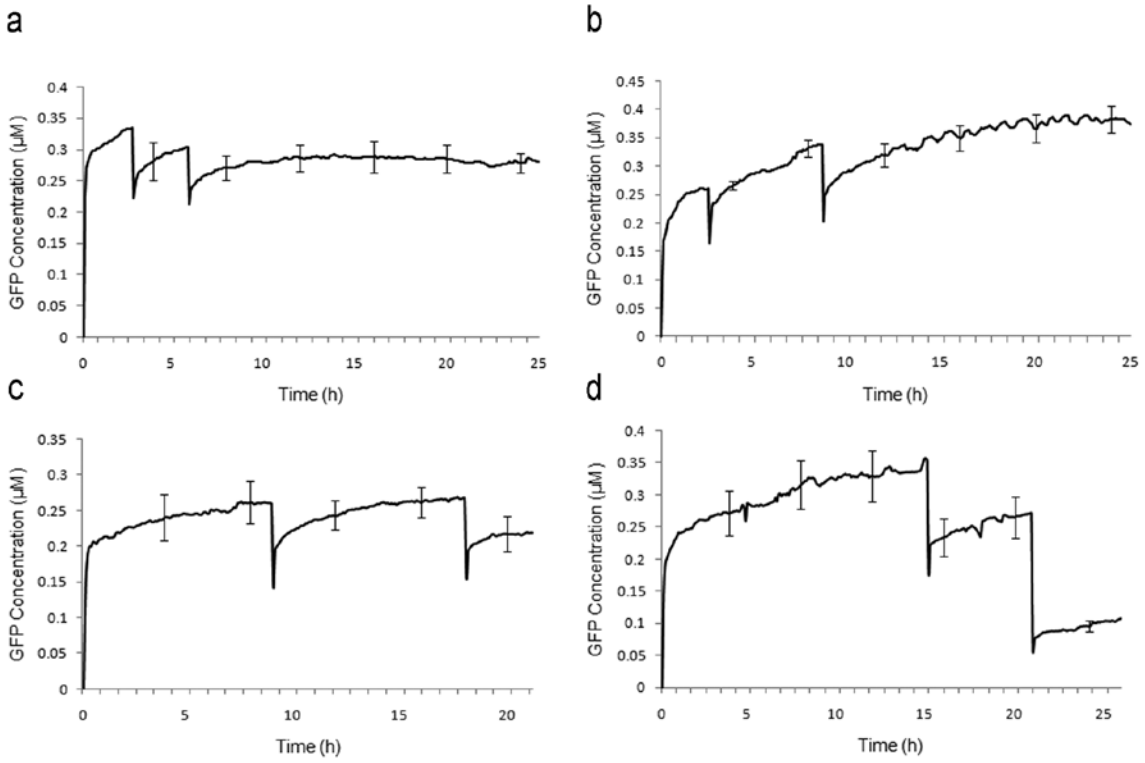

Figure 5-3: Protein synthesis recovery after photobleaching. The protein synthesis reaction in the cell mimic device was photobleached for 2.5 minutes after (a) 3 and 6 hours. (b) 3 and 9 hours. (c) 9 and 18 hours. (d) 15 and 21 hours. The reaction recovered after each photobleach and continued to synthesize EGFP, as indicated by the fluorescent recovery, beyond 24 hours. Each graph represents the protein concentration, corresponding to the observed fluorescence intensity, from three protein synthesis recovery after photobleaching experiments (3 individual devices on 3 separate chips). Error bars represent +/- one standard deviation and are shown at 4 hour intervals for clarity.

as protein synthesis recovery was not observed with bleach pulses that exceeded 3 minutes.

To assess the rate at which EGFP exits the cell mimic device, protein synthesis was blocked by adding chloramphenicol at selected time points. Chloramphenicol inhibits protein biosynthesis by binding to the peptidyl-transferase center of the ribosome and preventing peptide bond formation [212, 213]. Chloramphenicol was introduced by switching to an alternate flow stream, upstream of the fluidic chamber that contains the array of cell mimic devices. In each case 5 μg/mL chloramphenicol was combined with S30 Premix Plus and flowed for 60 minutes. After which, the flow stream was switched back to S30 Premix Plus. Fluorescence images were recorded at five minute intervals throughout the experiment (Figure 5.5). In each case, fluorescence decayed completely within 1 hour and new protein synthesis was not observed, even after removal of chloramphenicol. The rate of protein diffusion out of the device can be related to the fluorescence decay and found to be 5.25 nM/min at either time point. Collectively, the results of the photobleaching and chloramphenicol treatments indicate that protein synthesis is continuous throughout the reaction period and is balanced by diffusion of product from the cell mimic device. For the steady-state conditions observed it can be assumed that the diffusion of EGFP from the device, at a rate of 5.25nM/min, provides a conservative estimate of EGFP production.

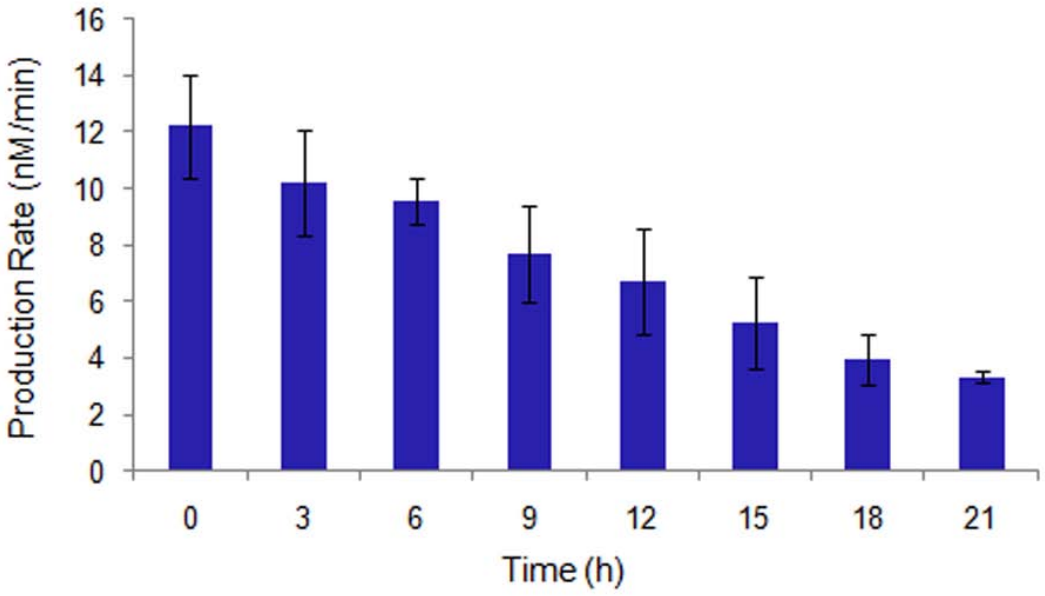

Figure 5-4: Fluorescence recovery rates. A steady decrease in the production rate, the rate of new protein synthesis as measured by the increase in fluorescence, is observed as reaction time progresses. Recovery rates were calculated by measuring the slope of photobleaching recovery curves for the first five minutes following the photobleach pulse. Error bars represent +/- one standard deviation

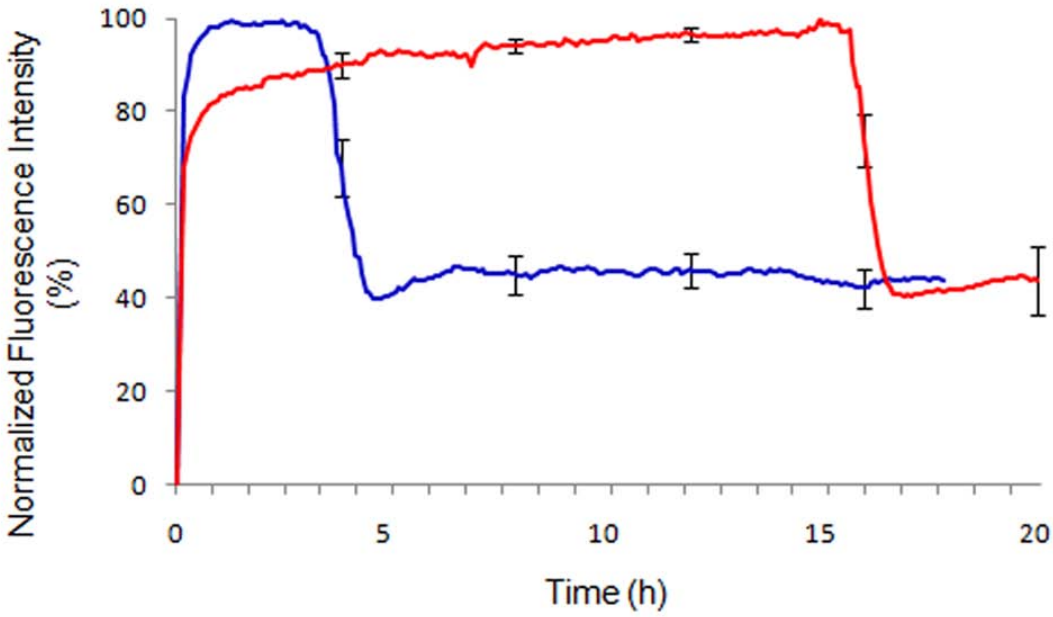

Figure 5-5: Blockage of protein synthesis by antibiotic treatment, . Adding chloramphenicol at selected time points blocked the protein synthesis reaction allowing estimation of protein loss from the device. Chloramphenicol was introduced in the reaction after 3 and 15 hours by switching to an alternate flow stream, upstream of the fluidic chamber that contains the array of cell mimic devices. The graph represents the average normalized intensity recorded from 3 individual reaction containers during 3 separate experiments. Error bars representing +/- one standard deviation are shown at 4 hour intervals for clarity.

5.4. Discussion

Understanding the myriad functions carried out by proteins represents an immense task. Addressing this challenge requires the ability to produce and characterize proteins, and, to this end, microscale protein synthesis is emerging as a valuable tool. By reducing the scale of synthesis, numerous proteins or protein variants can be produced economically and in parallel thereby facilitating functional analyses and comparisons. By preparing proteins in situ, such as in an array format, screening is greatly facilitated, as are applied uses such as integration with electronic or optical sensing methods. Prior demonstrations have employed small volume wells [63, 70, 131, 132, 134], or surface tethered DNA templates [214-217] to self-assemble protein arrays through localized transcription and translation. Microfluidics technology is especially well suited for small-scale synthesis [150] and can facilitate precise mixing of extremely small volumes and on-line detection techniques. Microdroplet-based reaction systems have been described and typically involve an emulsion generator to define the reaction volume [95, 218, 219]. These prior approaches are essentially batch reaction systems and cannot be fed metabolites or have toxic products removed. The implementation of continuous exchange systems at a reduced scale are beginning to emerge [133, 220], but these systems are carried out at relatively large volumes (microliter scale) and lack the ability to effectively exploit the fluid manipulation abilities or functional integration afforded by microfluidics technologies.

The cell mimic device described here enables cell free transcription and translation in a discreet volume while enabling reagent exchange. Continuous protein

production is observed beyond 24 hours and is enabled by the efficient diffusion-based mixing and the feeding/removal of metabolites and harmful byproducts. The ability to optically monitor the reaction and to chemically manipulate it allows for estimation of protein yield and related synthesis rate and material flux (Table 5.1). Protein synthesis after photobleaching measurements, as measured by fluorescence recovery, indicate that EGFP synthesis rates in the device can range from 12.2 nM/min to 3.3 nM/min, which correlates to ~2,300 molec/s to ~600 molec/s (Figure 5.4). These values are conservative estimates, as diffusive loss occurs as protein is produced. The peak synthesis rate occurs upon initiation of the reaction and steadily decreases throughout, as indicated by photobleaching experiments. The decrease in protein synthesis rate may result from accumulation of photo-induced damage to key proteins, or to the loss of essential reagents from the device. Large molecules and complexes, such as the DNA template and ribosomes, are expected to be significantly larger than the limiting aperture of the nanoporous membrane. However, essential translation proteins and the mRNA can be smaller and may escape the device over the long time course of the experiment. Such concerns have been noted as cause for decreased protein yield in conventional scale systems [60, 221, 222].

The membrane was designed to allow for slow release of the protein product. The rate of this release can be estimated from the chemically induced stopping of the reaction afforded by introduction of chloramphenicol. Upon cessation of the reaction, at either 3 or 15 hours after initiation, the loss of fluorescence from the device occurs at a rate of 5.25 nM/min, which correlates to ~1000 molecules/sec. This loss can be attributed to diffusion of EGFP out of the cell mimic device.

The similarity in the rates at 3 and 15 hours indicates that the pores remain open and that flux through the device remains fairly constant throughout the course of the experiment. When compared to the measured protein synthesis rates, product loss rate from the device appears to limit protein production. With this assumption, and that loss rate is constant throughout the experiment, the total amount of protein synthesized and released from a single 19 pl vessel is 0.15 fmoles. Comparison with the conventional scale batch reaction (Table 5.1) indicates that the amount produced is on the order of ~2.2 fold greater on a per volume basis.

Table 5-1: Summary of protein synthesis rates and yields for batch reactions and cell mimic devices.

Format	**Reaction Scale**	**Peak Synthesis Rate / Steady-State Synthesis Rate (nM/min)**	**Equilibrium Concentration (μM)**	**Total Yield**	**Yield (pg)/pL of reaction volume**
Batch	50 μL	32 / NA	3.66 ± 0.40	18.3 nmoles	0.108
Cell Mimic	19 pL	12* / 5.25**	0.35 ± 0.03	0.15 fmoles	0.234

* Peak synthesis rate calculated from the initial slope of protein synthesis curves (Fig. 2)
** Calculated based on percent of EGFP concentration decrease observed in cell mimic devices following chloramphenicol treatment. Under steady-state conditions, this loss rate corresponds to the steady-state EGFP production rate.

The quantitative evaluation of the CFT reactions provides insight into potential approaches to further optimize protein yield. Apparently, protein synthesis can occur at rates several fold higher than that observed under steady state conditions within the cell mimic platform. In comparison with the batch scale reactions, the peak synthesis rate can be 2.7 fold higher than that observed in the cell mimic device. Low protein flux and retention of reaction products within the device may limit protein production as has been observed with larger scale systems [223]. Potentially, increasing the diffusive loss rate, by increasing device permeability while retaining the ability to contain essential translation machinery may improve yield. In the current platform, this can be accomplished simply by changing the number of pores or the thickness of the membrane.

Another source for optimization is addressing the reduction in synthesis rate observed over the course of bleaching experiments. While some of this decrease in production rate may be attributed to photodamage of essential proteins, decreases may also result from diffusive loss of essential translation components. Depending on the intended protein target, tuning the size or chemical characteristics of the nanopore may help to retain essential translation components while facilitating product escape. Alternatively, co-synthesis of these translation components may prolong translation. Biochemical optimizations that improve translational yield can also be considered for enhancing protein production [224, 225]. Additionally, the microfluidic platform offers opportunity for even greater efficiency in protein synthesis. Metabolite conservation may be realized by careful metering of the feed metabolites and by potentially recycling this solution.

Beyond facile monitoring and optimization of reaction systems, the cell mimic platform offers a number of practical advantages. The relatively thin but robust nanoporous membrane that encapsulates the reaction volume can be tuned to facilitate a wide range of exchange rates and reaction volumes. Further, the ability to monolithically fabricate the structure and accompanying microfluidics greatly simplifies membrane integration and can enable creation of large-scale arrays. Such large-scale arrays can serve proteomic applications. Screening of protein activity can be conducted without the complications of using surface tethered reagents. Additionally, the platform can potentially meet the needs of larger scale protein production as required for biologic dosing. Based on the current synthesis yields, large-scale arrays can potentially produce the microgram quantities of biologics needed for a typical dose, while still being realized in a miniaturized platform. Additional functionalities, such as control elements, collection and purification systems, and quality assessment measures can be integrated into a common device and potentially meet future needs in personalized medicine. Moreover, the extended reaction periods afforded by the continuous flow system can make possible the understanding of biochemical networks, such as transcriptional regulation or metabolic pathways, in a cell free context [81, 224-226] This nano-enabled approach to synthetic biology can facilitate a bottom up understanding of complex systems [5, 227].

5.5. Conclusions

Protein synthesis in a cell mimic device has been demonstrated. The picoliter volume of the reaction allows for efficient mixing of reagents while the nanoporous container enables predictable flux of reactants and products. The device is easily integrated with

microfluidics, to reduce and manipulate the surrounding environment, and optical systems to monitor the progress of the reaction. Continuous protein production, for beyond 24 hours, and increased yield, on a per volume basis, over that of a conventional scale batch reaction has been demonstrated. The ability to engineer the volume, flux and environment of the device can facilitate its optimization for a variety of purposes. Production of proteins, based on programmable DNA based instructions, can greatly facilitate the high-throughput screening of protein function and the development and use of therapeutic proteins.

Chapter 6
Conclusions and future directions

6.1. Summary

The work presented here, represents a comprehensive development and investigation of a cell mimic based picoliter volume device that is able to mimic functional aspects of a biological cell, and function as a universal platform to study biochemical reactions within a cellular scale system. The nanoporous, cellular-scale devices have been created and modified using multi-scale fabrication techniques such as electron beam and contact lithography, cryogenic etching and plasma enhanced chemical vapor deposition. Size modification of the device pores allows for the confinement of larger species that represent information or functionality within a reaction system such as DNA, enzymes, proteins and cell free extract components while allowing smaller materials to freely pass through the porous membrane. The nanostructured device has been modified to tune material exchange and we have demonstrated functional size exclusion, fluorescence recovery after photobleaching, molecular containment, protein diffusion and a Lumped Capacitance Model for predicting transient changes in concentration within a nanoporous reaction vessel under moderate external flow.
In addition, the reaction device has been used under continuous-flow to conduct single and coupled enzyme reactions and measure enzyme kinetics. It is integrated with microfluidics, to reduce and manipulate the surrounding environment, and optical systems to monitor the progress of the reaction. Protein synthesis in the nanoporous device has also been demonstrated. Continuous protein production, for beyond 24 hours,

and increased yield, on a per volume basis, over that of a conventional scale batch reaction has been achieved. Many devices have been implemented in parallel, making the platform suitable for larger scale production of a single protein or for simultaneous functional analyses of multiple proteins.

6.2. Future Directions

Although we have demonstrated success with designing, optimizing and applying the nanoporous picoliter volume reaction devices for different biochemical reactions, there will always be a need to improve upon the existing platform. A better control of the pore structures and their selectivity is very important in optimization of the reaction devices. Changing the number of pores can have a direct effect on diffusion and transport of materials through the membrane of the device. The size of the pores can add the physical restriction that is necessary to contain certain size species inside of the device based on the type of application that is being used. However, chemical selectivity, which is achieved by functionalizing the surface of the pores through immobilizing different reactive molecules, could give the device more cell-like characteristics and provide a combined physical and chemical selectivity. The volume of the reaction device can also be optimized to mimic the size of certain cell types or compartments. This can be important in determining the effect of volume and crowding on biochemical reactions. The ability to engineer the volume, flux and environment of the device can facilitate its optimization for a variety of purposes.

The reaction devices may prove useful in fundamental studies of protein-based complex reaction systems and can enable the development of responsive sensors and

therapeutic platforms that rely upon the on-demand conversion or production of biological materials. They could also interact with biological systems, sense abnormal conditions and respond with appropriately dosed reagents.

The cell mimic devices could have a key role in probing biological systems and better understanding self-organization at the micro scale. Production of proteins, based on programmable DNA based instructions, can greatly facilitate the high-throughput screening of protein function and the development and use of therapeutic proteins. Another application for the reaction devices is to study cell-cell signaling. In a microfluidic coculture approach, substances released from cells or cell free transcription/translation confined in an up-stream reaction device can generate a response gradient in the down-stream devices. Cell-cell signaling studies can be used to coordinate biofilm formation at a single or multiple population at a desired cell density or for pattern formation in a mixed population. These studies can give us a better understanding of quorum sensing and biofilm formation. Most known bacteria live in complex surface-bound interactive communities called biofilms [228]. Biofilms consisting of interactive communities are common, however their mode of interaction and development are poorly understood. The picoliter volume reaction devices implemented into a microfluidic chip can serve as platforms to manipulate cell populations and would enable controlled studies of microbial ecosystem dynamics and microscale environmental manipulations. We have engineered cellular circuits, which can be used for unidirectional and bidirectional cell-cell communication network that can coordinate gene expression. The signaling network has been constructed in *E. coli* from components of the LasI/LasR quorum sensing systems found in *Pseudomonas aeruginosa*

[229, 230]. The network consists of a sender and receiver plasmid. The sender plasmid has a LasI gene (sender gene) controlled by a native promoter whereas the receiver plasmid has a LasR gene (receiver gene) also controlled by a native promoter and a GFP gene, which is controlled by a Las promoter. The signaling network works as follows: The sender plasmid is placed in the upstream reaction device and it undergoes cell free transcription/translation. The receiver plasmid is used to transform E.coli cells which are then placed in the downstream reaction device. The LasI protein, which is synthesized from the sender plasmid, uses S-adenosylmethionine (SAM) and 3-oxododecanoyl coenzyme A to form 3-oxododecanoyl homoserine lactone ($3OC_{12}HSL$). The newly formed $3OC_{12}HSL$ then travels downstream of the microfluidic channel. It is small enough to pass through the pores of the downstream reaction device that contains the cells that have been transformed with the receiver plasmid. After it passes through the membrane of the receiver cells, it forms a dimer with the LasR protein that has been synthesized from the receiver plasmid. The newly formed dimer (LasR-$3OC_{12}HSL$) then activates the Las promoter and GFP is allowed to be synthesized (Figure 6.1). Initial plate reader experiments have been performed to determine the amount of $3OC_{12}HSL$ that is required to activate GFP production in cells that have been transformed with the receiver plasmid (Figure 6.2). Other experiments that have already been performed consist of placing the receiver cells inside of a downstream reaction device and filling the channel with different concentrations of $3OC_{12}HSL$. The receiver cells started producing GFP after a few hours (Figure 6.3) with higher concentrations of $3OC_{12}HSL$ activating the receiver cells quicker than lower concentrations. Spatial and temporal behavior of this communication network can be characterized using the present microfluidic device.

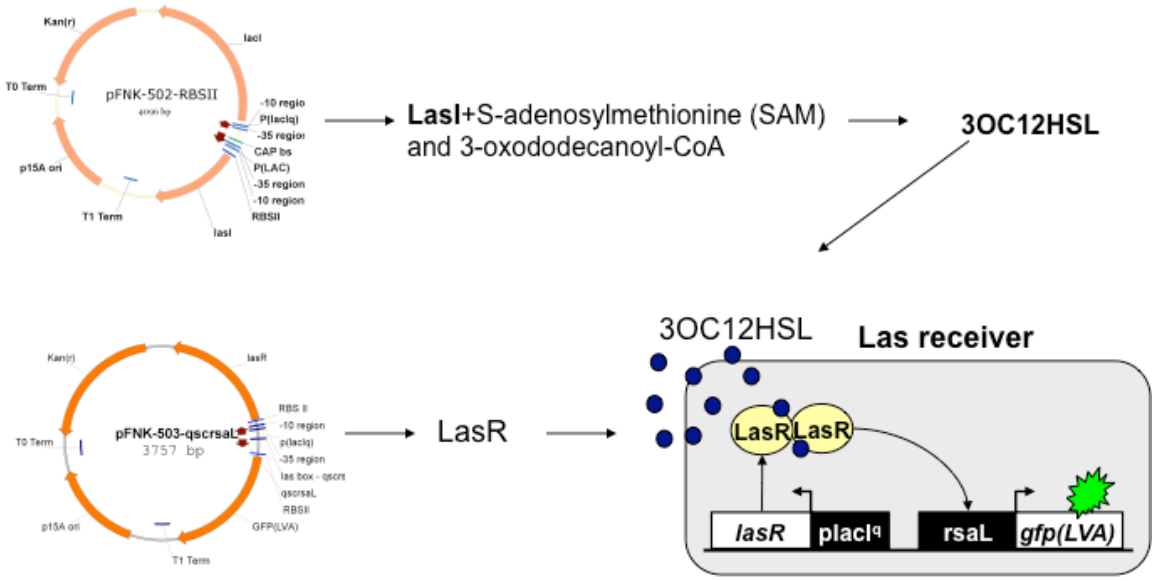

Figure 6-1: Sender-Receiver system in reaction devices. The sender plasmid containing LasI gene is located in the upstream reaction device. The LasI protein catalyzes synthesis of $3OC_{12}HSL$, which diffuses into the cells containing the receiver plasmid and forms a dimmer with LasR. The newly formed dimmer activates the Las promoter and allows for production of GFP.

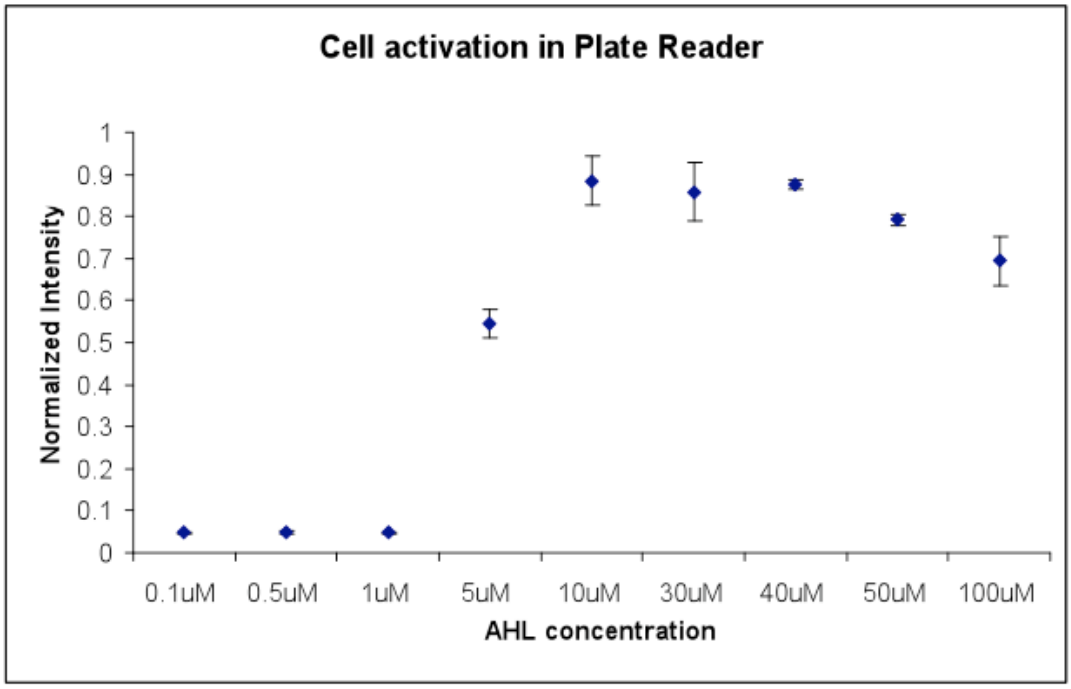

Figure 6-2: Receiver cell activation in a plate reader. Different concentrations of $3OC_{12}HSL$ ranging from 0.1 μM to 100 μM have been used to determine the minimum amount of $3OC_{12}HSL$ necessary to activate GFP production in receiver cells. Each point represents the normalized concentration, corresponding to the observed fluorescence intensity, from three experiments. Error bars represent +/- one standard deviation.

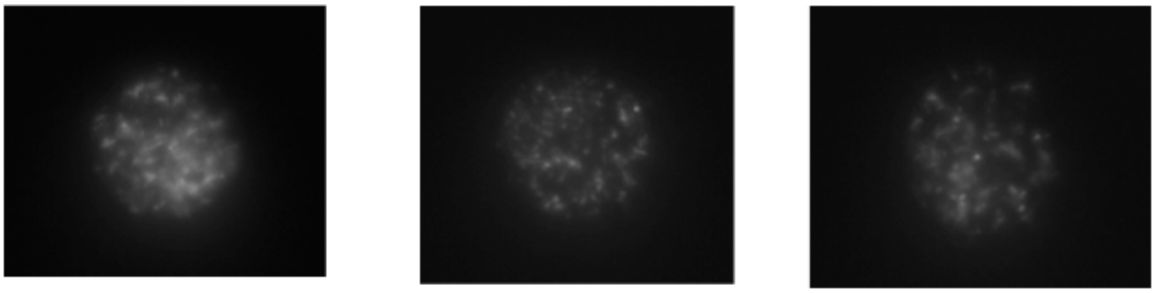

Figure 6-3: Activating receiver cells caged inside of a reaction device. LB media with different concentrations of $3OC_{12}HSL$ has been flown through the microfluidic channel. $3OC_{12}HSL$ has diffused through the pores of the device and through the cell membrane and activated GFP production from the receiver plasmid. Each image represents a different reaction device.

List of References

[1] J. Stelling, U. Sauer, Z. Szallasi, F. J. Doyle, 3rd, and J. Doyle, "Robustness of cellular functions," *Cell*, vol. 118, pp. 675-85, Sep 17 2004.
[2] P. W. Hochachka, "The metabolic implications of intracellular circulation," *Proc Natl Acad Sci U S A*, vol. 96, pp. 12233-9, Oct 26 1999.
[3] B. Hess and A. Mikhailov, "Self-organization in living cells," *Science*, vol. 264, pp. 223-4, Apr 8 1994.
[4] B. Hess and A. Mikhailov, "Microscopic self-organization in living cells: a study of time matching," *Journal of Theoretical Biology*, vol. 176, pp. 181-4, Sep 7 1995.
[5] M. J. Doktycz and M. L. Simpson, "Nano-enabled synthetic biology," *Mol Syst Biol*, vol. 3, p. 125, 2007.
[6] S. A. Benner and A. M. Sismour, "Synthetic biology," *Nat Rev Genet*, vol. 6, pp. 533-43, Jul 2005.
[7] E. Andrianantoandro, S. Basu, D. K. Karig, and R. Weiss, "Synthetic biology: new engineering rules for an emerging discipline," *Mol Syst Biol*, vol. 2, p. 2006 0028, 2006.
[8] B. Hobom, "[Gene surgery: on the threshold of synthetic biology]," *Med Klin*, vol. 75, pp. 834-41, Nov 21 1980.
[9] G. W. Salt, "Use of the Term Emergent-Properties - Comment," *American Naturalist*, vol. 113, pp. 145-148, 1979.
[10] S. A. Benner, "Redesigning Life - Organic-Chemistry and the Evolving Protein," *Chimia*, vol. 41, pp. 142-148, May 1987.
[11] J. W. Szostak, D. P. Bartel, and P. L. Luisi, "Synthesizing life," *Nature*, vol. 409, pp. 387-90, Jan 18 2001.
[12] P. L. Luisi, F. Ferri, and P. Stano, "Approaches to semi-synthetic minimal cells: a review," *Naturwissenschaften*, vol. 93, pp. 1-13, Jan 2006.
[13] K. Kobayashi, S. D. Ehrlich, A. Albertini, G. Amati, K. K. Andersen, M. Arnaud, K. Asai, S. Ashikaga, S. Aymerich, P. Bessieres, F. Boland, S. C. Brignell, S. Bron, K. Bunai, J. Chapuis, L. C. Christiansen, A. Danchin, M. Debarbouille, E. Dervyn, E. Deuerling, K. Devine, S. K. Devine, O. Dreesen, J. Errington, S. Fillinger, S. J. Foster, Y. Fujita, A. Galizzi, R. Gardan, C. Eschevins, T. Fukushima, K. Haga, C. R. Harwood, M. Hecker, D. Hosoya, M. F. Hullo, H. Kakeshita, D. Karamata, Y. Kasahara, F. Kawamura, K. Koga, P. Koski, R. Kuwana, D. Imamura, M. Ishimaru, S. Ishikawa, I. Ishio, D. Le Coq, A. Masson, C. Mauel, R. Meima, R. P. Mellado, A. Moir, S. Moriya, E. Nagakawa, H. Nanamiya, S. Nakai, P. Nygaard, M. Ogura, T. Ohanan, M. O'Reilly, M. O'Rourke, Z. Pragai, H. M. Pooley, G. Rapoport, J. P. Rawlins, L. A. Rivas, C. Rivolta, A. Sadaie, Y. Sadaie, M. Sarvas, T. Sato, H. H. Saxild, E. Scanlan, W. Schumann, J. F. Seegers, J. Sekiguchi, A. Sekowska, S. J. Seror, M. Simon, P. Stragier, R. Studer, H. Takamatsu, T. Tanaka, M. Takeuchi, H. B. Thomaides, V. Vagner, J. M. van Dijl, K. Watabe, A. Wipat, H. Yamamoto, M. Yamamoto, Y. Yamamoto, K. Yamane, K. Yata, K. Yoshida, H. Yoshikawa, U. Zuber, and N. Ogasawara, "Essential Bacillus subtilis genes," *Proc Natl Acad Sci U S A*, vol. 100, pp. 4678-83, Apr 15 2003.

[14] J. I. Glass, N. Assad-Garcia, N. Alperovich, S. Yooseph, M. R. Lewis, M. Maruf, C. A. Hutchison, 3rd, H. O. Smith, and J. C. Venter, "Essential genes of a minimal bacterium," *Proc Natl Acad Sci U S A,* vol. 103, pp. 425-30, Jan 10 2006.
[15] A. C. Forster and G. M. Church, "Towards synthesis of a minimal cell," *Mol Syst Biol,* vol. 2, p. 45, 2006.
[16] A. C. Forster and G. M. Church, "Synthetic biology projects in vitro," *Genome Res,* vol. 17, pp. 1-6, Jan 2007.
[17] G. Posfai, G. Plunkett, 3rd, T. Feher, D. Frisch, G. M. Keil, K. Umenhoffer, V. Kolisnychenko, B. Stahl, S. S. Sharma, M. de Arruda, V. Burland, S. W. Harcum, and F. R. Blattner, "Emergent properties of reduced-genome Escherichia coli," *Science,* vol. 312, pp. 1044-6, May 19 2006.
[18] M. K. Cho, D. Magnus, A. L. Caplan, and D. McGee, "Policy forum: genetics. Ethical considerations in synthesizing a minimal genome," *Science,* vol. 286, pp. 2087, 2089-90, Dec 10 1999.
[19] C. Zimmer, "Genomics. Tinker, tailor: can Venter stitch together a genome from scratch?," *Science,* vol. 299, pp. 1006-7, Feb 14 2003.
[20] S. E. Celniker, D. A. Wheeler, B. Kronmiller, J. W. Carlson, A. Halpern, S. Patel, M. Adams, M. Champe, S. P. Dugan, E. Frise, A. Hodgson, R. A. George, R. A. Hoskins, T. Laverty, D. M. Muzny, C. R. Nelson, J. M. Pacleb, S. Park, B. D. Pfeiffer, S. Richards, E. J. Sodergren, R. Svirskas, P. E. Tabor, K. Wan, M. Stapleton, G. G. Sutton, C. Venter, G. Weinstock, S. E. Scherer, E. W. Myers, R. A. Gibbs, and G. M. Rubin, "Finishing a whole-genome shotgun: release 3 of the Drosophila melanogaster euchromatic genome sequence," *Genome Biol,* vol. 3, p. RESEARCH0079, 2002.
[21] P. Chopra and A. Kamma, "Engineering life through Synthetic Biology," *In Silico Biol,* vol. 6, pp. 401-10, 2006.
[22] C. A. Hutchison, S. N. Peterson, S. R. Gill, R. T. Cline, O. White, C. M. Fraser, H. O. Smith, and J. C. Venter, "Global transposon mutagenesis and a minimal Mycoplasma genome," *Science,* vol. 286, pp. 2165-9, Dec 10 1999.
[23] J. C. Anderson, N. Wu, S. W. Santoro, V. Lakshman, D. S. King, and P. G. Schultz, "An expanded genetic code with a functional quadruplet codon," *Proc Natl Acad Sci U S A,* vol. 101, pp. 7566-71, May 18 2004.
[24] J. Hasty, D. McMillen, and J. J. Collins, "Engineered gene circuits," *Nature,* vol. 420, pp. 224-30, Nov 14 2002.
[25] D. Sprinzak and M. B. Elowitz, "Reconstruction of genetic circuits," *Nature,* vol. 438, pp. 443-8, Nov 24 2005.
[26] N. J. Guido, X. Wang, D. Adalsteinsson, D. McMillen, J. Hasty, C. R. Cantor, T. C. Elston, and J. J. Collins, "A bottom-up approach to gene regulation," *Nature,* vol. 439, pp. 856-60, Feb 16 2006.
[27] P. Ball, "Synthetic biology for nanotechnology," *Nanotechnology,* vol. 16, pp. R1-R8, Jan 2005.
[28] M. L. Simpson, G. S. Sayler, J. T. Fleming, and B. Applegate, "Whole-cell biocomputing," *Trends Biotechnol,* vol. 19, pp. 317-23, Aug 2001.
[29] M. B. Elowitz and S. Leibler, "A synthetic oscillatory network of transcriptional regulators," *Nature,* vol. 403, pp. 335-8, Jan 20 2000.

[30] T. S. Gardner, C. R. Cantor, and J. J. Collins, "Construction of a genetic toggle switch in Escherichia coli," *Nature,* vol. 403, pp. 339-42, Jan 20 2000.
[31] R. Jungmann, S. Renner, and F. C. Simmel, "From DNA nanotechnology to synthetic biology," *HFSP J,* vol. 2, pp. 99-109, Apr 2008.
[32] M. Koffas, C. Roberge, K. Lee, and G. Stephanopoulos, "Metabolic engineering," *Annu Rev Biomed Eng,* vol. 1, pp. 535-57, 1999.
[33] G. N. Vemuri and A. A. Aristidou, "Metabolic engineering in the -omics era: elucidating and modulating regulatory networks," *Microbiol Mol Biol Rev,* vol. 69, pp. 197-216, Jun 2005.
[34] M. L. Yarmush and S. Banta, "Metabolic engineering: advances in modeling and intervention in health and disease," *Annu Rev Biomed Eng,* vol. 5, pp. 349-81, 2003.
[35] L. C. You, R. S. Cox, R. Weiss, and F. H. Arnold, "Programmed population control by cell-cell communication and regulated killing," *Nature,* vol. 428, pp. 868-871, Apr 22 2004.
[36] D. Karig and R. Weiss, "Signal-amplifying genetic circuit enables in vivo observation of weak promoter activation in the Rhl quorum sensing system," *Biotechnol Bioeng,* vol. 89, pp. 709-18, Mar 20 2005.
[37] V. Noireaux, R. Bar-Ziv, and A. Libchaber, "Principles of cell-free genetic circuit assembly," *Proc Natl Acad Sci U S A,* vol. 100, pp. 12672-7, Oct 28 2003.
[38] B. A. Grzybowski, K. J. M. Bishop, C. J. Campbell, M. Fialkowski, and S. K. Smoukov, "Micro- and nanotechnology via reaction-diffusion," *Soft Matter,* vol. 1, pp. 114-128, Jul 14 2005.
[39] A. Pohorille and D. Deamer, "Artificial cells: prospects for biotechnology," *Trends Biotechnol,* vol. 20, pp. 123-8, Mar 2002.
[40] T. M. Chang, "Artificial cells for cell and organ replacements," *Artif Organs,* vol. 28, pp. 265-70, Mar 2004.
[41] V. Noireaux, R. Bar-Ziv, J. Godefroy, H. Salman, and A. Libchaber, "Toward an artificial cell based on gene expression in vesicles," *Phys Biol,* vol. 2, pp. P1-8, Sep 2005.
[42] D. S. Tawfik and A. D. Griffiths, "Man-made cell-like compartments for molecular evolution," *Nat Biotechnol,* vol. 16, pp. 652-6, Jul 1998.
[43] J. Song, Q. Cheng, S. M. Zhu, and R. C. Stevens, ""Smart" materials for biosensing devices: Cell-mimicking supramolecular assemblies and colorimetric detection of pathogenic agents," *Biomedical Microdevices,* vol. 4, pp. 213-221, Jul 2002.
[44] V. Noireaux and A. Libchaber, "A vesicle bioreactor as a step toward an artificial cell assembly," *Proc Natl Acad Sci U S A,* vol. 101, pp. 17669-74, Dec 21 2004.
[45] G. J. Pielak, "A model of intracellular organization," *Proc Natl Acad Sci U S A,* vol. 102, pp. 5901-2, Apr 26 2005.
[46] P. C. Marijuan, "Enzymes, artificial cells and the nature of biological information," *Biosystems,* vol. 35, pp. 167-70, 1995.
[47] T. Misteli, "The concept of self-organization in cellular architecture," *J Cell Biol,* vol. 155, pp. 181-5, Oct 15 2001.

[48] M. S. Long, C. D. Jones, M. R. Helfrich, L. K. Mangeney-Slavin, and C. D. Keating, "Dynamic microcompartmentation in synthetic cells," *Proc Natl Acad Sci U S A,* vol. 102, pp. 5920-5, Apr 26 2005.
[49] D. Deamer, "A giant step towards artificial life?," *Trends Biotechnol,* vol. 23, pp. 336-8, Jul 2005.
[50] T. Sawasaki, Y. Hasegawa, M. Tsuchimochi, N. Kamura, T. Ogasawara, T. Kuroita, and Y. Endo, "A bilayer cell-free protein synthesis system for high-throughput screening of gene products," *FEBS Lett,* vol. 514, pp. 102-5, Mar 6 2002.
[51] D. A. Vinarov, C. L. Loushin Newman, and J. L. Markley, "Wheat germ cell-free platform for eukaryotic protein production," *FEBS J,* vol. 273, pp. 4160-9, Sep 2006.
[52] M. J. Heller, "DNA microarray technology: devices, systems, and applications," *Annu Rev Biomed Eng,* vol. 4, pp. 129-53, 2002.
[53] J. Khandurina and A. Guttman, "Microchip-based high-throughput screening analysis of combinatorial libraries," *Curr Opin Chem Biol,* vol. 6, pp. 359-66, Jun 2002.
[54] J. Wolcke and D. Ullmann, "Miniaturized HTS technologies - uHTS," *Drug Discov Today,* vol. 6, pp. 637-646, Jun 1 2001.
[55] L. Jermutus, L. A. Ryabova, and A. Pluckthun, "Recent advances in producing and selecting functional proteins by using cell-free translation," *Curr Opin Biotechnol,* vol. 9, pp. 534-48, Oct 1998.
[56] F. Katzen, G. Chang, and W. Kudlicki, "The past, present and future of cell-free protein synthesis," *Trends Biotechnol,* vol. 23, pp. 150-6, Mar 2005.
[57] M. Nirenberg, "Historical review: Deciphering the genetic code--a personal account," *Trends Biochem Sci,* vol. 29, pp. 46-54, Jan 2004.
[58] M. C. Jewett and J. R. Swartz, "Mimicking the Escherichia coli cytoplasmic environment activates long-lived and efficient cell-free protein synthesis," *Biotechnol Bioeng,* vol. 86, pp. 19-26, Apr 5 2004.
[59] T. Kigawa and S. Yokoyama, "A continuous cell-free protein synthesis system for coupled transcription-translation," *J Biochem,* vol. 110, pp. 166-8, Aug 1991.
[60] D. M. Kim, T. Kigawa, C. Y. Choi, and S. Yokoyama, "A highly efficient cell-free protein synthesis system from Escherichia coli," *Eur J Biochem,* vol. 239, pp. 881-6, Aug 1 1996.
[61] M. W. Nirenberg and J. H. Matthaei, "The dependence of cell-free protein synthesis in E. coli upon naturally occurring or synthetic polyribonucleotides," *Proc Natl Acad Sci U S A,* vol. 47, pp. 1588-602, Oct 15 1961.
[62] N. Nishimura, Y. Kitaoka, A. Mimura, and Y. Takahara, "Continuous Protein-Synthesis System with Escherichia-Coli S30 Extract Containing Endogenous-T7 Rna-Polymerase," *Biotechnology Letters,* vol. 15, pp. 785-790, Aug 1993.
[63] P. Siuti, S. T. Retterer, C. K. Choi, J. D. Fowlkes, and M. J. Doktycz, "Cell Free Translation in Engineered Picoliter Volume Containers," *2009 First Annual Ornl Biomedical Science & Engineering Conference: Exploring the Intersections of Interdisciplinary Biomedical Research,* pp. 80-83
150, 2009.

[64] A. S. Spirin, "Ribosome Preparation and Cell-Free Protein-Synthesis," *Ribosome,* pp. 56-70
678, 1990.
[65] G. Zubay, M. Lederman, and J. K. DeVries, "DNA-directed peptide synthesis. 3. Repression of beta-galactosidase synthesis and inhibition of repressor by inducer in a cell-free system," *Proc Natl Acad Sci U S A,* vol. 58, pp. 1669-75, Oct 1967.
[66] J. Yang, G. Kanter, A. Voloshin, N. Michel-Reydellet, H. Velkeen, R. Levy, and J. R. Swartz, "Rapid expression of vaccine proteins for B-cell lymphoma in a cell-free system," *Biotechnol Bioeng,* vol. 89, pp. 503-11, Mar 5 2005.
[67] A. R. Goerke and J. R. Swartz, "Development of cell-free protein synthesis platforms for disulfide bonded proteins," *Biotechnol Bioeng,* vol. 99, pp. 351-67, Feb 1 2008.
[68] G. Kanter, J. Yang, A. Voloshin, S. Levy, J. R. Swartz, and R. Levy, "Cell-free production of scFv fusion proteins: an efficient approach for personalized lymphoma vaccines," *Blood,* vol. 109, pp. 3393-9, Apr 15 2007.
[69] Y. Elbaz, S. Steiner-Mordoch, T. Danieli, and S. Schuldiner, "In vitro synthesis of fully functional EmrE, a multidrug transporter, and study of its oligomeric state," *Proc Natl Acad Sci U S A,* vol. 101, pp. 1519-24, Feb 10 2004.
[70] Q. Mei, C. K. Fredrickson, S. Jin, and Z. H. Fan, "Toxin detection by a miniaturized in vitro protein expression array," *Anal Chem,* vol. 77, pp. 5494-500, Sep 1 2005.
[71] A. L. Grosvenor, A. Feltus, R. C. Conover, S. Daunert, and K. W. Anderson, "Development of binding assays in microfabricated picoliter vials: an assay for biotin," *Anal Chem,* vol. 72, pp. 2590-4, Jun 1 2000.
[72] D. M. Vriezema, M. Comellas Aragones, J. A. Elemans, J. J. Cornelissen, A. E. Rowan, and R. J. Nolte, "Self-assembled nanoreactors," *Chem Rev,* vol. 105, pp. 1445-89, Apr 2005.
[73] J. E. Barton and T. W. Odom, "Mass-limited growth in zeptoliter beakers: A general approach for the synthesis of nanocrystals," *Nano Letters,* vol. 4, pp. 1525-1528, Aug 2004.
[74] M. Karlsson, M. Davidson, R. Karlsson, A. Karlsson, J. Bergenholtz, Z. Konkoli, A. Jesorka, T. Lobovkina, J. Hurtig, M. Voinova, and O. Orwar, "Biomimetic nanoscale reactors and networks," *Annu Rev Phys Chem,* vol. 55, pp. 613-49, 2004.
[75] A. Napoli, M. Valentini, N. Tirelli, M. Muller, and J. A. Hubbell, "Oxidation-responsive polymeric vesicles," *Nat Mater,* vol. 3, pp. 183-9, Mar 2004.
[76] A. Ranquin, W. Versees, W. Meier, J. Steyaert, and P. Van Gelder, "Therapeutic nanoreactors: combining chemistry and biology in a novel triblock copolymer drug delivery system," *Nano Lett,* vol. 5, pp. 2220-4, Nov 2005.
[77] A. Napoli, M. J. Boerakker, N. Tirelli, R. J. Nolte, N. A. Sommerdijk, and J. A. Hubbell, "Glucose-oxidase based self-destructing polymeric vesicles," *Langmuir,* vol. 20, pp. 3487-91, Apr 27 2004.
[78] P. Walde and S. Ichikawa, "Enzymes inside lipid vesicles: preparation, reactivity and applications," *Biomol Eng,* vol. 18, pp. 143-77, Oct 31 2001.

[79] A. D. Bangham, M. M. Standish, and J. C. Watkins, "Diffusion of univalent ions across the lamellae of swollen phospholipids," *J Mol Biol,* vol. 13, pp. 238-52, Aug 1965.
[80] T. Oberholzer and P. L. Luisi, "The use of liposomes for constructing cell models," *Journal of Biological Physics,* vol. 28, pp. 733-744, 2002.
[81] Y. Shimizu, A. Inoue, Y. Tomari, T. Suzuki, T. Yokogawa, K. Nishikawa, and T. Ueda, "Cell-free translation reconstituted with purified components," *Nat Biotechnol,* vol. 19, pp. 751-5, Aug 2001.
[82] A. S. Spirin, V. I. Baranov, L. A. Ryabova, S. Y. Ovodov, and Y. B. Alakhov, "A continuous cell-free translation system capable of producing polypeptides in high yield," *Science,* vol. 242, pp. 1162-4, Nov 25 1988.
[83] S. M. Nomura, K. Tsumoto, T. Hamada, K. Akiyoshi, Y. Nakatani, and K. Yoshikawa, "Gene expression within cell-sized lipid vesicles," *Chembiochem,* vol. 4, pp. 1172-5, Nov 7 2003.
[84] T. Sunami, K. Sato, T. Matsuura, K. Tsukada, I. Urabe, and T. Yomo, "Femtoliter compartment in liposomes for in vitro selection of proteins," *Anal Biochem,* vol. 357, pp. 128-36, Oct 1 2006.
[85] W. Yu, K. Sato, M. Wakabayashi, T. Nakaishi, E. P. Ko-Mitamura, Y. Shima, I. Urabe, and T. Yomo, "Synthesis of functional protein in liposome," *J Biosci Bioeng,* vol. 92, pp. 590-3, 2001.
[86] K. Ishikawa, K. Sato, Y. Shima, I. Urabe, and T. Yomo, "Expression of a cascading genetic network within liposomes," *FEBS Lett,* vol. 576, pp. 387-90, Oct 22 2004.
[87] M. Yoshimoto, S. Wang, K. Fukunaga, P. Walde, R. Kuboi, and K. Nakao, "Preparation and characterization of reactive and stable glucose oxidase-containing liposomes modulated with detergent," *Biotechnol Bioeng,* vol. 81, pp. 695-704, Mar 20 2003.
[88] S. Wang, M. Yoshimoto, K. Fukunaga, and K. Nakao, "Optimal covalent immobilization of glucose oxidase-containing liposomes for highly stable biocatalyst in bioreactor," *Biotechnol Bioeng,* vol. 83, pp. 444-53, Aug 20 2003.
[89] I. Petrikovics, K. Hong, G. Omburo, Q. Z. Hu, L. Pei, W. D. McGuinn, D. Sylvester, C. Tamulinas, D. Papahadjopoulos, J. C. Jaszberenyi, and J. L. Way, "Antagonism of paraoxon intoxication by recombinant phosphotriesterase encapsulated within sterically stabilized liposomes," *Toxicol Appl Pharmacol,* vol. 156, pp. 56-63, Apr 1 1999.
[90] R. J. Y. Ho, B. T. Rouse, and L. Huang, "Interactions of Target-Sensitive Immunoliposomes with Herpes-Simplex Virus - the Foundation of a Sensitive Immunoliposome Assay for the Virus," *Journal of Biological Chemistry,* vol. 262, pp. 13979-13984, Oct 15 1987.
[91] F. J. Ghadessy, J. L. Ong, and P. Holliger, "Directed evolution of polymerase function by compartmentalized self-replication," *Proc Natl Acad Sci U S A,* vol. 98, pp. 4552-7, Apr 10 2001.
[92] A. D. Griffiths and D. S. Tawfik, "Man-made enzymes--from design to in vitro compartmentalisation," *Curr Opin Biotechnol,* vol. 11, pp. 338-53, Aug 2000.

[93] A. D. Griffiths and D. S. Tawfik, "Directed evolution of an extremely fast phosphotriesterase by in vitro compartmentalization," *EMBO J,* vol. 22, pp. 24-35, Jan 2 2003.
[94] A. Musyanovych, V. Mailander, and K. Landfester, "Miniemulsion droplets as single molecule nanoreactors for polymerase chain reaction," *Biomacromolecules,* vol. 6, pp. 1824-8, Jul-Aug 2005.
[95] P. S. Dittrich, M. Jahnz, and P. Schwille, "A new embedded process for compartmentalized cell-free protein expression and on-line detection in microfluidic devices," *Chembiochem,* vol. 6, pp. 811-4, May 2005.
[96] D. Dressman, H. Yan, G. Traverso, K. W. Kinzler, and B. Vogelstein, "Transforming single DNA molecules into fluorescent magnetic particles for detection and enumeration of genetic variations," *Proc Natl Acad Sci U S A,* vol. 100, pp. 8817-22, Jul 22 2003.
[97] M. Margulies, M. Egholm, W. E. Altman, S. Attiya, J. S. Bader, L. A. Bemben, J. Berka, M. S. Braverman, Y. J. Chen, Z. Chen, S. B. Dewell, L. Du, J. M. Fierro, X. V. Gomes, B. C. Godwin, W. He, S. Helgesen, C. H. Ho, G. P. Irzyk, S. C. Jando, M. L. Alenquer, T. P. Jarvie, K. B. Jirage, J. B. Kim, J. R. Knight, J. R. Lanza, J. H. Leamon, S. M. Lefkowitz, M. Lei, J. Li, K. L. Lohman, H. Lu, V. B. Makhijani, K. E. McDade, M. P. McKenna, E. W. Myers, E. Nickerson, J. R. Nobile, R. Plant, B. P. Puc, M. T. Ronan, G. T. Roth, G. J. Sarkis, J. F. Simons, J. W. Simpson, M. Srinivasan, K. R. Tartaro, A. Tomasz, K. A. Vogt, G. A. Volkmer, S. H. Wang, Y. Wang, M. P. Weiner, P. Yu, R. F. Begley, and J. M. Rothberg, "Genome sequencing in microfabricated high-density picolitre reactors," *Nature,* vol. 437, pp. 376-80, Sep 15 2005.
[98] J. Shendure, G. J. Porreca, N. B. Reppas, X. Lin, J. P. McCutcheon, A. M. Rosenbaum, M. D. Wang, K. Zhang, R. D. Mitra, and G. M. Church, "Accurate multiplex polony sequencing of an evolved bacterial genome," *Science,* vol. 309, pp. 1728-32, Sep 9 2005.
[99] A. Aharoni, G. Amitai, K. Bernath, S. Magdassi, and D. S. Tawfik, "High-throughput screening of enzyme libraries: thiolactonases evolved by fluorescence-activated sorting of single cells in emulsion compartments," *Chem Biol,* vol. 12, pp. 1281-9, Dec 2005.
[100] A. Aharoni, A. D. Griffiths, and D. S. Tawfik, "High-throughput screens and selections of enzyme-encoding genes," *Curr Opin Chem Biol,* vol. 9, pp. 210-6, Apr 2005.
[101] K. Bernath, M. Hai, E. Mastrobattista, A. D. Griffiths, S. Magdassi, and D. S. Tawfik, "In vitro compartmentalization by double emulsions: sorting and gene enrichment by fluorescence activated cell sorting," *Anal Biochem,* vol. 325, pp. 151-7, Feb 1 2004.
[102] A. V. Pietrini and P. L. Luisi, "Cell-free protein synthesis through solubilisate exchange in water/oil emulsion compartments," *Chembiochem,* vol. 5, pp. 1055-62, Aug 6 2004.
[103] M. Isalan, C. Lemerle, and L. Serrano, "Engineering gene networks to emulate Drosophila embryonic pattern formation," *PLoS Biol,* vol. 3, p. e64, Mar 2005.

[104] M. C. Roco, "Nanotechnology: convergence with modern biology and medicine," *Curr Opin Biotechnol,* vol. 14, pp. 337-46, Jun 2003.
[105] A. V. Davis, R. M. Yeh, and K. N. Raymond, "Supramolecular assembly dynamics," *Proc Natl Acad Sci U S A,* vol. 99, pp. 4793-6, Apr 16 2002.
[106] G. M. Whitesides and M. Boncheva, "Beyond molecules: self-assembly of mesoscopic and macroscopic components," *Proc Natl Acad Sci U S A,* vol. 99, pp. 4769-74, Apr 16 2002.
[107] M. N. Moore, "Biocomplexity: the post-genome challenge in ecotoxicology," *Aquat Toxicol,* vol. 59, pp. 1-15, Sep 10 2002.
[108] P. J. Borm, "Particle toxicology: from coal mining to nanotechnology," *Inhal Toxicol,* vol. 14, pp. 311-24, Mar 2002.
[109] J. J. Schmidt and C. D. Montemagno, "Using machines in cells," *Drug Discov Today,* vol. 7, pp. 500-3, May 1 2002.
[110] A. Ishijima and T. Yanagida, "Single molecule nanobioscience," *Trends Biochem Sci,* vol. 26, pp. 438-44, Jul 2001.
[111] D. J. Muller, H. Janovjak, T. Lehto, L. Kuerschner, and K. Anderson, "Observing structure, function and assembly of single proteins by AFM," *Prog Biophys Mol Biol,* vol. 79, pp. 1-43, May-Jul 2002.
[112] G. Baneyx, L. Baugh, and V. Vogel, "Coexisting conformations of fibronectin in cell culture imaged using fluorescence resonance energy transfer," *Proc Natl Acad Sci U S A,* vol. 98, pp. 14464-8, Dec 4 2001.
[113] R. F. Fox and M. H. Choi, "Rectified Brownian motion and kinesin motion along microtubules," *Phys Rev E Stat Nonlin Soft Matter Phys,* vol. 63, p. 051901, May 2001.
[114] S. Bhattacharya, J. S. Jang, L. J. Yang, D. Akin, and R. Bashir, "Biomems and nanotechnology-based approaches for rapid detection of biological entities," *Journal of Rapid Methods and Automation in Microbiology,* vol. 15, pp. 1-32, Mar 2007.
[115] G. Kodis, Herrero, Ch., Palacios, R., Marino-Ochoa, E., Gould, S., Garza, L., Grondelle, R., Gust, D., Moore, T.A., Moore, A.L., Kennis, J.T.M.,, "Light Harvesting and Photoprotective Functions of Carotenoids in Compact Artificial Photosynthetic Antenna Designs," *The Journal of Physical Chemistry B,* vol. 108, pp. 414-425, 2004.
[116] M. Bazhenov, M. Stopfer, M. Rabinovich, H. D. Abarbanel, T. J. Sejnowski, and G. Laurent, "Model of cellular and network mechanisms for odor-evoked temporal patterning in the locust antennal lobe," *Neuron,* vol. 30, pp. 569-81, May 2001.
[117] J. Li, D. Stein, C. McMullan, D. Branton, M. J. Aziz, and J. A. Golovchenko, "Ion-beam sculpting at nanometre length scales," *Nature,* vol. 412, pp. 166-9, Jul 12 2001.
[118] A. J. Storm, J. H. Chen, X. S. Ling, H. W. Zandbergen, and C. Dekker, "Fabrication of solid-state nanopores with single-nanometre precision," *Nat Mater,* vol. 2, pp. 537-40, Aug 2003.
[119] C. R. Martin, "Nanomaterials: a membrane-based synthetic approach," *Science,* vol. 266, pp. 1961-6, Dec 23 1994.

[120] L. R. Huang, E. C. Cox, R. H. Austin, and J. C. Sturm, "Continuous particle separation through deterministic lateral displacement," *Science,* vol. 304, pp. 987-990, May 14 2004.
[121] B. L. Fletcher, T. E. McKnight, J. D. Fowlkes, D. P. Allison, M. L. Simpson, and M. J. Doktycz, "Controlling the Dimensions of Carbon Nanofiber Structures through the Electropolymerization of Pyrrole," *Synth Met,* vol. 157, pp. 282-289, Apr 2007.
[122] B. L. Fletcher, S. T. Retterer, T. E. McKnight, A. V. Melechko, J. D. Fowlkes, M. L. Simpson, and M. J. Doktycz, "Actuatable membranes based on polypyrrole-coated vertically aligned carbon nanofibers," *Acs Nano,* vol. 2, pp. 247-54, Feb 2008.
[123] D. Gust, T. A. Moore, and A. L. Moore, "Mimicking photosynthetic solar energy transduction," *Acc Chem Res,* vol. 34, pp. 40-8, Jan 2001.
[124] G. H. Seong, J. Heo, and R. M. Crooks, "Measurement of enzyme kinetics using a continuous-flow microfluidic system," *Anal Chem,* vol. 75, pp. 3161-7, Jul 1 2003.
[125] A. M. Girelli and E. Mattei, "Application of immobilized enzyme reactor in on-line high performance liquid chromatography: a review," *J Chromatogr B Analyt Technol Biomed Life Sci,* vol. 819, pp. 3-16, May 5 2005.
[126] L. Ma, X. Gong, and E. S. Yeung, "Combinatorial screening of enzyme activity by using multiplexed capillary electrophoresis," *Anal Chem,* vol. 72, pp. 3383-7, Jul 15 2000.
[127] P. L. Urban, D. M. Goodall, and N. C. Bruce, "Enzymatic microreactors in chemical analysis and kinetic studies," *Biotechnol Adv,* vol. 24, pp. 42-57, Jan-Feb 2006.
[128] N. J. Gleason and J. D. Carbeck, "Measurement of enzyme kinetics using microscale steady-state kinetic analysis," *Langmuir,* vol. 20, pp. 6374-81, Jul 20 2004.
[129] Y. Rondelez, G. Tresset, K. V. Tabata, H. Arata, H. Fujita, S. Takeuchi, and H. Noji, "Microfabricated arrays of femtoliter chambers allow single molecule enzymology," *Nat Biotechnol,* vol. 23, pp. 361-5, Mar 2005.
[130] D. M. Rissin and D. R. Walt, "Digital concentration readout of single enzyme molecules using femtoliter arrays and Poisson statistics," *Nano Lett,* vol. 6, pp. 520-3, Mar 2006.
[131] P. Angenendt, L. Nyarsik, W. Szaflarski, J. Glokler, K. H. Nierhaus, H. Lehrach, D. J. Cahill, and A. Lueking, "Cell-free protein expression and functional assay in nanowell chip format," *Anal Chem,* vol. 76, pp. 1844-9, Apr 1 2004.
[132] T. Kinpara, R. Mizuno, Y. Murakami, M. Kobayashi, S. Yamaura, Q. Hasan, Y. Morita, H. Nakano, T. Yamane, and E. Tamiya, "A picoliter chamber array for cell-free protein synthesis," *J Biochem,* vol. 136, pp. 149-54, Aug 2004.
[133] Q. Mei, C. K. Fredrickson, A. Simon, R. Khnouf, and Z. H. Fan, "Cell-free protein synthesis in microfluidic array devices," *Biotechnol Prog,* vol. 23, pp. 1305-11, Nov-Dec 2007.
[134] M. Tabuchi, M. Hino, Y. Shinohara, and Y. Baba, "Cell-free protein synthesis on a microchip," *Proteomics,* vol. 2, pp. 430-5, Apr 2002.

[135] P. Angenendt, H. Lehrach, J. Kreutzberger, and J. Glokler, "Subnanoliter enzymatic assays on microarrays," *Proteomics,* vol. 5, pp. 420-5, Feb 2005.
[136] M. M. C. Cheng, G. Cuda, Y. L. Bunimovich, M. Gaspari, J. R. Heath, H. D. Hill, C. A. Mirkin, A. J. Nijdam, R. Terracciano, T. Thundat, and M. Ferrari, "Nanotechnologies for biomolecular detection and medical diagnostics," *Current Opinion in Chemical Biology,* vol. 10, pp. 11-19, Feb 2006.
[137] M. M. Cheng, G. Cuda, Y. L. Bunimovich, M. Gaspari, J. R. Heath, H. D. Hill, C. A. Mirkin, A. J. Nijdam, R. Terracciano, T. Thundat, and M. Ferrari, "Nanotechnologies for biomolecular detection and medical diagnostics," *Curr Opin Chem Biol,* vol. 10, pp. 11-9, Feb 2006.
[138] D. Hulsenberg, "Glasses for microsystems technology," *Microelectronics Journal,* vol. 28, pp. 419-432, May 1997.
[139] D. J. Beebe, G. A. Mensing, and G. M. Walker, "Physics and applications of microfluidics in biology," *Annu Rev Biomed Eng,* vol. 4, pp. 261-86, 2002.
[140] M. A. Unger, H. P. Chou, T. Thorsen, A. Scherer, and S. R. Quake, "Monolithic microfabricated valves and pumps by multilayer soft lithography," *Science,* vol. 288, pp. 113-6, Apr 7 2000.
[141] S. R. Quake and A. Scherer, "From micro- to nanofabrication with soft materials," *Science,* vol. 290, pp. 1536-40, Nov 24 2000.
[142] G. M. Whitesides, E. Ostuni, S. Takayama, X. Jiang, and D. E. Ingber, "Soft lithography in biology and biochemistry," *Annu Rev Biomed Eng,* vol. 3, pp. 335-73, 2001.
[143] H. Hillborg and U. W. Gedde, "Hydrophobicity recovery of polydimethylsiloxane after exposure to corona discharges," *Polymer,* vol. 39, pp. 1991-1998, May 1998.
[144] D. C. Duffy, J. C. McDonald, O. J. A. Schueller, and G. M. Whitesides, "Rapid prototyping of microfluidic systems in poly(dimethylsiloxane)," *Analytical Chemistry,* vol. 70, pp. 4974-4984, Dec 1 1998.
[145] R. Karnik, K. Castelino, and A. Majumdar, "Field-effect control of protein transport in a nanofluidic transistor circuit," *Applied Physics Letters,* vol. 88, pp. -, Mar 20 2006.
[146] J. R. Anderson, D. T. Chiu, R. J. Jackman, O. Cherniavskaya, J. C. McDonald, H. Wu, S. H. Whitesides, and G. M. Whitesides, "Fabrication of topologically complex three-dimensional microfluidic systems in PDMS by rapid prototyping," *Anal Chem,* vol. 72, pp. 3158-64, Jul 15 2000.
[147] L. Martynova, L. E. Locascio, M. Gaitan, G. W. Kramer, R. G. Christensen, and W. A. MacCrehan, "Fabrication of plastic microfluid channels by imprinting methods," *Anal Chem,* vol. 69, pp. 4783-9, Dec 1 1997.
[148] A. C. Henry, T. J. Tutt, M. Galloway, Y. Y. Davidson, C. S. McWhorter, S. A. Soper, and R. L. McCarley, "Surface modification of poly(methyl methacrylate) used in the fabrication of microanalytical devices," *Analytical Chemistry,* vol. 72, pp. 5331-5337, Nov 1 2000.
[149] D. N. Breslauer, P. J. Lee, and L. P. Lee, "Microfluidics-based systems biology," *Mol Biosyst,* vol. 2, pp. 97-112, Feb 2006.
[150] P. S. Dittrich and A. Manz, "Lab-on-a-chip: microfluidics in drug discovery," *Nat Rev Drug Discov,* vol. 5, pp. 210-8, Mar 2006.

[151] H. Becker and C. Gartner, "Polymer microfabrication methods for microfluidic analytical applications," *Electrophoresis,* vol. 21, pp. 12-26, Jan 2000.
[152] J. C. McDonald, D. C. Duffy, J. R. Anderson, D. T. Chiu, H. Wu, O. J. Schueller, and G. M. Whitesides, "Fabrication of microfluidic systems in poly(dimethylsiloxane)," *Electrophoresis,* vol. 21, pp. 27-40, Jan 2000.
[153] S. Takayama, E. Ostuni, P. LeDuc, K. Naruse, D. E. Ingber, and G. M. Whitesides, "Subcellular positioning of small molecules," *Nature,* vol. 411, p. 1016, Jun 28 2001.
[154] K. Takahashi, S. N. Arjunan, and M. Tomita, "Space in systems biology of signaling pathways--towards intracellular molecular crowding in silico," *FEBS Lett,* vol. 579, pp. 1783-8, Mar 21 2005.
[155] M. A. Burns, C. H. Mastrangelo, T. S. Sammarco, F. P. Man, J. R. Webster, B. N. Johnsons, B. Foerster, D. Jones, Y. Fields, A. R. Kaiser, and D. T. Burke, "Microfabricated structures for integrated DNA analysis," *Proc Natl Acad Sci U S A,* vol. 93, pp. 5556-61, May 28 1996.
[156] A. T. Woolley and R. A. Mathies, "Ultra-high-speed DNA sequencing using capillary electrophoresis chips," *Anal Chem,* vol. 67, pp. 3676-80, Oct 15 1995.
[157] E. D. Steinle, D. T. Mitchell, M. Wirtz, S. B. Lee, V. Y. Young, and C. R. Martin, "Ion channel mimetic micropore and nanotube membrane sensors," *Anal Chem,* vol. 74, pp. 2416-22, May 15 2002.
[158] Q. Wei, C. Bechinger, and P. Leiderer, "Single-file diffusion of colloids in one-dimensional channels," *Science,* vol. 287, pp. 625-7, Jan 28 2000.
[159] S. T. Retterer, P. Siuti, C. K. Choi, D. K. Thomas, and M. J. Doktycz, "Development and fabrication of nanoporous silicon-based bioreactors within a microfluidic chip," *Lab on a Chip,* vol. 10, pp. 1174-1181, 2010.
[160] J. Beaudouin, F. Mora-Bermudez, T. Klee, N. Daigle, and J. Ellenberg, "Dissecting the contribution of diffusion and interactions to the mobility of nuclear proteins," *Biophysical Journal,* vol. 90, pp. 1878-94, Mar 15 2006.
[161] B. L. Sprague and J. G. McNally, "FRAP analysis of binding: proper and fitting," *Trends Cell Biol,* vol. 15, pp. 84-91, Feb 2005.
[162] D. E. Smith, Perkins, T.T., Chu, S., "Dynamical Scaling of DNA Diffusion Coefficients " *Macromolecules,* vol. 29, pp. 1372-1373, 1996.
[163] J. Langowski, M. Hammermann, K. Klenin, R. May, and K. Toth, "Superhelical DNA studied by solution scattering and computer models," *Genetica,* vol. 106, pp. 49-55, 1999.
[164] N. Periasamy and A. S. Verkman, "Analysis of fluorophore diffusion by continuous distributions of diffusion coefficients: application to photobleaching measurements of multicomponent and anomalous diffusion," *Biophysical Journal,* vol. 75, pp. 557-67, Jul 1998.
[165] R. Y. Tsien, "The green fluorescent protein," *Annu Rev Biochem,* vol. 67, pp. 509-44, 1998.
[166] D. Piszkiewicz, "Positive cooperativity in micelle-catalyzed reactions," *J Am Chem Soc,* vol. 99, pp. 1550-7, Mar 2 1977.
[167] B. Gavish and M. M. Werber, "Viscosity-dependent structural fluctuations in enzyme catalysis," *Biochemistry,* vol. 18, pp. 1269-75, Apr 3 1979.

[168] C. A. Vernon, "The mechanisms of hydrolysis of glycosides and their revelance to enzyme-catalysed reactions," *Proc R Soc Lond B Biol Sci,* vol. 167, pp. 389-401, Apr 18 1967.
[169] A. Warshel and M. Levitt, "Theoretical studies of enzymic reactions: dielectric, electrostatic and steric stabilization of the carbonium ion in the reaction of lysozyme," *J Mol Biol,* vol. 103, pp. 227-49, May 15 1976.
[170] S. Matosevic and B. M. Paegel, "Stepwise synthesis of giant unilamellar vesicles on a microfluidic assembly line," *Journal of the American Chemical Society,* vol. 133, pp. 2798-800, Mar 9 2011.
[171] M. J. Doktycz and M. L. Simpson, "Nano-enabled synthetic biology," *Molecular Systems Biology,* vol. 3, pp. -, Jul 2007.
[172] S. Matosevic, G. J. Lye, and F. Baganz, "Design and characterization of a prototype enzyme microreactor: quantification of immobilized transketolase kinetics," *Biotechnol Prog,* vol. 26, pp. 118-26, Jan 2010.
[173] P. Walde and S. Ichikawa, "Enzymes inside lipid vesicles: Preparation, reactivity and applications," *Biomolecular Engineering,* vol. 18, pp. 143-177, Oct 31 2001.
[174] M. Karlsson, M. Davidson, R. Karlsson, A. Karlsson, J. Bergenholtz, Z. Konkoli, A. Jesorka, T. Lobovkina, J. Hurtig, M. Voinova, and O. Orwar, "Biomimetic nanoscale reactors and networks," *Annual Review of Physical Chemistry,* vol. 55, pp. 613-649, 2004.
[175] A. Taubert, A. Napoli, and W. Meier, "Self-assembly of reactive amphiphilic block copolymers as mimetics for biological membranes," *Curr Opin Chem Biol,* vol. 8, pp. 598-603, Dec 2004.
[176] R. J. Y. Ho, H. Pingbeall, B. T. Rouse, and L. Huang, "Kinetic and Ultrastructural Studies of Interactions of Target Sensitive Immunoliposome with Herpes-Simplex Virus," *Biophysical Journal,* vol. 51, pp. A155-A155, Feb 1987.
[177] A. Yamaguchi, P. Jin, H. Tsuchiyama, T. Masuda, K. Sun, S. Matsuo, and H. Misawa, "Rapid fabrication of electrochemical enzyme sensor chip using polydimethylsiloxane microfluidic channel," *Analytica Chimica Acta,* vol. 468, pp. 143-152, Sep 10 2002.
[178] D. M. Vriezema, M. C. Aragones, J. A. A. W. Elemans, J. J. L. M. Cornelissen, A. E. Rowan, and R. J. M. Nolte, "Self-assembled nanoreactors," *Chemical Reviews,* vol. 105, pp. 1445-1489, Apr 2005.
[179] W. Zhan, G. H. Seong, and R. M. Crooks, "Hydrogel-based microreactors as a functional component of microfluidic systems," *Analytical Chemistry,* vol. 74, pp. 4647-4652, Sep 15 2002.
[180] H. Mao, T. Yang, and P. S. Cremer, "Design and characterization of immobilized enzymes in microfluidic systems," *Anal Chem,* vol. 74, pp. 379-85, Jan 15 2002.
[181] S. Y. Jung, Y. Liu, and C. P. Collier, "Fast mixing and reaction initiation control of single-enzyme kinetics in confined volumes," *Langmuir,* vol. 24, pp. 4439-42, May 6 2008.
[182] A. G. Hadd, D. E. Raymond, J. W. Halliwell, S. C. Jacobson, and J. M. Ramsey, "Microchip device for performing enzyme assays," *Anal Chem,* vol. 69, pp. 3407-12, Sep 1 1997.

[183] B. J. Burke and F. E. Regnier, "Stopped-flow enzyme assays on a chip using a microfabricated mixer," *Anal Chem,* vol. 75, pp. 1786-91, Apr 15 2003.
[184] D. C. Duffy, H. L. Gillis, J. Lin, N. F. Sheppard, and G. J. Kellogg, "Microfabricated centrifugal microfluidic systems: Characterization and multiple enzymatic assays," *Analytical Chemistry,* vol. 71, pp. 4669-4678, Oct 15 1999.
[185] Y. Tanaka, M. N. Slyadnev, K. Sato, M. Tokeshi, H. B. Kim, and T. Kitamori, "Acceleration of an enzymatic reaction in a microchip," *Anal Sci,* vol. 17, pp. 809-10, Jul 2001.
[186] A. Nomura, S. Shin, O. O. Mehdi, and J. M. Kauffmann, "Preparation, characterization, and application of an enzyme-immobilized magnetic microreactor for flow injection analysis," *Anal Chem,* vol. 76, pp. 5498-502, Sep 15 2004.
[187] K. Sakai-Kato, M. Kato, and T. Toyo'oka, "Creation of an on-chip enzyme reactor by encapsulating trypsin in sol-gel on a plastic microchip," *Anal Chem,* vol. 75, pp. 388-93, Feb 1 2003.
[188] M. A. Holden, S. Y. Jung, and P. S. Cremer, "Patterning enzymes inside microfluidic channels via photoattachment chemistry," *Anal Chem,* vol. 76, pp. 1838-43, Apr 1 2004.
[189] J. Boudrant and C. Cheftel, "[Application of the theory of oxygen transfer: determination of the Michaelis constant of glucose oxidase with respect to oxygen]," *Biochimie,* vol. 57, pp. 117-22, 1975.
[190] S. Zimmermann, D. Fienbork, B. Stoeber, A. W. Flounders, and D. Liepmann, "A microneedle-based glucose monitor: Fabricated on a wafer-level using in-device enzyme immobilization," *Boston Transducers'03: Digest of Technical Papers, Vols 1 and 2,* pp. 99-102
1938, 2003.
[191] D. T. Chiu, C. F. Wilson, F. Ryttsen, A. Stromberg, C. Farre, A. Karlsson, S. Nordholm, A. Gaggar, B. P. Modi, A. Moscho, R. A. Garza-Lopez, O. Orwar, and R. N. Zare, "Chemical transformations in individual ultrasmall biomimetic containers," *Science,* vol. 283, pp. 1892-5, Mar 19 1999.
[192] B. Hess and A. Mikhailov, "Microscopic self-organization in living cells: a study of time matching," *J Theor Biol,* vol. 176, pp. 181-4, Sep 7 1995.
[193] J. M. Cooper, "Towards electronic Petri dishes and picolitre-scale single-cell technologies," *Trends Biotechnol,* vol. 17, pp. 226-30, Jun 1999.
[194] S. R. May, A. M. Ashique, M. Karlen, B. Wang, Y. Shen, K. Zarbalis, J. Reiter, J. Ericson, and A. S. Peterson, "Loss of the retrograde motor for IFT disrupts localization of Smo to cilia and prevents the expression of both activator and repressor functions of Gli," *Dev Biol,* vol. 287, pp. 378-89, Nov 15 2005.
[195] S. E. Brenner, "A tour of structural genomics," *Nat Rev Genet,* vol. 2, pp. 801-9, Oct 2001.
[196] A. Hoos, G. Parmiani, K. Hege, M. Sznol, H. Loibner, A. Eggermont, W. Urba, B. Blumenstein, N. Sacks, U. Keilholz, and G. Nichol, "A clinical development paradigm for cancer vaccines and related biologics," *J Immunother,* vol. 30, pp. 1-15, Jan 2007.

[197] J. A. Kramer, J. E. Sagartz, and D. L. Morris, "The application of discovery toxicology and pathology towards the design of safer pharmaceutical lead candidates," *Nat Rev Drug Discov,* vol. 6, pp. 636-49, Aug 2007.
[198] S. L. Johnston, "Biologic therapies: what and when?," *J Clin Pathol,* vol. 60, pp. 8-17, Jan 2007.
[199] F. Baneyx, "Recombinant protein expression in Escherichia coli," *Curr Opin Biotechnol,* vol. 10, pp. 411-21, Oct 1999.
[200] D. C. Andersen and L. Krummen, "Recombinant protein expression for therapeutic applications," *Curr Opin Biotechnol,* vol. 13, pp. 117-23, Apr 2002.
[201] Y. Shimizu, Y. Kuruma, B. W. Ying, S. Umekage, and T. Ueda, "Cell-free translation systems for protein engineering," *FEBS J,* vol. 273, pp. 4133-40, Sep 2006.
[202] T. Sawasaki, T. Ogasawara, R. Morishita, and Y. Endo, "A cell-free protein synthesis system for high-throughput proteomics," *Proc Natl Acad Sci U S A,* vol. 99, pp. 14652-7, Nov 12 2002.
[203] D. Busso, R. Kim, and S. H. Kim, "Expression of soluble recombinant proteins in a cell-free system using a 96-well format," *J Biochem Biophys Methods,* vol. 55, pp. 233-40, Mar 28 2003.
[204] S. H. Kang, D. M. Kim, H. J. Kim, S. Y. Jun, and K. Y. Lee, "Cell-free production of aggregation-prone proteins in soluble and active forms," *Biotechnol Prog,* vol. 21, pp. 1412-9, Sep-Oct 2005.
[205] G. Yin and J. R. Swartz, "Enhancing multiple disulfide bonded protein folding in a cell-free system," *Biotechnol Bioeng,* vol. 86, pp. 188-95, Apr 20 2004.
[206] J. Tian, H. Gong, N. Sheng, X. Zhou, E. Gulari, X. Gao, and G. Church, "Accurate multiplex gene synthesis from programmable DNA microchips," *Nature,* vol. 432, pp. 1050-4, Dec 23 2004.
[207] D. M. Kim and J. R. Swartz, "Prolonging cell-free protein synthesis with a novel ATP regeneration system," *Biotechnol Bioeng,* vol. 66, pp. 180-8, 1999.
[208] Y. Endo, S. Otsuzuki, K. Ito, and K. Miura, "Production of an enzymatic active protein using a continuous flow cell-free translation system," *J Biotechnol,* vol. 25, pp. 221-30, Sep 1992.
[209] D. M. Kim and C. Y. Choi, "A semicontinuous prokaryotic coupled transcription/translation system using a dialysis membrane," *Biotechnol Prog,* vol. 12, pp. 645-9, Sep-Oct 1996.
[210] B. L. Fletcher, E. D. Hullander, A. V. Melechko, T. E. McKnight, K. L. Klein, D. K. Hensley, J. L. Morrell, M. L. Simpson, and M. J. Doktycz, "Microarrays of biomimetic cells formed by the controlled synthesis of carbon nanofiber membranes," *Nano Letters,* vol. 4, pp. 1809-1814, Oct 2004.
[211] B. R. Srijanto, S. T. Retterer, J. D. Fowlkes, and M. J. Doktycz, "Nanostructured silicon membranes for control of molecular transport," *Journal of Vacuum Science & Technology B,* vol. 28, pp. C6p48-C6p52, Nov 2010.
[212] O. Pongs, R. Bald, and V. A. Erdmann, "Identification of chloramphenicol-binding protein in Escherichia coli ribosomes by affinity labeling," *Proc Natl Acad Sci U S A,* vol. 70, pp. 2229-33, Aug 1973.

[213] T. Siibak, L. Peil, L. Xiong, A. Mankin, J. Remme, and T. Tenson, "Erythromycin- and chloramphenicol-induced ribosomal assembly defects are secondary effects of protein synthesis inhibition," *Antimicrob Agents Chemother,* vol. 53, pp. 563-71, Feb 2009.
[214] S. Brenner and R. A. Lerner, "Encoded combinatorial chemistry," *Proc Natl Acad Sci U S A,* vol. 89, pp. 5381-3, Jun 15 1992.
[215] A. Buxboim, M. Bar-Dagan, V. Frydman, D. Zbaida, M. Morpurgo, and R. Bar-Ziv, "A single-step photolithographic interface for cell-free gene expression and active biochips," *Small,* vol. 3, pp. 500-10, Mar 2007.
[216] C. M. Niemeyer, T. Sano, C. L. Smith, and C. R. Cantor, "Oligonucleotide-directed self-assembly of proteins: semisynthetic DNA--streptavidin hybrid molecules as connectors for the generation of macroscopic arrays and the construction of supramolecular bioconjugates," *Nucleic Acids Res,* vol. 22, pp. 5530-9, Dec 25 1994.
[217] A. V. Oleinikov, M. D. Gray, J. Zhao, D. D. Montgomery, A. L. Ghindilis, and K. Dill, "Self-assembling protein arrays using electronic semiconductor microchips and in vitro translation," *J Proteome Res,* vol. 2, pp. 313-9, May-Jun 2003.
[218] H. W. Wu, Y. C. Huang, C. L. Wu, and G. B. Lee, "Exploitation of a microfluidic device capable of generating size-tunable droplets for gene delivery," *Microfluidics and Nanofluidics,* vol. 7, pp. 45-56, Jul 2009.
[219] Y. Zhu and B. E. Power, "Lab-on-a-chip in vitro compartmentalization technologies for protein studies," *Adv Biochem Eng Biotechnol,* vol. 110, pp. 81-114, 2008.
[220] Q. Mei, R. Khnouf, A. Simon, and Z. H. Fan, "Protein synthesis in a device with nanoporous membranes and microchannels," *Lab Chip,* vol. 10, pp. 2541-5, Oct 7 2010.
[221] Y. Kitaoka, N. Nishimura, and M. Niwano, "Cooperativity of stabilized mRNA and enhanced translation activity in the cell-free system," *J Biotechnol,* vol. 48, pp. 1-8, Jul 18 1996.
[222] M. Hino, Y. Shinohara, K. Kajimoto, H. Terada, and Y. Baba, "Requirement of continuous transcription for the synthesis of sufficient amounts of protein by a cell-free rapid translation system," *Protein Expr Purif,* vol. 24, pp. 255-9, Mar 2002.
[223] N. Nishimura, Y. Kitaoka, and M. Niwano, "Improvement of Escherichia coli cell-free system by utilization of cell extract having additional property. Problems and countermeasures," *Appl Biochem Biotechnol,* vol. 53, pp. 29-35, Apr 1995.
[224] M. C. Jewett, K. A. Calhoun, A. Voloshin, J. J. Wuu, and J. R. Swartz, "An integrated cell-free metabolic platform for protein production and synthetic biology," *Mol Syst Biol,* vol. 4, p. 220, 2008.
[225] N. Park, S. H. Um, H. Funabashi, J. Xu, and D. Luo, "A cell-free protein-producing gel," *Nat Mater,* vol. 8, pp. 432-7, May 2009.
[226] J. Kim and E. Winfree, "Synthetic in vitro transcriptional oscillators," *Mol Syst Biol,* vol. 7, p. 465, Feb 1 2011.
[227] M. L. Simpson, "Cell-free synthetic biology: a bottom-up approach to discovery by design," *Mol Syst Biol,* vol. 2, p. 69, 2006.

[228] K. Brenner, D. K. Karig, R. Weiss, and F. H. Arnold, "Engineered bidirectional communication mediates a consensus in a microbial biofilm consortium," *Proc Natl Acad Sci U S A,* vol. 104, pp. 17300-4, Oct 30 2007.
[229] J. P. Pearson, E. C. Pesci, and B. H. Iglewski, "Roles of Pseudomonas aeruginosa las and rhl quorum-sensing systems in control of elastase and rhamnolipid biosynthesis genes," *J Bacteriol,* vol. 179, pp. 5756-67, Sep 1997.
[230] E. C. Pesci, J. P. Pearson, P. C. Seed, and B. H. Iglewski, "Regulation of las and rhl quorum sensing in Pseudomonas aeruginosa," *J Bacteriol,* vol. 179, pp. 3127-32, May 1997.

VITA

Piro Siuti was born Kucove, Albania in 1981. He graduated from Shkolla e Mesme in 2000. That fall he began his undergraduate education at New York College, in Athens Greece and then transferred to the University of Southern Indiana, Indiana, to complete his degree in Biology in 2005. It was at USI that he started to develop a greater appreciation for molecular and cellular research. In February of 2006, he was accepted in the Genome Science and Technology program at the University of Tennessee-Knoxville. He completed his PhD degree in the summer of 2011.